

The Radio/Optical Catalog of the SSA13 Field

E. B. Fomalont, K. I. Kellermann

National Radio Astronomy Observatory, Charlottesville, VA 22903

efomalon@nrao.edu, kkellerm@nrao.edu

L. L. Cowie¹, P. Capak^{1,2}, A. J. Barger^{1,3,4}

¹*Institute for Astronomy, Honolulu, HI 96822*

²*California Institute of Technology, Pasadena, CA 91125*

³*University of Wisconsin-Madison, Madison, WI 53706*

⁴*University of Hawaii, Honolulu, HI 96822*

cowie@ifa.hawaii.edu, capak@astro.caltech.edu, barger@astro.wisc.edu

R. B. Partridge¹, R. A. Windhorst², E. A. Richards³

¹*Haverford College, Haverford, PA 19041*

²*Arizona State University, Tempe, AZ 85287*

³*Talladega College, Talladega, AL 35160*

bpartrid@haverford.edu, Rogier.Windhorst@asu.edu, erichards@talladega.edu

ABSTRACT

We present a 1.4-GHz catalog of 810 radio sources (560 sources in the complete sample) found in the SSA13 field (RA=13^h12^m, DEC=42°38′). The 1.4-GHz radio image was obtained from a 91-hour VLA integration with an rms noise level of 4.82 μ Jy/beam at the field center. Optical images in r-band (6300Å) and z-band (9200Å) with three- σ detection magnitudes of 26.1 and 24.9, respectively, were obtained from three observing nights on the 8-m Subaru Telescope. We find that $88 \pm 2\%$ of the radio sources are identified with an optical counterpart. There is significantly more reddening for the optical counterparts that are fainter than 24-mag, probably caused by the somewhat larger redshift of these faint galaxies. The radio and optical parameters are tabulated, and source morphologies are displayed by radio contours overlaying optical false-color images. The brightness distributions show a wealth of complexity and these are classified into a small number of categories. About one-third of the radio sources are larger than 1.2'' and their orientation is often similar to that of the associated galaxy or binary-galaxy system. Radio emission is sometimes located outside of the nuclear regions of the galaxy. The density of sources in the SSA13 field above 75 μ Jy is 0.40 (arcmin)⁻², with a slope of -2.43 in the differential counts. This source density is about a factor of two higher than that in the HDF-north. The radio spectral index may steepen for sources below 75 μ Jy and is consistent with the difference in the slope of the source counts observed between 1.4 GHz and 8.4 GHz. We estimate that at most 40% of the microJansky radio sources are dominated by AGN processes while the remainder are mostly the consequence of star formation and associated supernovae activity.

Subject headings: Galaxies:Active; Galaxies:Starburst; Radio Continuum:Galaxies

1. Introduction

One of the fundamental problems in astrophysics is the formation and evolution of stars, galaxies and black holes, and their properties as a function of cosmic time. Many radio sources stronger than about 1 mJy are associated with luminous galaxies with an active galactic nucleus (AGN) that contains a super massive black hole (SMBH). The energy generated by interactions near the SMBH produces most of the observed electromagnetic emission, some of which extends up to several megaparsecs from the AGN. These extended active galaxies are often referred to as ‘classical double radio sources’. With the increased sensitivity of radio observations, now extending to microJansky levels, a different population is detected (Mitchell & Condon 1985; Oort & Windhorst 1985). These sources are dominated by emission from massive star formation in a galaxy or in groups of galaxies, have redshifts typically between 0.5 and 2.0, and appear to evolve strongly with cosmological time. AGN activity, although not as dominant as in the brighter radio sources, may still be an important ingredient in the formation and evolution of the microJansky sources.

Since these processes have a complicated signature throughout the electromagnetic spectrum, multi-band observations are needed to understand the physical phenomena and evolution. Sensitive radio observations are a crucial part of the data base for many reasons: surveys provide an unbiased sample of a large number of objects in a relatively small field of view; the radio position accuracy of $\approx 0.2''$ is crucial in finding sub-mm/optical/X-ray counterparts; the radio emission is not significantly absorbed by dust; the FIR/radio correlation is an indication of redshift; and finally, the radio source spectrum, angular size and the precise location with respect to the galaxy nucleus can often distinguish between AGN processes and starforming processes.

The Small Selected Area 13 (SSA13) field is one of the Hawaii Deep Fields that has been studied at a variety of wavelengths, comparable to studies of the Hubble Deep Field (HDF). The first deep VLA radio observations of SSA 13 were made at 8.4 GHz (Windhorst et al. 1995; Fomalont et al. 2002) where about 50 sources were detected in the relatively small part of the SSA13 region that

was imaged. In this paper we report on additional deep VLA observations at 1.4 GHz over the entire SSA13 field to a detection level of $25.8 \mu\text{Jy}/\text{beam}$. Our deep r-band and z-band images from the 8-m Subaru Telescope allows us to present a radio/optical catalog of over 800 radio sources and describe their radio and optical properties.

The radio observations, data reduction and images are described in §2, and the optical observations in §3. The radio/optical catalog is given in §4 in tabular and graphical form, including descriptive notes for the more interesting objects. The identification rate, the radio/optical morphologies, and the radio properties are discussed in §5, §6 and §7, respectively. A summary is given in §8. Further discussion of the properties of the sources in the SSA13 field is given elsewhere (Cowie et al. 2004).

2. The Radio Data

2.1. The Observations and Reductions

The SSA13 observations were made with the VLA at 1.4 GHz for a total of 104 hours on nine separate observing days, as shown in Table 1. Excluding calibration observations, 91 hours of data were obtained on the SSA13 field. For eight of the days, the VLA was in the A-configuration (a maximum baseline of 35 km), and on one day we observed in the B-configuration (maximum baseline of 10 km) in order to increase the image sensitivity to sources larger than about $5''$ in angular size. The field center of the radio observations was at R.A. = $13^h 12^m 17.4^s$, DEC = $+42^\circ 38' 05.0''$ (J2000), and the observations were taken at two frequencies, 1.355 GHz and 1.455 GHz, each with dual circular polarization. In order to minimize the image distortion and loss of sensitivity over the area of sky covered by the optical images, the data in each frequency/polarization channel were split into 7 channels, each of 3.125-MHz bandwidth, and the data were sampled every 5 seconds (see §2.4). A few percent of the data from each observing session were deleted for occasional short periods of interference, during periods of known technical problems, for telescope shadowing, and during inclement weather conditions.

Each observing session lasted between 8 and 13 hours, with observations alternating between 12 min on SSA13 and 3 min on the nearby

calibrator source J1327+4326, located at $\alpha = 13^{\text{h}}27^{\text{m}}20.9790^{\text{s}}$, $\delta = 43^{\circ}26'27.997''$; J2000, (Beasley et al. 2002). This absolute position of J1327+4326 with respect to the International Celestial Reference Frame has been measured with the Very Long Baseline Array to an accuracy less than $0.01''$ (Ma et al. 1998). The relative positional accuracy obtained between J1327+4326 and the SSA13 radio field depends on their angular separation, the apriori calibration of VLA astrometric parameters, and weather conditions. Based on many astrometric VLA observations, the relative positional accuracy at 1.4 GHz in the A-configuration is $< 0.1''$ and we have used this value as the minimum position error in each coordinate for any source in the SSA13. The amplitude scale was derived from two observations of 3C286 on each day, assuming a flux density of 14.55 Jy at 1.4 GHz. The derived flux density of J1327+4326 was 0.558 Jy and did not vary by more than 1% over the entire observation period. Two weak radio sources of 0.01 Jy located about $10'$ from J1327+4326 were noted, but their large distance from the main radio source decorrelated their effect; we determined the overall gain calibration with an accuracy better than 1%.

The telescope-based temporal gain and phase fluctuations were determined every 15 minutes from the calibrator observations. The gain variations between successive calibrator scans was generally less than 2%, apart from the decreasing loss of sensitivity at elevations below 15° of about 30% caused by the additional noise from ground emission. The phase fluctuations between calibrator scans were typically 2° to 10° on the short to the long spacings, respectively. During periods of inclement weather and at sunrise or sunset when ionospheric activity can be large, phase changes of 15° over a few minutes occurred on baselines longer than about 10 km. Linear interpolation of the gain and phase calibration, determined from the calibrator every 15 minutes, was applied to the SSA13 data.

2.2. Self-Calibration and Imaging

The self-calibration and imaging of the VLA data were complicated by two factors: First, sources more than about $5'$ from the field center are distorted by the finite bandwidth of each 3 MHz channel (chromatic aberration), the data

sampling interval, and sky curvature. Secondly, the non-circularity of the VLA primary beam produces an apparent variability of sources because of the relative rotation between the plane of the sky and the primary antenna sensitivity pattern during an observation day. Both of these effects produce artifacts near bright sources near the 1% level. Since the brightest source in the image at 1.4 GHz was 20 mJy, these artifacts were about $50 \mu\text{Jy}/\text{beam}$, well above the rms noise level of $5 \mu\text{Jy}/\text{beam}$ after 91 hours of integration. Thus, special imaging and self-calibration techniques were necessary to reduce these artifacts below the level expected from receiver noise alone.

After applying the calibrations, based on the measurements of J1327+4326, a clean (deconvolved) image of radius $40'$ centered on SSA13 was made using the AIPS task IMAGR (Greisen 1988). We used a data weighting scheme (called robust=0) which weights the visibility data in order to produce a relatively smooth distribution of the sampled synthesized aperture, and thus a point-spread function with lower side-lobe levels than for natural weighting that considers only the apriori rms noise per data point. The image resolution associated with this weighting was $1.8''$, and a $0.5''$ pixel size was used. The SSA13 field was covered with 38 overlapping 1024×1024 ($512'' \times 512''$) images. The individual image size was chosen to limit the amplitude distortion, caused by the sky curvature, to under 5% at the edge of each image. We also made smaller images around the 15 brightest sources within $90'$ of the field center; these were all stronger than 1 mJy, the strongest being 20 mJy. Because of the relatively accurate calibration of the data using J1327+4326, the initial radio images were of good quality, although the above mentioned artifacts remained.

We continued with the next calibration step, the standard self-calibration technique (CALIB and IMAGR in AIPS), to improve the calibration of the SSA13 data. Because of the redundancy of the number of baselines (351) compared with the number of telescopes (27), it is possible to improve the telescope calibration of SSA13 using a source model, which is in fact the first-pass clean image (Cornwell & Fomalont 1989). With the self-calibration algorithm, each telescope residual phase was determined every four minutes for each polarization and frequency. The signal-to-

noise in each of these intervals was about 30:1, so robust solutions were obtained. As expected, these residual phase determinations were generally less than 5° , although there were times when the phases were as large as 30° ; these coincided with periods when there were significant phase change in the original calibration with J1327+4236¹. Because these residual phases were primarily associated with the troposphere and ionosphere above each telescope, the four phase determinations—derived from two frequencies and two polarization—agreed to within a few degrees. During the rare periods when there was either poor agreement among the four determinations, or lack of reasonable continuity among the telescope solutions, further inspection indicated data problems and these data were deleted. With the improved phase calibration and additional data editing, new cleaned images were then made.

In order to remove the artifacts due to the apparent source variability from the non-circular VLA beam shape, we next imaged and cleaned the data in four-hour observing blocks, which produced about three images per observing day and 24 images for the entire experiment. The sum of these images reproduced the cleaned image made from all of the data, but the brightest 15 sources clearly appeared to vary over the day. We then subtracted the contribution from these 15 bright sources in each 4-hour time segment directly from the data base, and formed a residual data base from which these 15 apparently-varying sources were removed. We then imaged and deeply cleaned this residual data in the 38 overlapping 1024x1024 images to the $10 \mu\text{Jy}/\text{beam}$ level ($2.8\text{-}\sigma$) to produce the final image. Finally, the cleaned images of the 15 subtracted sources (averaged over all 24 separate time-sliced images) were added to the final image so that all of the emission from all sources is included in the final image.

2.3. The 1.4 GHz Image and the Initial Radio Source List

The final cleaned image, covering a $34' \times 34'$ region with $1.8''$ -resolution at the center, is shown

¹The residual amplitude calibration was also determined; however, it was close to unity and significant departures were indicative of periods of poor data quality, rather than improved gain calibration.

in Fig. 1. The image rms noise is $4.82 \mu\text{Jy}/\text{beam}$ and is uniform to 2% over the entire image, except very close to the six brightest sources, and within $2'$ of the central region where the rms is $4.95 \mu\text{Jy}/\text{beam}$. The conversion of the image to the sky sensitivity and resolution is discussed in the next section.

We also made an image with $6''$ resolution by convolving the data. This convolved image has an rms noise of $13.8 \mu\text{Jy}/\text{beam}$, and was used to determine the structure and flux density of the more extended sources. The formal completeness level of the uncorrected image is a peak image flux density of $25.8 \mu\text{Jy}/\text{beam}$ (or $> 70 \mu\text{Jy}/\text{beam}$ on the lower resolution image), which is 5.35 times the rms noise level. Based on the almost Gaussian noise characteristics of the image, there is less than a 0.5% chance that an apparent source in the image at the completeness level is merely a noise fluctuation. The largest negative peak on the image of $-24.5 \mu\text{Jy}/\text{beam}$ is consistent with our chosen completeness level chosen.

An initial list of about 900 radio sources was generated from the region within $17'$ of the field center. We included sources with peak flux density greater than $\sim 20 \mu\text{Jy}/\text{beam}$ on the $1.8''$ -image, or above $65 \mu\text{Jy}/\text{beam}$ on the $6''$ image. These search limits were selected to be somewhat below the completeness level of the image.

The properties of each source in the radio image were determined by fitting the brightness distribution to one or two elliptical Gaussian components. The six independent parameters for each component were the peak flux density, the x- and y-coordinates, the major axis, the minor axis sizes, and orientation of the major axis. If the source was not appreciably resolved (the difference between the peak flux density and the integrated flux density was less than two times the rms noise in the image), then the average of the measured peak and integrated flux densities was assigned as the final integrated flux density, with the appropriate diameter limits. Another estimate of the integrated flux density was obtained from the peak flux density on the $6''$ resolution image, since it is less affected by resolution degradation or instrumental distortion effects. This estimate was used if it was more the $2\text{-}\sigma$ higher than that on the higher resolution image.

For sources with an image peak flux density less

than $50 \mu\text{Jy}/\text{beam}$ (10 times the rms noise), non-linear interaction of the image noise with the deconvolution process make the integrated flux density and the angular size parameters and error estimates somewhat more difficult to estimate than the peak flux density and source position (Windhorst, van Heerde & Katgert 1984). From simulations of the model fitting of weak sources on a radio image, we determined conservative estimates of the true angular size of the source or upper limits as a function of signal-to-noise ratio (SNR), and the relationship of these parameters to the integrated flux density and its estimated error. For this reason, the ratio of the integrated flux density to its estimated error is often less than the ratio of the peak flux density to its estimated error (the SNR of the peak).

2.4. Image Correction to the Sky

In order to obtain a true surface brightness model of a source from the image model, three effects must be removed. First, because of the finite primary beam size of the individual VLA antennas the sky sensitivity of the observations decreases with radial distance from the field center, with a full-width at half-power (FWHP) of $31.5'$. The radial attenuation function, which has been measured to an accuracy of 2%, is nearly circular, and is shown in Fig. 2 as the primary beam sensitivity. Second, because of the chromatic aberration, there is an additional smearing in the image which broadens a source in the radial direction. For example, for a point source that is $17'$ from the field center its peak flux density is 62% of its field center value although the integrated flux density remains unchanged. This decrease of the peak flux density as a function of distance from the field center is also plotted in Fig. 2. Finally, there is also a slight decrease in sensitivity caused by the 5-sec sampling time and the effective sensitivity loss for this is also plotted in Fig. 2 as the time smear. The combined attenuation of a source on the image as a function of distance from the field center is shown by the solid curve in Fig. 2. At a distance of $17'$ from the field center, the sky sensitivity is 24% of that at the field center. The chromatic aberration also produces a decrease of the effective sky resolution in the radial direction from the field center. The resolution ranges from $1.8''$ at the field center to $2.9''$ at a distance of $17'$ from

the field center.

Although a radio catalog could have been made after the above analyses and corrections to the radio image, the relatively high density of discrete, but often extended, radio sources caused considerable ambiguity in determining whether closely spaced radio sources should be considered as components of *one independent source* or as two independent sources. Since radio emission at the micro-Jansky level is often identified with galaxies between 17-mag and 24-mag, we have established the catalog of sources using both radio and optical information. Hence, each cataloged radio source (sometimes composed of several components) is associated with one optical object, or a close group of objects. Whatever segregation method is used to define a cataloged source, there will be ambiguous situations, and these are noted in §5.4.5. These sources may turn out to be among the more interesting objects in the image.

3. The Optical Data

3.1. The Observations and Reductions

Observations of the SSA13 field were made with the 8-m Subaru Telescope and the Suprime-Cam prime focus camera with a $34' \times 27'$ field of view (Miyazaki et al. 1998). Two filters were used: The z-filter band pass is between 8600 and 9800 Å, and the r-filter band pass is between 5800 and 6800 Å. We will designate these two wavebands as the z-band and r-band. Data were collected on 2001 February 2, April 22, and April 23, and all nights except April 22 were photometric. During the February run, the Suprime-Cam was still in a commissioning phase, and 9 of the 10 chips were usable. The missing chip producing a $7' \times 14.5'$ hole in the SE corner of the image. During the April observations, the camera had one chip in the NE corner with a bad anti-reflective coating, and this reduced the throughput in this region by 50% or more. The camera was also severely vignetted near the edge of the field, reducing throughput by up to 60% for objects more than $14'$ from the center of the field.

On 2001 February 2, we collected 1920 sec of r-band data with the commissioning camera. A further 2400 sec of r-band and 3230 sec of z-band data were collected on April 22 and 23. The camera was offset by one arc minute between expo-

tures in a five-point dither pattern. The dither pattern and large steps were chosen to fill in gaps between chips, optimize flat fielding, and allow for chip to chip photometric calibration. The camera was rotated by 90 degrees between dither patterns for z-band observations to remove bleeding from bright stars, and to move the bad chip to the NW corner for some of the exposures.

These data were reduced using Kaiser’s IMCAT software² which is optimized for reducing large data sets on parallel computers. Median sky flats were used to flat field the images. The z-band flat was smoothed by 32 pixels to remove fringing. A median fringe frame was generated for the z-band images, scaled to the sky level in each image, and subtracted. A second phase of flattening was performed on each set of 5 images to remove flat fielding errors caused by flexure in the instrument. A second order polynomial was fit to the sky level and subtracted from each frame to remove the sky emission. Objects detected at $3\text{-}\sigma$ and pixels brighter than 200 counts were then masked out and a surface tessellated on a 64 pixel grid. This background was then subtracted to remove scattered light in the image. This was particularly important in this field because of the 10th magnitude star in the field, and scattered light from the moon in the z-band images. Chip to chip and exposure to exposure photometric offsets were then calculated and an airmass correction was applied using a standard Mauna Kea extinction curve. The preliminary photometric zero points were calculated using the HDF-N as a standard frame. Landolt standards were also taken, but were found to be less reliable because of the short exposure times required to ensure that they did not saturate. The four-minute readout of Suprime-Cam during these runs also limited the number of standard star exposures which could be taken. Further calibration of the magnitude scale is described in §3.4.

The Subaru images were then re-sampled onto a final grid of $0.2''$ pixel-separation and a photometric distortion correction was applied. The re-sampled images were then median combined, weighted by the rms noise in each chip and in each image. The final images have a usable field of view of $34' \times 27'$ in r-band and $34' \times 34'$ in z-band. The resolution of both images, determined from

the minimum angular size of stellar-like objects, is $1.1''$. The $3\text{-}\sigma$ limiting magnitude is 26.1 in r-band and 24.9 in z-band, and was determined by laying down blank $3''$ apertures on the image at least $15''$ from a detected object.

3.2. The Optical Images

The z-band (9200\AA) Subaru optical image is shown in Fig. 3. The detection level in the image is 24.9 mag ($3\text{-}\sigma$) and objects brighter than a peak magnitude of 18 to 19 mag-sec⁻² become saturated. There are some evident artifacts associated with the bright 10-mag star, and there are other blemishes near the southern edge of the image.

3.3. Final Radio/Optical Registration

Objects brighter than 19-mag are saturated in the r-band images, making it difficult to reliably register the images to the USNO-A catalog (<http://archive.eso.org/servers/usnoa>). To avoid this problem, an initial astrometric solution was calculated using a standard star field. This resolution was applied to each individual solution, and these corrected images were then registered to one another. A refined astrometric distortion was then calculated for each image by minimizing the scatter in the position of stars from image to image. In the absence of an external astrometric reference, several systematics are present. First, anamorphic magnification from differential atmospheric refraction is present in the images. Secondly, in addition to the readout problem in one of the commissioning chips, the relative position of the chips was misaligned by up to $1''$, especially in declination.

The final detailed registration of the r-band and z-band optical images to the radio image was determined by comparing the positions of bright, small-diameter radio sources with an obvious optical counterpart in order to determine the small offset, rotation and magnification between the radio and optical images, and the chip-to-chip registration offsets. There are over 400 secure identifications, but about 25% of the identifications have significant radio-optical offsets, and 50% are not of high astrometric quality since they are associated with distorted galaxies and/or extended and complex radio structures. Hence, a total of 95 high-quality identifications established the fi-

²<http://www.ifa.hawaii.edu/~kaiser/imcat>

nal radio/optical alignment. The distribution of the radio-optical positions after the registration is shown in Fig. 4. The dashed circle with radius of $0.2''$ shows the one-sigma registration error. Since the radio source and galaxy positions have a typical positional accuracy of about $0.1''$, the scatter is consistent with the measurement errors with perhaps small residual radio-optical offsets. The quality of the registration clearly suggests that measured offsets between the radio and optical emission peaks larger than $0.5''$ are real offsets associated with the source, at least for sources well above the radio and optical thresholds.

3.4. Magnitude Calibration and Measurement

The final calibration of the zero point of the magnitude scale was determined by selecting over a 100 isolated, compact optical objects, securely identified with a radio source, that were also in the Sloan Digital Sky Survey (SDSS)³, then comparing SDSS and our Subaru magnitudes. Fig. 5 shows the linearity and scatter of the Subaru magnitudes of isolated sources in the SSA13 catalog, listed in Table 2, versus the SDSS magnitudes (interpolated to r- and z-bands). After this calibration, the rms error per galaxy is 0.3-mag in r-band and 0.5-mag in z-band, but there is no systematic difference greater than 0.2-mag.

We then determined the r-band and z-band magnitude of all relevant objects at or near each radio source, using this SDSS-based magnitude calibration. For objects fainter than about 22 mag, the magnitude was determined by the sum of intensities within a radius of $3''$ from the galaxy center. For brighter and more extended galaxies the area was increased as necessary. For close binary galaxy-pairs, the area was adjusted to include only the emission from the relevant galaxy. The emission associated with faint halos of galaxies was not included in the estimated magnitudes. In all cases, the same area was used to determine the magnitude for both filters. For radio sources with no apparent optical counterpart, we used the $2\text{-}\sigma$ noise level as the magnitude limit. This limit increased near the image edges and near the bright star in the field.

³<http://www.sdss.org/science/index.html>

4. The Radio/Optical Catalog

4.1. Compilation of the Radio/Optical Catalog

We then carefully compared the optical and radio fields for the preliminary list of 900 radio sources which we had compiled using only the radio data. With the radio and optical registration of $0.2''$, objects as faint as $z=24.9$ and $r=26.2$ could be identified with a radio source, based on proximity alone. Thus, the astrometric accuracy was crucial in determining the most probable identification or lack of identification for the radio sources, some of which are extended by several arcsec and are located in relatively crowded optical fields. It is also clear that the centroids of some radio sources are significantly offset from the center of the optical counterpart. The individual identifications are discussed more fully in §4.5.

4.2. The Complete Sample

The radio/optical catalog, listed in Table 2, contains 810 radio sources within $17'$ of the field center. Because of the significant attenuation and distortion of sources near the edge of the field, we limited the area of formal completeness to a radius of $15'$ from the field center, and a peak *image* flux density greater than $25.8 \mu\text{Jy}/\text{beam}$. This corresponds to a *sky* completeness of $75 \mu\text{Jy}/\text{beam}$ within the $15'$ radius.

Of the 810 sources in the catalog, 560 sources are in this complete sample, and it is only this sample which is used for statistical analysis of the properties of the radio sources. The additional 250 sources, while not part of the complete sample, are useful additions in understanding the complex radio and optical morphologies found at the lower flux density levels. The probability that these weak sources are real is $> 95\%$. Thus we estimate that fewer than ten to fifteen of the 810 cataloged sources may not be real.

4.3. The SSA13 Radio/Optical Catalog

The radio/optical catalog of the SSA13 Field is given in Table 2. It is arranged in right ascension order, although components of a single source are kept together.

- Column 1: The radio source number used in

this paper. The letter **N** before the number indicates that it is **NOT** in the complete sample: either the peak flux density on the image is less than $25.8 \mu\text{Jy}/\text{beam}$; or it lies more than $15'$ from the field center. If the radio source is composed of several discrete radio components, these are separately listed underneath as A, B, etc.

- Column 2: The IAU designation for each source. Individual radio components of a cataloged source are not given separate IAU designations, but should use that of the source as a whole.
- Column 3: The SNR of the radio source and radio components, given by the peak image flux density divided by the rms noise. Those sources with $\text{SNR} < 5.35$ are not in the complete catalog.
- Column 4: The source integrated flux density and error estimates in microJansky, *corrected to the sky for all instrumental effects*. The determination of this parameter is discussed in §2.4.
- Column 5: The right ascension and error estimate of the radio emission. For sources larger than $8''$, the position is that of the brightest emission peak in the source, not the centroid. The minimum error is 0.010s, as discussed in §2.1.
- Column 6: The declination and error estimate defined as in column 5. The minimum error is $0.10''$.
- Columns 7, 8, 9: The radio FWHP major axis and minor axis in arcsec, and position angle, north through east, in degrees. All instrumental and noise corrections have been made and this angular size is the best estimate of the true angular size or its limit. The size of each individual radio component is also given. The angular size limit is a strong function of SNR. Based on simulations, we estimate that there is more than 85% confidence that a source with a tabulated angular size is really resolved.
- Column 10: The radio/optical morphology category (ROM). These are defined in Table

3 and discussed in the next section. The major categories are: EG = Extended Active Galaxies; S = Stellar Object; G = Galaxy; B = Binary Galaxy System; C = Complex; F = Faint ID; U=Unidentified. The sub-categories in lower case letter are: c = radio emission centered on optical object; e = extended radio source; d = radio source is displaced from optical center. There is some subjectivity among the categories. Individual optical identifications for radio components in a cataloged source are also listed when applicable. A question mark (?) indicates that there is a note associated with this catalog entry. For the small portion of the radio field covered only by the SDSS and not the deeper Subaru images, the optical classifications are limited to: sg=galaxy, su=unidentified.

- Column 11: The r-band integrated magnitude of the optical counterpart to the radio source (or components where applicable).
- Column 12: The z-band integrated magnitude of the optical counterpart.

4.4. The SSA13 Radio/Optical Plots

The comparison of the radio and optical emission for all 810 sources in the catalog is shown in Figs. 6-1 to 6-33. Most fields in these figures are $12'' \times 12''$ in size, although some plots are as large $30'' \times 30''$ to display all of the radio and optical emission of extended or complex sources. *The full-set of plots are found in ftp://ftp.cv.nrao.edu/pub/NRAO-staff/efomalon/ssa13_diagrams/.*

The contours show the *radio* emission with the lowest contour value at $10.0 \mu\text{Jy}/\text{beam}$, and levels at -1,1,2,4,16 times this value. For the brightest radio sources, the lowest radio contour level has been increased to remove low level artifacts. The colored display shows the optical emission, usually at z-band unless the r-band image is of superior quality. The color transfer function for each source has been adjusted in order to show the salient morphological features of the optical emission, and to limit the noise contribution in regions of lower optical sensitivity. For those sources with no optical information from Subaru, only the radio contours

are shown, with a pink color background; however, Table 2 does contain any identifications and magnitudes obtained from the SDSS.

4.5. Comments on Individual Sources

Individual comments on selected radio/optical fields are given below. Most references to SDSS are associated with point-like optical emission where the colors can distinguish between stars and quasars.

009. The smaller object to the south-west is a star (SDSS).
020. The smaller object to the west is a star (SDSS).
021. The radio emission is displaced north-west of the optical center. It is extended to the east and is associated with a faint optical galaxy.
027. The extended radio source is about $8''$ south of group of bright galaxies. It is unidentified, but faint background optical emission lies near the radio emission.
032. The radio source is well displaced from the galactic nucleus. There is a spur of optical emission near the radio centroid.
050. The main part of the radio emission is associated with a 23-mag galaxy. There is radio emission extending to the galaxies to the east and west.
053. The extended radio emission is associated with a close binary system.
069. This extended radio source is identified with a symmetric galaxy. The contour plot of the entire radio source (Fig. 8) shows a morphology closer to FRI than FRII (lobes are diffuse with no hot spot).
091. The radio source is displaced $3''$ west of the galaxy nucleus. It may be a background unidentified source, or it may be associated with a faint spur toward the west from the galaxy.
096. The radio source is identified with a faint galaxy. There is extended radio emission connected to another galaxy about $7''$ to the south.
101. One radio component is associated with the nucleus of the galaxy. A second radio component (101B) is located $2''$ north, roughly in the direction of the extended optical core.
104. The radio source is located at the nucleus of the southern galaxy of a close pair. Source 105 is to the north. The circular object to the west is a star (SDSS).
105. The radio source is located at the nucleus of the northern galaxy of a close pair. Source 104 is to the south.
109. Most of the radio emission is associated with the southern galaxy. The object about $3''$ to the north-west is a star (SDSS), with a hint of faint radio emission.
112. The object $4''$ to the west is a star (SDSS).
122. The radio source lies in the middle of a group of galaxies, but is considered unidentified since there is no optical emission coincident with the radio source.
141. The identification is uncertain.
143. The main radio emission is associated with a 23-mag galaxy. There are indications of extended emission associated with two nearby galaxies.
156. The radio source is located near a bright star (SDSS) that is saturated on the image. Source 158 is on the left lower border of the frame.
158. The radio emission is located within the glare of a bright star (SDSS).
159. The identification is uncertain.
169. The radio source is associated with a blue stellar object (SDSS). It could be a quasar.
171. The identification is uncertain.
175. The large-scale radio emission is associated with several galaxies.
177. The identification is uncertain.
183. The optical object $3''$ to the west is a star (SDSS).
185. Three objects show radio emission. However, the northern-most radio source (185C) is a slightly red stellar object (SDSS), while components 185A and 185B are associated with individual galaxies.
188. The radio emission associated with the elliptical galaxy is complex. A bright star is located about $10''$ north-east.
195. The radio emission lies between a circular galaxy to the north and a fainter galaxy to the south-west (morphology unknown).
201. Two of the three galaxies have radio emission (components 201A and 201B). They are cataloged as one radio source since the galaxies appear interacting.
212. The radio contours here just show the radio core of an extended active galaxy with lobes $38''$ to the south and $45''$ to the north. See the contour plot of the entire source in Fig. 8. This source has a classic FRII morphology.
229. The radio source is lost in the glare of a bright star (SDSS).
234. The identification is uncertain.
236. The bright object to the north-east is a star (SDSS).
239. The fainter object to the south-west is a star (SDSS).
244. The brighter radio source is identified with a 20-mag, slightly red stellar object (SDSS). The weaker component $3''$ to the south-west is unidentified. Perhaps it is a background galaxy which is obscured.
254. Unidentified. With source 255 it could be a pair of radio lobes associated with the galaxy located between them.
255. See note for source 254.
257. Extended radio emission has a similar orientation to the optical galaxy. This source is $10''$ west of 263.
263. The orientation of the radio emission is similar to the optical light of the galaxy, and points to a fainter binary component. This source is $10''$ east of 257, and is assumed to be an independent source.
264. Most of the radio emission is offset from the nucleus of the galaxy, but coincident with a faint optical feature. It is classified as a binary.
266. There is extended radio emission along the minor axis of the galaxy. It could be an extended AGN.
267. The identification is uncertain.

268. The main radio component (268A) is near the galaxy center. Two fainter arms of radio emission are also present.
275. The identification is uncertain.
280. The major component is offset $2''$ south-west of a galaxy. A brighter galaxy with faint emission lies about $7''$ to the north.
294. The relationship of the radio emission and the faint galaxies within $2''$ is unclear.
295. The small-diameter radio source is significantly displaced from the center of an elliptical galaxy. There is a star (SDSS) located $8''$ to the north-east.
299. The optical object is a red stellar object (SDSS).
304. An extended active galaxy with an intermediate FRI-II morphology. See contour plot in Fig. 8.
314. Most of the extended radio emission is located in the center of a bright galaxy; however there is extended radio emission toward a faint companion to the west.
315. A group of galaxies contains radio emission associated with two of the galaxies. There is additional extended radio emission.
319. The radio emission is displaced south-west of the core of the galaxy. The relationship to the bright galaxy $8''$ to the north-east is unclear.
330. A complicated group of galaxies. Two galaxies have significant radio emission (330A, 330B). The source 335 is south-east of this region.
335. A line of three galaxies, with the southern two having radio emission. The radio sources are $15''$ south-east of the complex of sources 330.
340. The radio source is in the glare of the 10-mag star.
346. The radio emission contains two components, each probably identified with a faint galaxy. It is classified as a binary, but could be considered as two independent identifications.
350. The radio source is close to the 10-mag star.
353. The radio emission is relatively weak and extended. It is cataloged as one source with two components, the southern one identified with a galaxy and the more extended northern component leading toward a fainter galaxy to the north-east. However, the source is weak and this association is uncertain.
359. The radio source is identified with a faint galaxy. There is an elliptical galaxy $2''$ to the west, and it is unknown if there is a physical connection between these two optical objects.
360. The radio source is too close to a 10-mag star to be identified.
385. The two radio components are identified with two galaxies in a crowded group of galaxies. The bright object to the south-east is stellar.
386. The radio source is unidentified. Source 391, which is $6''$ north-west is also unidentified. It is possible that 386 and 391 are radio lobes of the galaxy lying roughly between them, but there is no detection of a radio core.
390. The object north of the radio identification is stellar (SDSS).
391. The radio source is unidentified. Source 386, which is $6''$ south-east, is also unidentified. It is possible that 386 and 391 are radio lobes associated with the galaxy between them.
400. The redshift is 0.322 (Fomalont et al. 2002).
403. The optical object is blue stellar object (SDSS). It is a quasar with a redshift of 2.561 (Fomalont et al. 2002).
407. The radio source is associated with a faint, diffuse object that is $2''$ east of a brighter galaxy. The two galaxies may be part of a binary.
409. The peak emission of the radio source lies $1.5''$ south-west of the center of the galaxy, and may be associated with an optical spur to the south-west.
412. The optical object is a red stellar object (SDSS).
413. The radio emission is associated with a galaxy. The bright object is stellar (SDSS). The low surface brightness of the extended optical emission is puzzling.
416. The optical object is a blue stellar object (SDSS). It is probably a quasar.
418. The extended radio source is identified with a faint object at the edge of the image of a bright star (SDSS).
419. The optical object is a blue stellar object (SDSS). It is probably a quasar.
431. The nature of this radio source is puzzling. One radio component (B) is associated with faint emission south-east of the nucleus of the brighter object. The brighter radio source is north-west of the bright galaxy, although it could be associated with a faint spur (or an unrelated faint background object) to the north-west. These components could also be the radio lobes associated with the bright galaxy with no detectable core emission from the nucleus. However, the near coincidence of this possible radio lobe to the south-east with optical emission argues somewhat against a twin-lobed radio source. The 8-GHz radio image (source 29=J131219+423608 in the 8-GHz catalog) with lower resolution blends these two radio components with no indication of emission from the galaxy nucleus (Fomalont et al. 2002).
434. The identification is uncertain.
435. A complex region of radio and optical emission. The peak of the radio emission is near a faint spur from the most southern galaxy.
438. The redshift is 0.302 (Fomalont et al. 2002).
442. The redshift is 0.180 (Fomalont et al. 2002).
443. The bright radio component lies near the center of the galaxy. There is also a faint radio component (443B) $4''$ to the east. It is unknown if this is related to the galaxy or associated with a faint background object.
446. The peak of the radio emission is coincident with a circular galaxy. Radio jets emanate north and south of the core for $5''$, and the source has been classified as an FRI galaxy. See contour plot in Fig. 8.
449. The optical object north-east of the radio source is stellar (SDSS). The identification is uncertain.
450. The radio source is centered on a blue stellar object (SDSS), a quasar with redshift 2.561 (Fomalont et al. 2002).
453. The object north-east of the radio source is a red stellar object (SDSS). Hence, it is unlikely to be part of a binary system.
457. The redshifts of both galaxies are 0.401 (Fomalont et al. 2002).

461. Some of the radio emission extends from the center of the fainter galaxy toward the brighter galaxy.
462. The radio emission is extended and may be associated with three closely-grouped galaxies.
466. The fainter extended source of a close, weak pair. Source 471 about $3''$ to the north-east is more compact. Both sources are unidentified and not in the complete catalog.
469. The brighter radio source lies near the center of a galaxy. The fainter radio source (469B) is associated with another galaxy to the east. These two objects have been cataloged as one source because the galaxies appear to be interacting.
471. The brighter compact source of a close, weak pair. Source 466 about $3''$ to the south-west is more extended. Both sources are unidentified and not in the complete catalog.
477. There is faint extended radio emission from the optical identification toward another galaxy $8''$ to the north.
483. The radio source is identified with an elliptical galaxy that is near a bright red stellar object (SDSS).
490. The radio source is coincident with a galaxy that is about $2''$ south of a stellar object (SDSS).
503. An extended active galaxy with a morphology closer to FRI than to FRII. See contour plot in Fig. 8.
504. The radio source is coincident with a galaxy that lies near two bright stars (SDSS).
507. This radio source is north of the northern lobe of the extended active galaxy 503 (Fig. 8). It is identified with a faint galaxy and probably not part of source 503.
515. The main radio source is located $1''$ east of a bright red stellar object (SDSS). This identification is classified as stellar, but may be a compact red galaxy. There may be an extended, faint radio emission along the galaxy north-south line.
535. The radio emission lies on a galaxy to the north of a bright star (SDSS).
549. The strong radio core and the emission to the west and east are associated with an extended active galaxy. It could be an FRII source, but the lobes are too weak to be certain. See Fig. 8.
563. The radio source is coincident with a faint optical object that is $5''$ east of a bright circular galaxy. We have classified this as a binary system.
566. The compact radio emission is located $3''$ west of a bright galaxy, perhaps identified with a faint optical object. A faint radio extension toward the bright galaxy suggests that the compact radio emission is associated with the bright galaxy.
567. The two radio components have been classified as a binary; however, they may be independent sources.
569. The nucleus of this bright galaxy has a slightly extended radio source. Source 578 is located $10''$ to the north-west.
575. The slightly extended radio source is identified with a faint galaxy. The bright object to the west is stellar (SDSS).
582. The radio source is associated with a faint binary visible above the glare of the nearby bright star.
589. The identification is uncertain.
594. Most of the radio emission comes from an optical spur to the north-east of the galaxy nucleus. Some extended emission covers the other spur and the galactic nucleus.
601. The radio emission is located at the western edge of a 25-mag galaxy which is probably in a binary pair.
611. The radio source is centered on a faint object between two brighter objects.
621. The extended radio emission is an asymmetric FRI source. See Fig. 8.
626. The radio source is clearly displaced from the galaxy. The probability that this is a random association is about 10%.
634. The radio emission is coincident with a galaxy that is located in the glare of the bright star.
654. This region, near the plate edge, has poor optical sensitivity. The western component might be identified with a faint galaxy, the eastern is not. Classified as unidentified.
660. The radio emission lies on an optical bridge between two galaxies.
668. A large diffuse radio source with two extended components is associated with a group of galaxies.
676. The radio component is clearly displaced from a galaxy core and not associated with an optical feature. It is unlikely to be associated with another, invisible background galaxy. The probability that this source is unrelated to the bright galaxy is $< 10\%$. The source to the east is 680.
680. The radio source is coincident with a compact galaxy which is $7''$ east of a brighter galaxy. Source 676 lies to the west.
685. The radio source is associated with a faint galaxy near the edge of the image of a bright star (SDSS). The identification is uncertain.
711. The two galaxies in this binary each have radio emission which is oriented along each galaxy's major axis. They could be considered as two independent sources, although the optical objects appear interacting.
715. The identification is uncertain.
721. The identification with a very faint optical object has only a 50% probability. Faint extended radio emission to the east may be associated with another galaxy $3''$ to the east.
738. The radio emission is extended and covers several galaxies.
740. The unresolved radio emission peak is located between two 23-mag galaxies. It is considered as unidentified, although it may be associated to one or both of the nearby galaxies. Source 741 can be seen in the upper left and is assumed to be unrelated to 740.
748. A bright source at the edge of the z-band image with reduced optical sensitivity and some distortion. The identification is uncertain.
753. The radio emission is extended and may be associated with several galaxies in this group.
754. The radio source is close to a 26-mag object that is $1''$ north of a brighter galaxy. This identification is uncertain.
771. The radio source is extended, and located between the galaxy nucleus and an optically brightened region about $1''$

to the east.

779. The probability of identification of this radio source with the faint object that is $2''$ north of a binary system is 80%. It is unknown if the faint optical emission is associated with the brighter binary.

790. The radio source lies $1''$ north of a 24-mag galaxy. It could be associated with this galaxy, but may also be identified with a faint optical object. It is tentatively considered as unidentified.

792. The extended radio source is coincident with a faint galaxy that is $8''$ south-west of a much brighter galaxy. We assume that the faint galaxy is a background object.

800. The radio source is associated with faint diffuse emission that is $3''$ north of a brighter galaxy. There is also faint radio emission near the bright galaxy.

806. The extended radio source is centered on a faint object that lies between two binary systems. The radio emission extends to the northern galaxy of a binary system to the north-west.

5. Optical Properties of Radio Sources

5.1. Identification Rate

The identification rate for the sources in the complete sample, as indicated in Table 2, is close to 90%. Of the 551 sources for which there is z-band and/or r-band Subaru coverage (nine sources have only SDSS coverage), 499 (90.6%) are optically identified with a $3\text{-}\sigma$ detection level of $r=26.1$ mag or $z=24.9$ mag. In determining an identification of a radio source, the high optical and radio resolution and the $0.2''$ -rms astrometric alignment of the images allowed us to use optical and radio structure properties, as well as just the radio and optical centroid offset. Ignoring this additional information and using straight-forward identification algorithms to calculate likelihood percentages of identifications (Sutherland & Saunders 1992) that are based solely on the radio-optical offset and the radio and optical densities gives a somewhat lower rate of identifications.

For a more conservative determination of the identification rate, we have excluded faint identifications (Table 2, ROM=F?) where there is some doubt ($< 75\%$ chance) about the identification, and excluded all identifications with a significant optical radio offset (Table 2, ROM=Gd) although there may be morphological and statistical evidence for an association. The number of identifications then drops from 499 to 483 for the more conservative identification rate of 87.7%. This rate is similar to the i-band (7700\AA) identification rate of 85% for the HDF above a limited magnitude of

25-mag (Richards et al. 1998; Muxlow et al. 2005) and the 82% k-band detection rate of the deepest Phoenix Deep Field (PDF) (Sullivan et al. 2004). For the brighter galaxies alone, the identification rate from the entire PDF is 73% down to $r=24.0$ mag (Afonso et al. 2000), whereas the identification rate from the SSA13 field to the same magnitude limit is 55% (269 ID's out of 489). Hence, the identification rate is about 65% for a limit of $r=24$. We conclude that the identification rate of microJansky radio sources in the SSA13 field is at least $88\% \pm 2\%$ with r-band and z-band magnitude limits of 26.1 and 24.9, respectively.

5.2. Magnitude Distributions

The distribution of magnitudes for the complete sample of sources are shown in Fig. 7a for z-band and Fig. 7b for r-band. The number distribution for the z-band galaxy magnitudes is relatively flat between 20-mag and 23-mag (per magnitude interval), and then drops off significantly for fainter galaxies. Only 9% of the radio sources are unidentified. The distribution of the r-band magnitudes, on the other hand, continues to rise with a peak at about $r=24.0$ mag and a drop-off at fainter magnitudes. Since only 11% of the radio sources are not identified in this band, the drop-off must be real. The drop-off in the number distribution of identifications at $r=23$ mag in the PDF survey (Afonso et al. 2000) (in their Fig. 1) is consistent with their optical detection level limit of $r=24$ mag, and their lower radio resolution that makes their identifications with faint objects more ambiguous.

The color distribution (r-z magnitude) for the SSA13 complete sample with detections at both bands (440 sources) is shown in Fig. 7c. The average r-band (6300Å) minus z-band (9200Å) magnitude difference is 1.3 mag, and about 25% of the galaxies have a reddening (r-z) greater than 1.8 mag. This amount of r-z reddening corresponds to the $r - k$ band reddening demarcation of about 5.0 mag which defines an extremely red object (ERO). Hence, the percentage of microJansky sources in the SSA13 which are ERO's is consistent with that found using the wider-separated wave bands (Moriondo, Cimatti & Daddi 2000).

The histogram also shows that the fainter galaxies near $r=24$ mag are significantly redder than galaxies with $r=22$ mag. This is consistent with the correlation of redshift and identification

magnitude found in the PDF (Afonso et al. 2000): the fainter optical sources are more redshifted so that restframe emission is at shorter wavelengths where the reddening is more apparent.

6. The Radio/Optical Morphologies (ROM)

Two major goals of this paper are the presentation of the catalog of microJansky radio sources in the SSA13 field, and the comparison of the radio and optical morphologies of these sources. In order to facilitate the concise description of the radio and optical properties of a source, we use a radio/optical morphological (ROM) classification system used in Column 10 of Table 2 and described in the table headings. The number of sources in each of the classifications is given in Table 3, both for all 810 sources and for those in the complete sample of 560 sources. The classification of single and binary systems, and the reliability of the faint identifications, are discussed below.

6.1. Radio Sources Associated with Isolated Galaxies: ROM=G

Of the 560 source in the complete sample, only 390 had identifications which are sufficiently bright so that an assessment of the optical complexity could be determined. About 60% of these sources have an optical identifications ($z < 24.0$) to allow us to classify them as associated with a relatively isolated galaxy. We use the average density of galaxies from SDSS in the SSA13 field and the HDF down to 25 mag, to determine the average separation of galaxies brighter than $r=25m, 24m, 23m, 22m, 21m$ and $20m$, which is $7'', 11'', 17'', 25'', 37'',$ and $55''$, respectively. If two galaxies are closer than about one-third the expected mean separation (corresponding to 10% or less chance of random associated), they are probably a physical pair. However, other considerations related to the morphology and shape of the neighboring galaxies and radio sources are also used to distinguish isolated galaxies from binary or more complex systems.

The radio emission from about 40% of the isolated galaxies is resolved, with an angular size that is typically $< 1.2''$. The orientation of the radio emission is often related to the orientation of the galaxy, as shown in the following sources: 72, 90, 135, 180, 190, 194, 196, 198, 277, 289, 307,

308, 320, 403, 430, 447, 459, 514, 543, 590, 628, 670 and 758. In most cases the radio orientation is aligned along the galaxy major axis, but some sources have a clear radio extension along the minor axis.

About 8% (30 out of 390) of the single galaxy identifications have radio components clearly displaced by several arcsec from the galaxy nucleus (ROM=Gd), although some radio emission may also be associated with the galaxy nucleus. In many cases there is optical enhancement or asymmetry outside of the central region that appears associated with the radio emission; hence, they may be in binaries in the latter stages of merging. Some of these sources are: 15, 38, 186, 271, 345, 497, 515, 519, 532, 594, 679 and 690. Two sources, 91 and 676, are significantly displaced from the galaxy center (still only $3''$), but the identifications are likely, based on the probability of $< 10\%$ that these are a chance occurrence.

6.2. Binary and Complex Systems: ROM = Bc, Be, B2, C

About 40% of the radio sources with sufficiently bright optical counterparts are associated with binary or more complicated optical systems (ROM=B or C). Since most of the radio emission is usually confined to only one galaxy, this classification is determined by the proximity of other galaxies, and the morphology and shape of the optical and radio emission that suggest these are interacting systems.

Binary systems which contain a majority of the radio emission in an unresolved radio source in the center of one of the galaxies are common. Some examples are: 9, 23, 84, 109, 127, 128, 134, 140, 183, 231, 298, 341, 377, 390, 420, 508, 545, 551, 552, 643, 666, 723 and 741. In some of these cases, there is a hint of radio emission toward or associated with the other galaxy, but the emission is too faint to be cataloged. Binary systems with extended radio emission (ROM=Be) often show a correlation between the orientation of the radio emission and the binary position angle, and examples are: 16, 28, 49, 99, 119, 131, 199, 209, 237, 239, 279, 322, 338, 372, 392, 393, 414, 425, 453, 457, 461, 473, 502, 510, 541, 574, 579, 587, 595, 610, 639, 672, 683, 688, 707, 737, 743 and 750. Because of the difficulty in deriving angular sizes for the weaker sources, the physical differ-

ence between the ROM=Bc and Be sources may be somewhat artificial.

About 10% of the binaries have significant radio emission associated with both galaxies (ROM=B2) where both radio components are strong enough to be individually cataloged. Examples are: 35, 166, 286, 310, 361, 629, 694 and 711. Some of the ROM=Be sources are probably similar, but with the emission from the fainter galaxy somewhat below our detection limit.

Those few radio/optical sources which are labeled as complex generally contain more than two galaxies, and/or two radio components which are not simply related to the optical emission. The radio properties are often similar to those of binary systems, but with additional complexity. These sources are more fully discussed in the notes to Table 2 and include numbers 185, 188, 353, 385, 431 (might be an AGN), 435, 668, 738, 753 and 806.

6.3. Radio Sources Associated with a Stellar Object: ROM=S

Eight sources are associated with stellar objects: 169, 299, 403, 412, 416, 419, 450 and 515. Five of them—169, 403 (confirmed redshift of 2.561), 416, 419, and 450 (confirmed redshift also of 2.561)—are blue and probably all are quasars. Sources 299, 412 and 515 are red and probably are stars. The radio emission of source 515 is displaced about 1" east of the center of the red stellar object and there may be extended emission. Two sources cataloged as complex have part of their radio emission apparently associated with a stellar object, 185 and 244. See the notes to these sources. Hence, up to 1% of the microJansky sources are galactic stars, comparable to detection rates found in other deep radio surveys.

6.4. Extended AGNs: ROM=EA

AGNs are defined by a radio component that is co-located with the active nucleus of a galaxy. However, some active galaxies also have extended radio emission that is often bi-polar and contains narrow jets and relatively compact radio components in the jets or in the lobes. These sources are called ‘classical doubles’. If the jets are dominant and the hot spots are located near the beginning of the jets, they are called FRI. If the

bright hot spots are dominant and at the edge of the lobes, they are called FR II (Fanaroff & Riley 1974). We were able to detect these large sources because the component sizes are generally smaller than 8", the angular size where our radio observations become insensitive. Extended AGNs with compact lobes that extend more than about 20" can be difficult to identify because the lobe may overlap with other faint radio sources. For example, source 212 contains a radio core that is identified with a faint galaxy. Two asymmetric radio sources, about 40" away, have no co-located optical counterpart, have a structure that is suggestive of an FR II double source and are symmetrically disposed with respect to the suggested core component.

Seven apparently extended ‘classical’ extended radio galaxies were found in the SSA13 field, and the corresponding radio/optical fields are shown in Fig. 8. Five are in the complete sample, and two are located outside of the 15' region defined for the completeness limit. All seven active galaxies are relatively strong radio sources, with the weakest having a total flux density of 149 μ Jy while three are well above 1 mJy.

Even with this small sample, we find examples of the different types of classical extended radio galaxies, seen at milliJansky and Jansky levels. Only one extended AGN has a classic FR II structure, source 212. Source 503 is closer to an FRI than an FR II (the small component the north is source 507), and Source 304 is intermediate type with well-resolve hot spots. Source 549 is too weak to determine if it is FRI or FR II. The other three sources are FRI, including Source 69 that does not have hot spots but a strong symmetric jet.

A potential extended AGN could be comprised of sources 254 and 255. They are separated by 7", with a bright galaxy between them. We classified them as independent radio sources because one of them is identified with a faint optical counterpart. Source 266 has a strong core with a possible weak jet emanating to the east. Sources 386 and 391 could possibly be associated with a galaxy between them. Another uncertainty concerns the compact source 507 near the northern tip of the extended AGN, source 503. Because source 507 is clearly coincident with a galaxy, it has been cataloged as an independent object.

The relative numbers of extended AGN found

in the SSA13 field are somewhat sparse as expected from other surveys at somewhat higher flux densities (Jackson 2004). At about 1 mJy, the density of FRI sources is about four times that of FR II sources. This ratio is difficult to determine from our sample, but is consistent with 25% of them as FRI or primarily FR II. While the extended radio galaxies comprise about 30% of the sources at about 1 mJy, only about 10% of the extended sources are larger than about $8''$, according to the SIRTf FLS VLA survey⁴. If this ratio holds for the microJansky population, we would expect that out of a sample of 510 sources that approximately 15 should be extended radio galaxies. This is considerably larger than the five extended AGN that we detected in the complete sample.

6.5. Faint Identifications: ROM=F and Unidentified Sources: ROM=U

Most of the faint identifications are secure with better than 90% confidence. This is because the registration accuracy of the radio/optical images is accurate to $0.2''$, so that proximity of the radio source to even a 25.5-mag galaxy (where the mean separation of objects is $5''$) is sufficient for a confident identification. Identifications that are less secure than 90% are: 141, 159, 171, 177, 234, 267, 275, 434, 449, 589, 685, 715, 721, 748 and 754. Thus, considering all these less secure identifications as unidentified would only increase the number to 55 sources or 11% of the sample.

6.6. Comparison with the Hubble Deep Field North

The only other sensitive observations currently available with sufficient resolution to compare detailed radio and optical morphologies are the combined MERLIN/VLA observations of the Hubble Deep Field North (Muxlow et al. 2005) with $0.2''$ resolution and 92 sources in the complete sample (see §7.1). The variety and relative numbers of the different radio/optical morphologies are similar in both fields, with most HDF identifications associated with relatively isolated galaxies. Although many sources in the HDF sample have radio emission coincident with the galactic nucleus, there is often additional radio emission with an angular

⁴http://www.cv.nrao.edu/sirtf_fls

extension that is correlated with the galaxy orientation. Slight displacements of the radio centroid from the nucleus are clearly observed in both the HDF and SSA13 fields, and in both surveys, approximately 10% of the sources have radio emission which is well-displaced from the galaxy nucleus.

These surveys show that with arcsecond or sub-arcsecond resolution both the optical and radio emission brightness distributions are complex in a significant part of the microJansky source population. Not only can solid identifications be made, but a detailed comparison and modeling of the radio and optical brightness distributions can lead to a deeper understanding of the role of both AGN and starburst activity in the evolution of galaxies.

7. Radio Properties

7.1. Angular Size Distribution

The size of each radio source is given in columns 7, 8 and 9 of Table 2. An unbiased distribution of the true angular size is difficult to determine for at least two reasons: the inability to measure the angular size is a strong function of SNR, and the definition of what constitutes a single radio source is ambiguous. With these caveats, Fig. 9a shows the number distribution of the largest angular size (LAS: the major axis size or separation in the cases of multi-component sources) of the 289 sources in the complete sample which have $\text{SNR} > 8$, equivalent to sources with $S_{1.4} > 40 \mu\text{Jy}/\text{beam}$ at the field center. With this high SNR, source diameters larger than $1.2''$ can be reliably determined, and we find that about 64% (186 of 289) of the sources are smaller than this angular size.

Five of the 13 sources larger than $4''$ in the SSA13 field are extended active galaxies (212, 304, 446, 503 and 621). Two sources (72 and 758) are associated with a bright flattened galaxy with a large radio disk component; three sources (330, 385 and 629) are associated with several galaxies in a tight group of galaxies; two sources (188 and 517) have diffuse radio emission associated with one galaxy. Source 711 is associated with a binary galaxy and it could be interpreted as two independent sources. About 20 other radio sources have hints of extended structure larger than $4''$, but are too faint to be reliably measured.

Fig. 9b shows the angular size distribution ob-

tained by the combined MERLIN/VLA observations of the Hubble field with a resolution of $0.2''$ (Muxlow et al. 2005). Although there are only 92 sources in this sample, virtually all of them are resolved and have a measured largest angular size. The proportion of sources with LAS small than $1.2''$ is similar for the SSA13 and HDF fields, and most of the remaining sources are smaller than $4''$. The median angular size is about $1.2''$, but there are two parts to the angular distribution: a Gaussian shaped distribution centered near $0.7''$ (resolved only by the MERLIN observations), and a tail which decreases roughly as the inverse angular size.

There have been several investigations on the number of ‘missing’ large-diameter, microJansky sources in VLA catalogs (Garrett et al. 2000; Muxlow et al. 2005). The Westerbork surveys and the SIRTF FLS surveys with $\approx 10''$ resolution find that about 15% to 20% of the sources at the $300 \mu\text{Jy}$ level are larger than about $4''$, whereas only 4% of the sources from our SSA13 catalog are at least this large. But, when observations with higher angular resolution are available, a significant fraction of this excess of apparently large sources found in low resolution observations is explained by the blending of weak, close sources which thus appear as a single resolved source. This type of ambiguity is also seen for a few of the cataloged sources in the SSA13 field. Nevertheless, it is possible that some relatively large and diffuse sources are missing (resolved out) in our higher resolution radio images. We thus conclude that about $8 \pm 4\%$ of the microJansky radio sources are larger than $4''$ in angular size. The upper limit nearly reaches the proportions seen in lower-resolution surveys, and the lower limit is about that observed in the SSA13 field.

7.2. Spectral Index

Observation of a small solid angle near the central part of the SSA13 field have been made at 8.4 GHz (Fomalont et al. 2002). Within a radius of $273''$, 34 sources were detected above an image level of $7.5 \mu\text{Jy}/\text{beam}$ ($5\text{-}\sigma$). In order to determine the spectral index of a complete sample defined at 1.4 GHz, we have examined the field within $180''$ from the field center where the rms sky noise at 8.4 GHz is $< 4.3 \mu\text{Jy}/\text{beam}$ and at 1.4 GHz is $< 5.5 \mu\text{Jy}/\text{beam}$. In this region, 47 sources are

detected at 1.4 GHz in the complete sample, all of which are seen on the 8.4 GHz image, above the $2.5\text{-}\sigma$ level. Although the number of measured spectral indices is small, the detection levels at 1.4 GHz and 8.4 GHz were well-matched so that the strong bias in the derived spectral index distribution that can occur because of a non-detection at one of the frequencies is not present in this sample.

The spectral index histogram ($S \propto \nu^\alpha$) for the complete sample of 47 sources at 1.4 GHz is shown in Fig. 10a. The mean spectral index is -0.84 ± 0.08 . For comparison, the spectral index distribution based on the complete sample of 34 sources at 8 GHz (Fomalont et al. 2002) is shown in Fig. 10b. The average spectral index is -0.68 with a standard deviation of the mean of 0.08.

Fig. 11 shows the radio contour/optical images of the six sources with the flattest ($\alpha > -0.5$) and the steepest ($\alpha < -1.1$) spectral indices. Some possible differences are: 1) The flat-spectrum sources are identified with relatively isolated galaxies (434 is probably unidentified) that are relatively undistorted; whereas the steep-spectrum sources tend to have more complex optical emission. 2) The flatter-spectrum sources contain a dominant component with an angular size less than $0.9''$, whereas the steep sources are both large and small. 3) The average (r-z) magnitude color difference for the flat-spectrum sources is 1.8, compared with 0.7 for the steep sources. With such a small sample, this difference is not significant.

We have divided the 1.4 GHz sample, based on total flux density at 1.4 GHz, into those stronger than $75 \mu\text{Jy}$ (19 sources) and those weaker than $75 \mu\text{Jy}$ (28 sources), and these distributions are shown in Fig. 12a and b. The mean spectral index for the stronger sources is $\alpha = -0.78 \pm 0.04$ and for the weaker sources is $\alpha = -0.87 \pm 0.05$. Although both distributions contain several steep and flat spectrum objects, the peak of the spectral indices is slightly flatter for the stronger sources. The probability that these two distributions come from the same population is 20%.

7.3. The Counts of Radio Sources

With this survey we are able to determine the density of radio sources in the sky from $26 \mu\text{Jy}$ to about $2000 \mu\text{Jy}$. Table 4 shows the observed

source counts as a function of sky flux density for the 560 sources in the complete sample. Columns 1, 2 and 3 give the source total flux density binning information, and column 4 gives the number of sources found within each bin. Column 5 gives the effective weight of the data in this bin. A weight of 15.0 for the lowest flux density bin, for example, means that on average a source within this flux density range would have a peak image flux density greater than the completeness threshold of $25.8 \mu\text{Jy}/\text{beam}$ in only $1/15.0$ of the $15'$ radius region. The determination of the weighting factor is described in the following paragraph. Columns 6 then gives the derived integral count and column 7 gives the differential count for each flux density bin. In Column 8 the differential count is normalized to a Euclidean count of $1 \times S^{-2.5} dS \text{ sr}^{-1} \text{ Jy}^{-1}$. The errors in the count are derived from the number of sources in each bin.

The weight in column 5 corrects for the smaller area in which weaker sources can be detected above the image detection (completeness) level. The weight depends strongly on the radial dependence of observational sensitivity over the field of view, shown in Fig. 2, but also takes account of the angular size distribution of the microJansky sources (see Fig. 9) and the statistical noise of the image. Simulations of a sky filled with point sources, then convolved with the above effects, were used to determine the weights as a function of flux density for each source.

The derived normalized counts for the SSA13 field, from Column 8 in Table 4, is plotted in Fig. 13. We have also included the counts from other observations of comparable sensitivity at 1.4 GHz. References to the other data are: PDFS and PDF (Hopkins et al. 1998), MC85 (Mitchell & Condon 1985), OW84 (Oort & Windhorst 1985), ELIAS (Cilegi et al. 2000) and HDF (Richards 2000)). The SSA13 field has a somewhat higher density of sources than other fields at these flux densities, particularly the HDF field which has only 60% of the source density seen in SSA13.

The field to field apparent differences in the counts at and below the one milliJansky level have been predicted (Benn & Wall 1995) and previously noted (Hopkins et al. 1998). With a typical field size of one degree, the inhomogeneity between the counts of various deep fields corresponds to a fluctuation volume scale size of order 100 Mpc^3 . Some

of the variations in the counts can be caused by various instrumental defects; however, there are a sufficient number of deep survey using the same instrument and observational set-up that show significantly different counts; such as the SSA13 and HDF fields. The observed differences in these counts in this case reflects real cosmic variance.

The best fit power-law to the SSA13 alone (neglecting the lowest flux density bin between $25.8 \mu\text{Jy}$ and $37.5 \mu\text{Jy}$ which may be incomplete), is shown by the dashed line in Fig. 13, and can be expressed in several ways. The differential count to the best fit power law is $n(S)dS = (9.2 \pm 0.8)S^{(-2.43 \pm 0.13)} \text{ sr}^{-1} \text{ Jy}^{-1}$. The integral form of this best fit is

$$N(> S) = (0.40 \pm 0.04) \left(\frac{S}{75 \mu\text{Jy}} \right)^{(-1.43 \pm 0.13)} \quad (1)$$

where N is the number of sources $(\text{arcmin})^{-2}$ with a flux density $> S(\mu\text{Jy})$. This is consistent with the Euclidean value of -1.50 .

There is some indication that the density of sources is beginning to decrease below about $48 \mu\text{Jy}$, since the count in the $37.5 \mu\text{Jy}$ to $48.0 \mu\text{Jy}$ bin is low. However, the decreased density observed near the lower flux density limit of the count can be caused by a slight error in the weight of the sources, or an underestimated rms noise near the center of the image where the blurring of faint sources and image artifacts may be occurring (a minor fall-off at low flux is also seen in the HDF counts). Extrapolation of the best fit slope of -2.43 to one microJansky gives a source density of $148 \text{ sources} (\text{arcmin})^{-2}$, which corresponds to a mean separation between sources of $5''$. However, the true separation could be as much as a factor of two larger if the count of sources does in fact decrease below about $48 \mu\text{Jy}$.

Fig. 14 shows the comparison of the source counts at 1.4 GHz and at 8.4 GHz (Fomalont et al. 2002) for the SSA13 field. The slope of the 8.4 GHz counts, $\gamma = 2.11 \pm 0.18$, is considerably different from the 1.4 GHz value, $\gamma = 2.43 \pm 0.13$, although the difference is compatible with the change of the spectral index distribution at $S_{1.4} \sim 75 \mu\text{Jy}$. To show that this change of the slope in the count is consistent with the spectral index versus flux density relationship shown in Fig. 12, we assumed the best power-law fit at 1.4 GHz (the top line in Fig. 14) and convolved it with

this spectral index distribution. The dashed line in Fig. 14 is the predicted count at 8.4 GHz, and it is in good agreement with that observed. Thus, the source count change between 1.4 GHz and 8.4 GHz supports the steepening of the spectral index at 1.4 GHz for sources fainter than about $70 \mu\text{Jy}$.

8. Summary

We present a catalog of over 800 radio sources in the SSA13 field, derived from VLA observations at 1.4 GHz. About 90% of the sources in the complete sample are identified with an optical counterpart on Subaru r-band or z-band images. Even with conservative assumptions at least 88% of the sources are reliably identified. Table 2 lists the radio and optical parameters for each source. In Fig. 6, radio contours are overlaid on optical false-color displays for all sources in order to display the morphological properties of the radio/optical emission. This catalog, especially the 560 sources in the complete sample, can be used as a basis for further studies of the nature of faint radio sources. For example, the evolution of ultra-luminous infrared galaxies has been investigated using data from this survey (Cowie et al. 2004)

With the relatively high radio and optical resolution and sensitivity of this work, the complexity of the radio/optical morphologies has become evident. We analyzed the morphological properties into a small number of classifications that depend on the radio emission size, the complexity of the optical region, and the relative location of the radio and optical emission. More than half of the radio sources are identified with isolated galaxies, and about 30% with binary or more complex optical systems. Only seven sources are identified with FRI or FRII active galaxies, and eight stellar objects (half of which are blue and are probably quasars) have been detected. The centroid of the radio emission is significantly displaced from the galaxy nucleus for about 8% of the sources. The radio orientation, when resolved, is often similar to that of the galaxy or binary system, and suggests that the radio and optical emission are associated with extended, starforming regions.

The radio spectral index between 1.4 and 8.4 GHz steepens for sources fainter than about $75 \mu\text{Jy}$, and this trend is confirmed by the different slopes found in the source counts at these two fre-

quencies. The count of microJansky radio sources at 1.4 GHz is close to the Euclidean value down to $50 \mu\text{Jy}$. Although the observed count appears to fall off below about $40 - 50 \mu\text{Jy}$, this may be the result of incompleteness at the faint end of the catalog.

The proportion of sources which are dominated by AGN or by starforming mechanisms can not be well-determined without more detailed observations of the sources at other wavebands, but both mechanisms are clearly present. Extended radio galaxies ($> 4''$), quasars and galactic stars comprise only a few percent of the sample.

The observed radio spectra reflect the decreasing numbers of AGN at flux densities below $100 \mu\text{Jy}$. Although the proportion of sources with a spectral index > -0.5 is about 10% over all flux density ranges, there is a clear increase in the number of steep-spectrum sources ($\alpha < -0.9$) at flux densities below $75 \mu\text{Jy}$. The emission from these weaker sources is more likely caused by remnant plasma from starburst and supernova phenomena, than by AGN-induced jets and lobes.

The radio/optical morphology is also a useful discriminant between emission from starbursts and/or AGN activity. From Table 3, approximately 40% of the radio sources contain radio emission that is located in the galactic nuclear region and is less than $< 1.5''$ in extent. Although these sources could be regions of dense star formation near the nuclear regions as in Arp220 (Anantharamaiah et al. 2000), these statistics at least provide an upper limit of 40% to the fraction of sources which could be AGN cores. The angular size of the radio emission is not a definite discriminator between AGN and starburst phenomena unless resolutions better than $0.05''$ can be reached. Recent VLBA+GBT observations of the Bootes field (Garrett et al. 2001; Garrett, Wrobel & Morganti 2005) show that approximately 8% of the sub-mJy sources have appreciable flux density in a components with a brightness temperature greater than 10^5 K; whereas 29% of the sources stronger than 1 mJy have such a bright, non-thermal component.

With the high sensitivities and resolutions now available from radio, optical and X-ray observations, it is already clear that most galaxies formed at early cosmological epochs show complexity in emission mechanisms and morphological struc-

ture. These are only now being probed with the most recent observations, which may lead to a deeper understanding of AGN formation and the starburst phenomenon, and the interaction between them.

9. Acknowledgments

The National Radio Astronomy Observatory is a facility of the National Science Foundation operated under cooperative agreement by Associated Universities, Inc. EAR was supported by a Hubble Fellowship and RBP was supported by the NSF grant AST-0071192 to Haverford College. We thank the referee for the careful reading and significant improvements in the text.

REFERENCES

- Afonso, J., Georgakakis, A., Almeida, C., Hopkins, A. M., Cram, L. E., Mobasher, B. & Sullivan, M. 2005, *ApJ*, 624, 135
- Anantharamaiah, K. R., Viallefond, F., Mohan, N. R., Goss, W. M. & Zhao, J. H. 2000, *ApJ* 537, 613
- Beasley, A. J., Gordon, D., Peck, A. B., Petrov, L., MacMillan, D. S., Fomalont, E. B. & Ma, C. 2002, *ApJ Suppl.*, 141, 13
- Benn, C. R. & Wall, J. V. 1995, *MNRAS*, 272, 678
- Cilegi, P., et al. 2000, *MNRAS*, 302, 22
- Cornwell, T. & Fomalont, E. B. 1989, in *Synthesis imaging in Radio Astronomy*, ed. R. Perley, F. Schwab & A. Bridle, (San Francisco: PASP) 185
- Cowie, L. L., Barger, A. J., Fomalont, E. B. & Capak, P. 2004, *ApJ*, 603, 69
- Fanaroff, B. L. & Riley, J. M. 1974, *MNRAS*, 167, 31P
- Fomalont, E. B., Kellermann, K. I., Partridge, R. B., Windhorst, R. A. & Richards, E. A. 2002, *AJ*, 123, 2402.
- Garrett, M. A., deBruyn, A. G., Giroletti, M., Baan, W. A & Schilizzi, R. T. 2000, *A&A*, 361, L41.
- Garrett, M. S., Muxlow, T. W. B., Garrington, S. T., Alex, W., Alberdi, A., van Langevelde, H. J., Venturi, T., Polatidis, A. G., Kellermann, K. I., Baan, W. A. 2001, *A&A*, 366, 5
- Garrett, M. A., Wrobel, J. M. & Morganti, R. 2005, *ApJ*, 619, 105
- Garrett, M. A. 2002, *A&A*, 384, L19
- Greisen, E. W. 1988, in *Acquisition, Processing and Archiving of Astronomical Images*, ed. G. Longo & G. Sedmak (Napoli: Osservatorio Astronomico di Capodimonte), 125
- Hopkins, A. M., Mobasher, B., Cram, L. & Rowan-Robinson, M. 1998, *MNRAS*, 296, 839
- Hopkins, A. M., Afonso, J., Cram, L & Mobasher, B. 1999, *ApJ*, 519, L59
- Jackson, C. A. 2004, *NewAR*, 48, 1187.
- Ma, C., Arias, E. F., Eubanks, T. M., Fey, A. L., Gontier, A.-M., Jacobs, C. S., Sovers, O. J., Archinal, B. A. & Charlot, P. 1998, *AJ*, 116, 516
- Mitchell, K. J. & Condon, J. J. 1985, *AJ*, 90, 1987
- Miyazaki, S., Sekiguchi, M., Imi, K., Okada, N., Nakata, F., & Komiyama, Y. 1998, *Characterization and mosaicking of CCDs and the applications to the Subaru wide-field camera (Suprime-Cam)*, in *Proc. SPIE 3355: Optical Astronomical Instrumentation*, ed. S. D'Odorico, 363
- Moriondo, G., Cimatti, A. & Daddi, E. 2000, *A&A*, 364, 26
- Muxlow, T. W. B., Richards, A. M. S., Garrington, S. T., Wilkinson, P. N., Anderson, B., Richards, E. A., Axon, D. J., Fomalont, E. B., Kellermann, K. I., Partridge, R. B. & Windhorst, R. A. 2005, *MNRAS*, 358, 1159
- Oort, J. A. & Windhorst, R. A. 1985, *A&A*, 195, 21
- Richards, E. A. 2000, *ApJ*. 533, 611
- Richards, E. A., Fomalont, E. B., Kellermann, K. I., Windhorst, R. A., Partridge, R. B., Cowie, L. L. & Barger, A. J. 1999, *ApJ*, 526, L73

- Richards, E. A., Kellermann, K. I., Fomalont, E. B., Windhorst, R. A. & Partridge, R. B. 1998, *AJ*, 116, 1039
- Sullivan, M., Hopkins, A. M., Afonso, J., Georgakakis, B., Chan, L. E., Mobasher, B. & Almeida, C. 2003, *ApJ*, 155, 1
- Sutherland, W. & Saunders, W. 1992, *MNRAS*, 259, 413
- de Vries, W. H., Morganti, R., Rottgering, H. J. A., Vermeulen, R., van Breugel, W., Rengelink, R & Jarvis, M. J. 2002, *ApJ*, 123, 1784
- Windhorst, R. A., van Heerde, G. M. & Katgert, P. 1984, *A&A Suppl.*, 58, 1
- Windhorst, R. A., Fomalont, E. B., Kellermann, K. I., Partridge, R. B., Richards, E. A., Franklin, B. E., Pascarella, S. M. & Griffiths, R. E. 1995, *Nature*, 375, 471

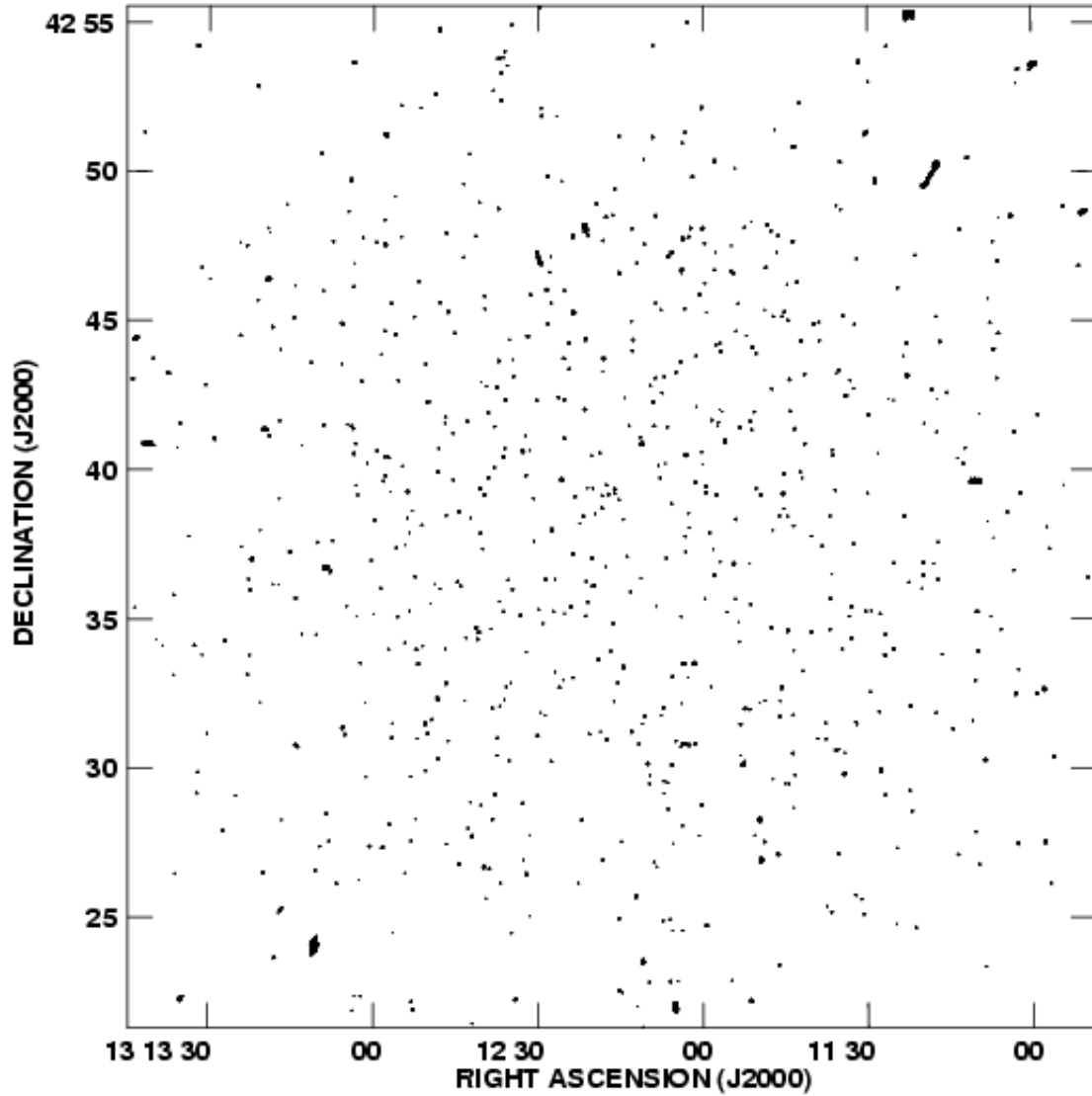


Fig. 1.— **The SSA13 1.4-GHz Radio Image.** The inner $34' \times 34'$ area of the cleaned radio image of SSA13. The image is *not* corrected for instrumental distortions and the decreased sky sensitivity as a function of distance from the field center (see Fig. 2 for the dependence of the sensitivity versus radial distance from the field center). All of the dark spots are sources above the detection level. A few extended sources are visible.

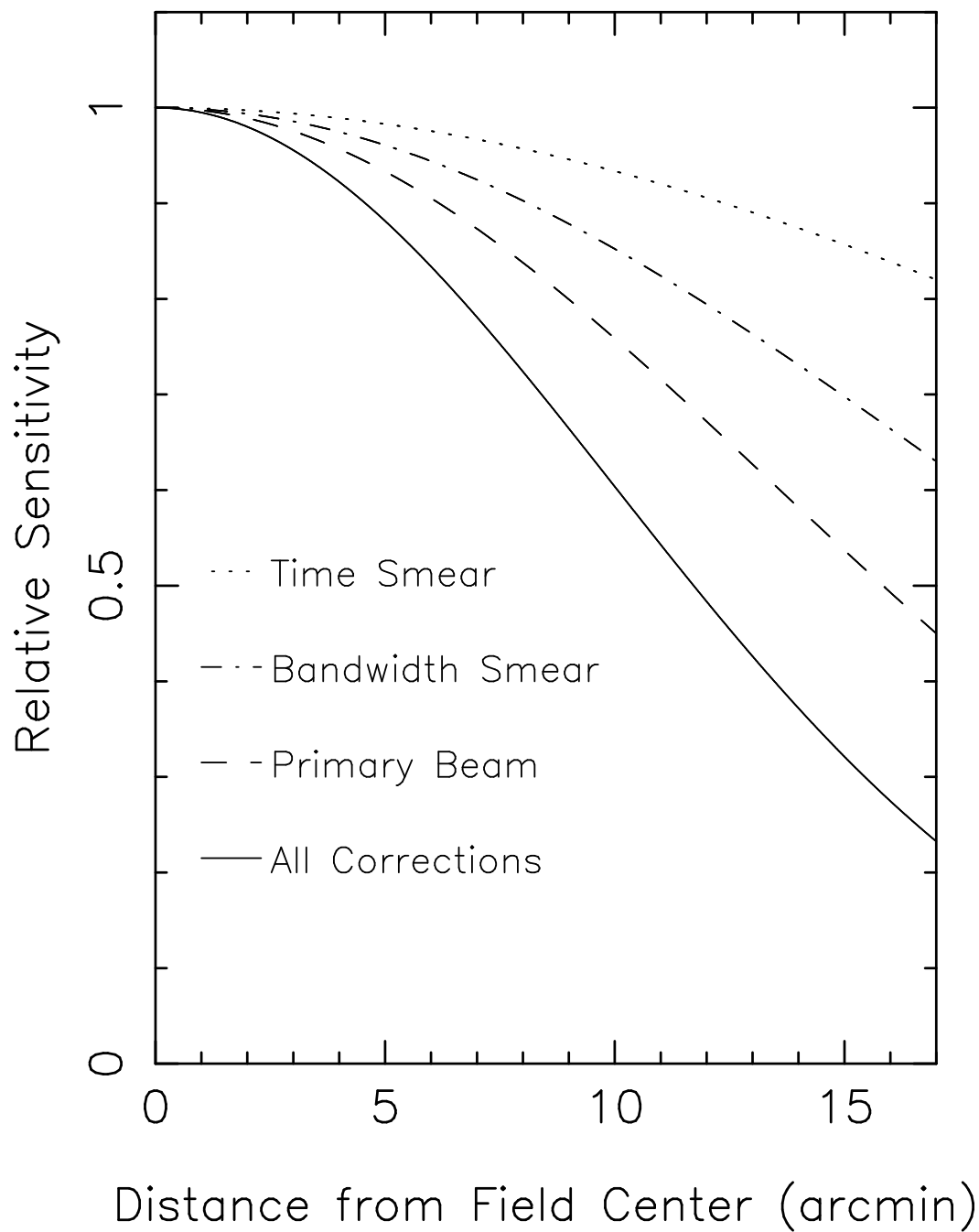


Fig. 2.— **The Relative Sensitivity Across the Radio Image.** The ordinate shows the ratio (sky sensitivity / image sensitivity) associated with the peak intensity of a radio source as a function of radial distance from the field center. The fractional sensitivity loss due to the three factors is discussed in the text, and the net sensitivity is shown by the solid line.

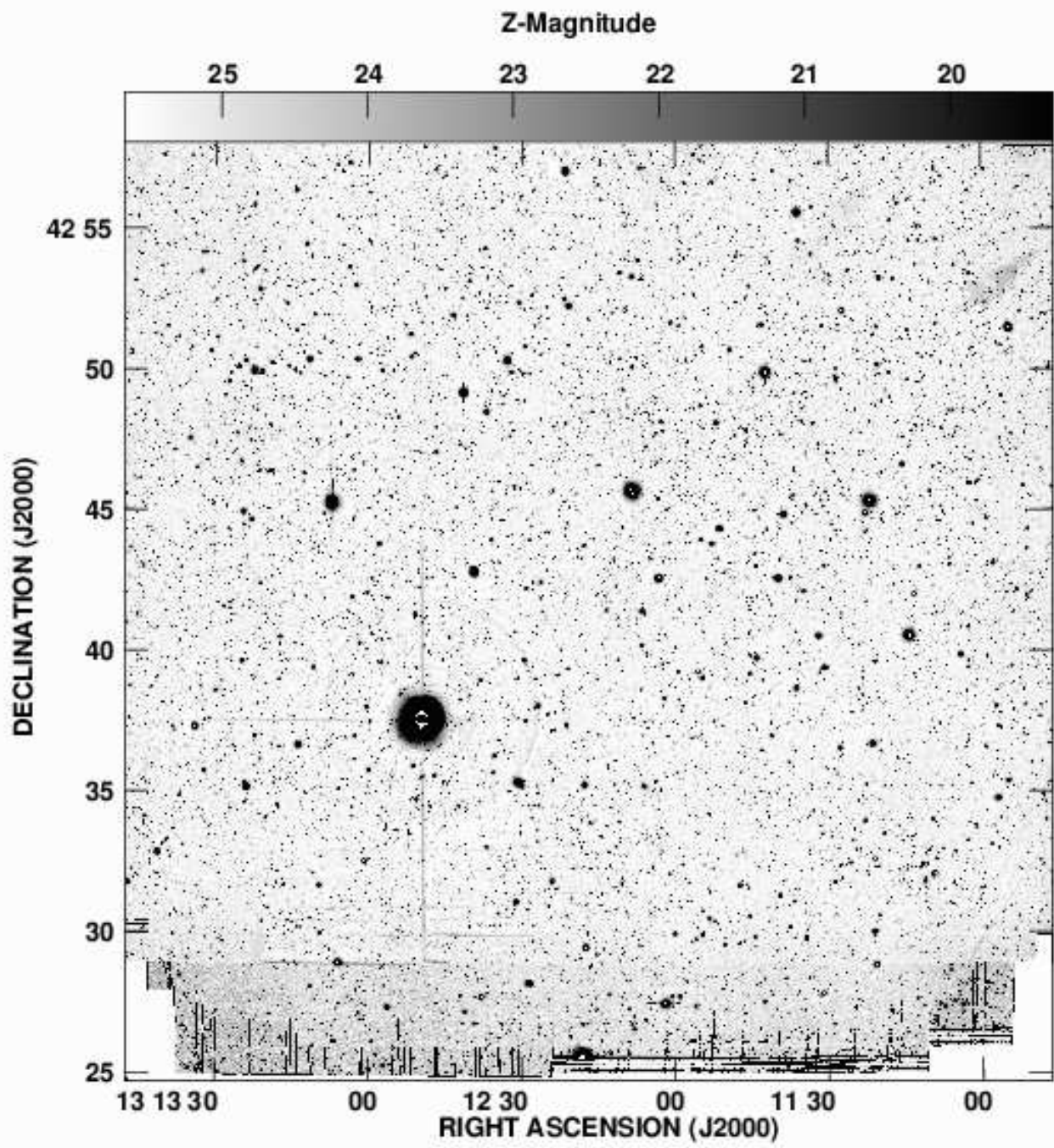


Fig. 3.— **The SSA13 z-Band Image:** A gray-scale representation of the entire z-band image. The contrast, expressed in magnitudes, is shown by the wedge above the image.

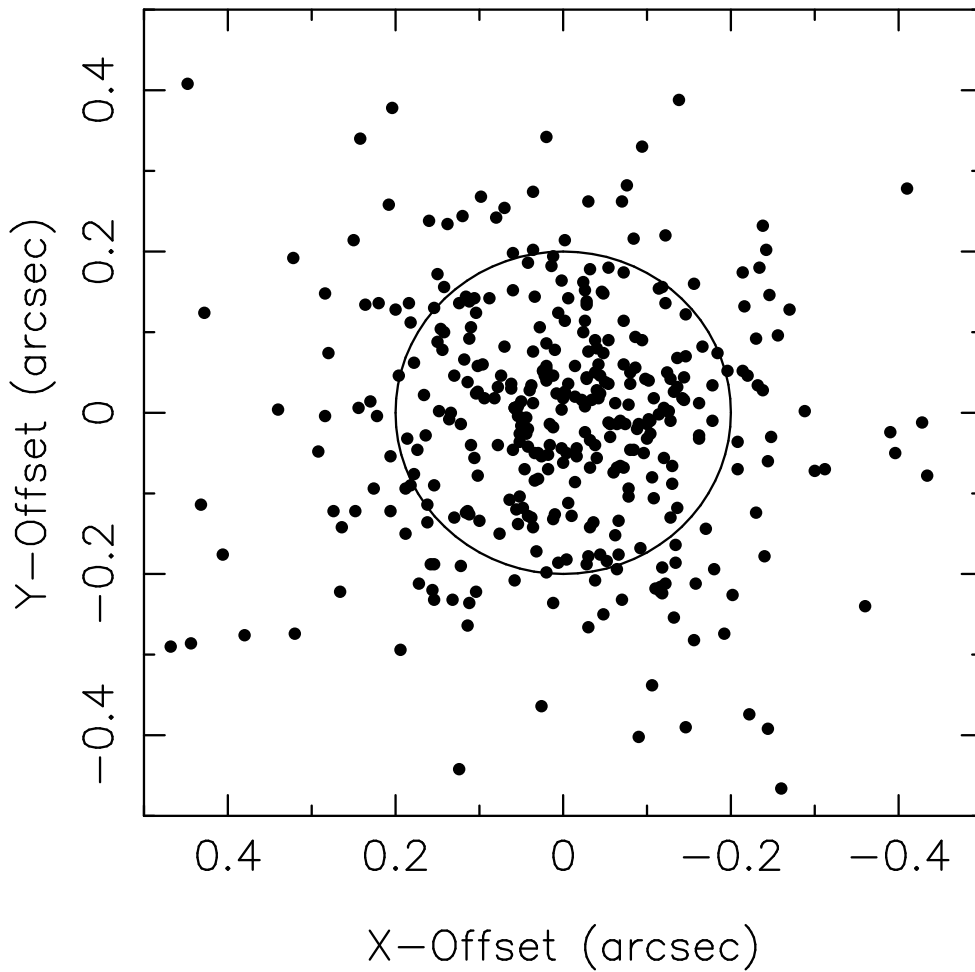


Fig. 4.— **Radio-Optical Registration:** The difference between the radio and optical positions for 95 high-quality identifications. The circle indicates the one-sigma error of $0.2''$.

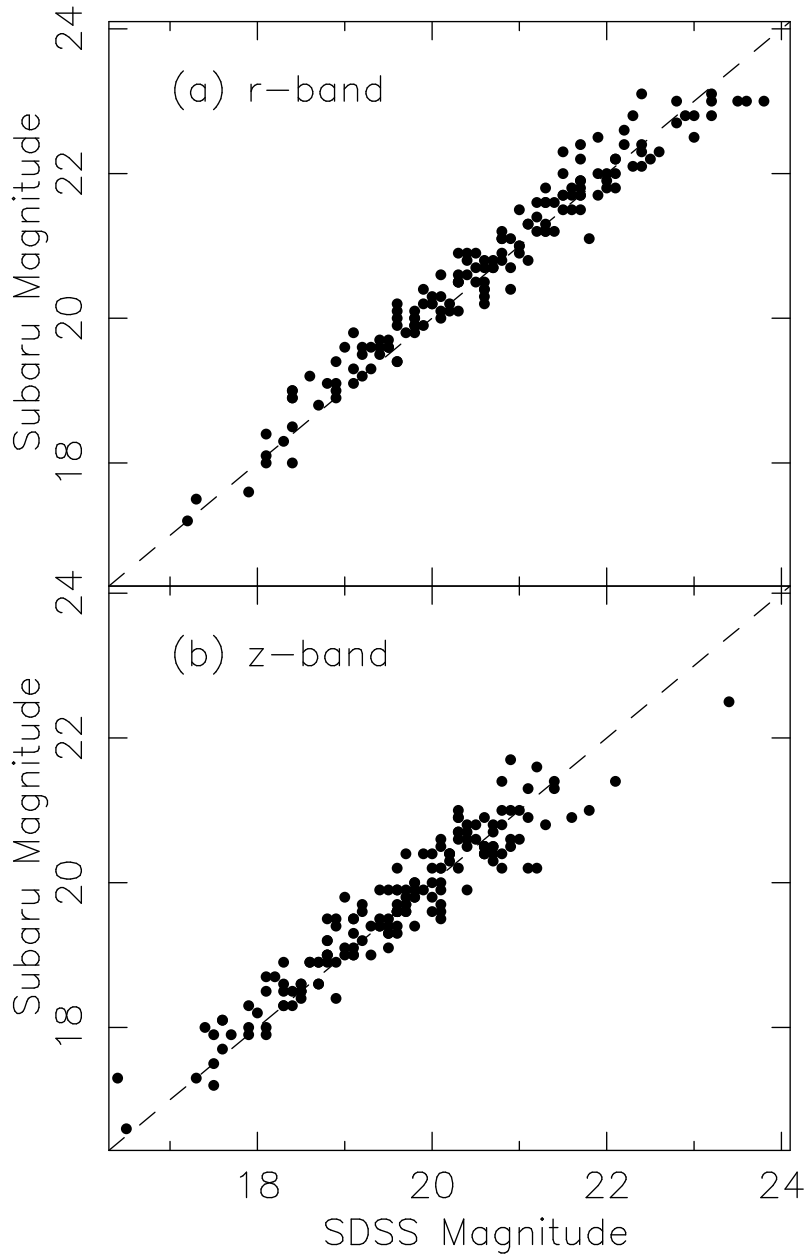


Fig. 5.— **Subaru vs SDSS Magnitude Comparisons:** (a) The comparison of Subaru and SDSS r-magnitudes for 110 galaxies. (b) The comparison of Subaru and SDSS z-magnitudes for 113 galaxies. The comparison is made after zero-point correction of the Subaru r-magnitude by 0.1 mag and z-magnitude by 0.4 mag.

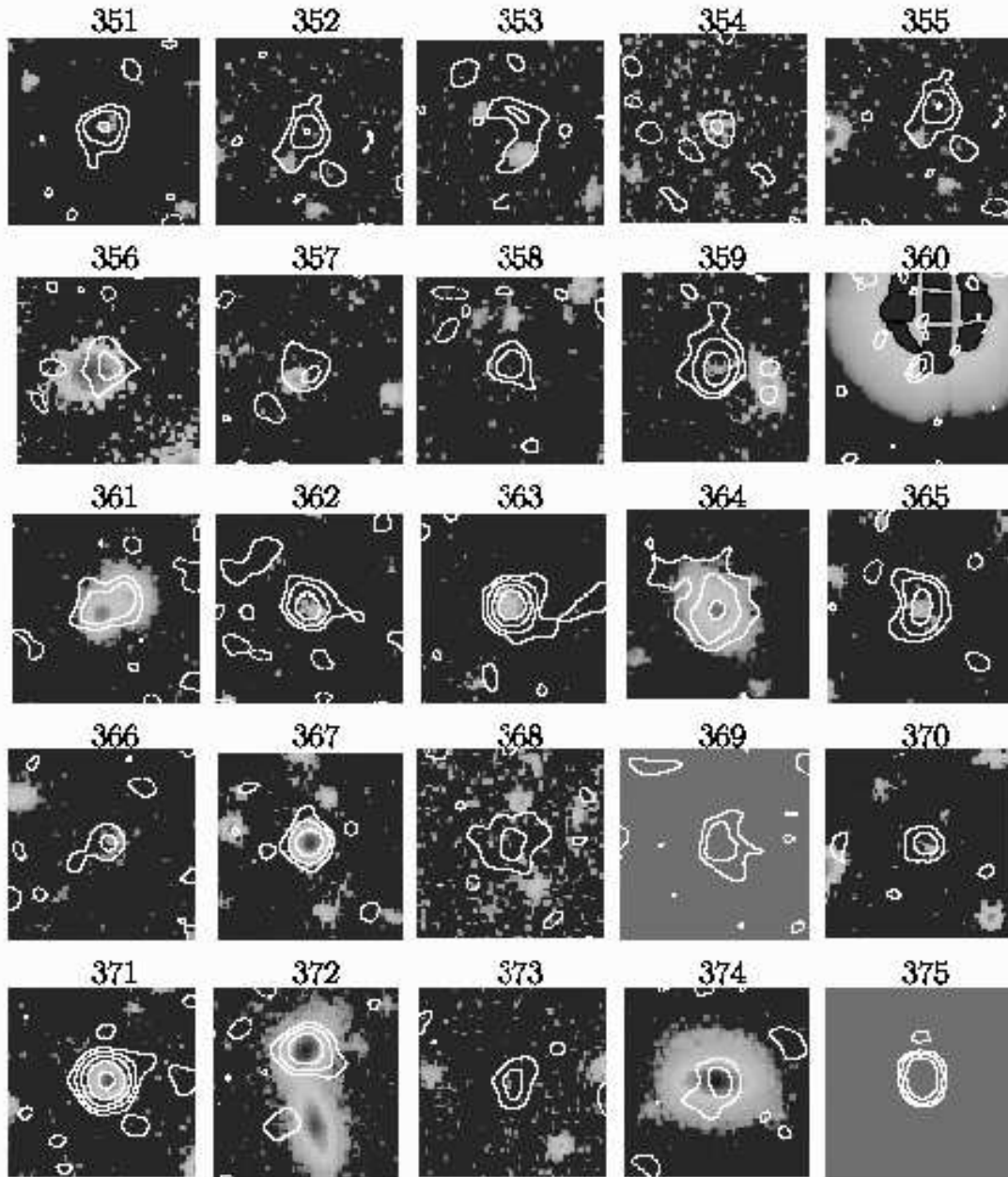


Fig. 6.— **The Radio/Optical Images:** The catalog number is shown above each diagram. The contours show the radio emission taken directly from the image of Fig. 1 (that is, uncorrected for the decrease of sky sensitivity with linear distance from the field center). The lowest radio contour value is $10.0 \mu\text{Jy}/\text{beam}$ and levels are shown at $-1, 1, 2, 4, 16$ times the lowest value (except for the brightest sources where the lowest contour level has been increased). The optical emission (usually z-band) is shown by the false-color image, adjusted to display the optical morphology. Bright sources (360) can be saturated. A uniform pink background is used when no Subaru optical data are available. **NOTE: All 33 pages of color images can be downloaded from ftp://ftp.cv.nrao.edu/pub/NRAO-staff/efomalon/ssa13_diagrams/**

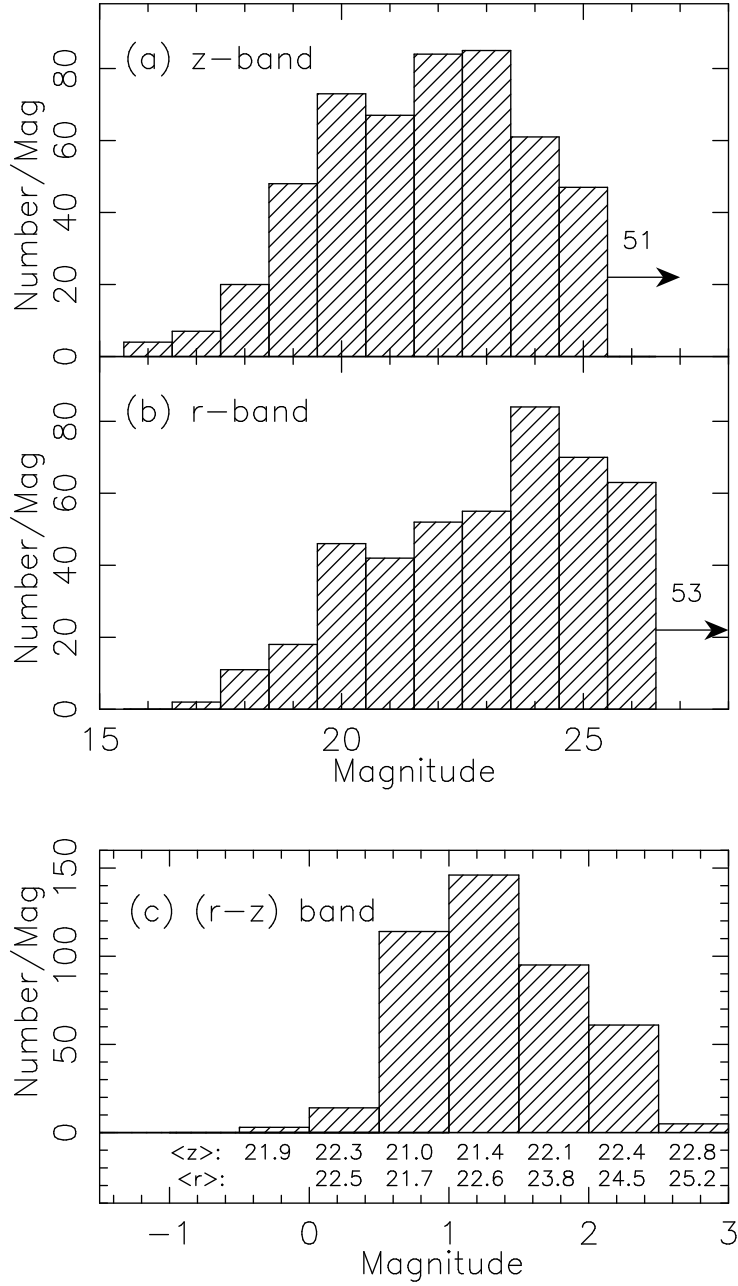


Fig. 7.— **Magnitude Distributions for Optical Identifications:** (a) The distribution of the z-band identifications for the the 532 sources in the complete sample with Subaru z-band data. Fifty-one sources are not identified. (b) The distribution of the r-band identifications for the 480 sources in the complete sample with Subaru r-band data. Fifty-three are not identified; (c) the distribution of the r-z color distribution for 441 sources with both r-band and z-band measurements. The average r-band and z-band magnitude is listed under each color magnitude bin; note the trend in $\langle r \rangle$.

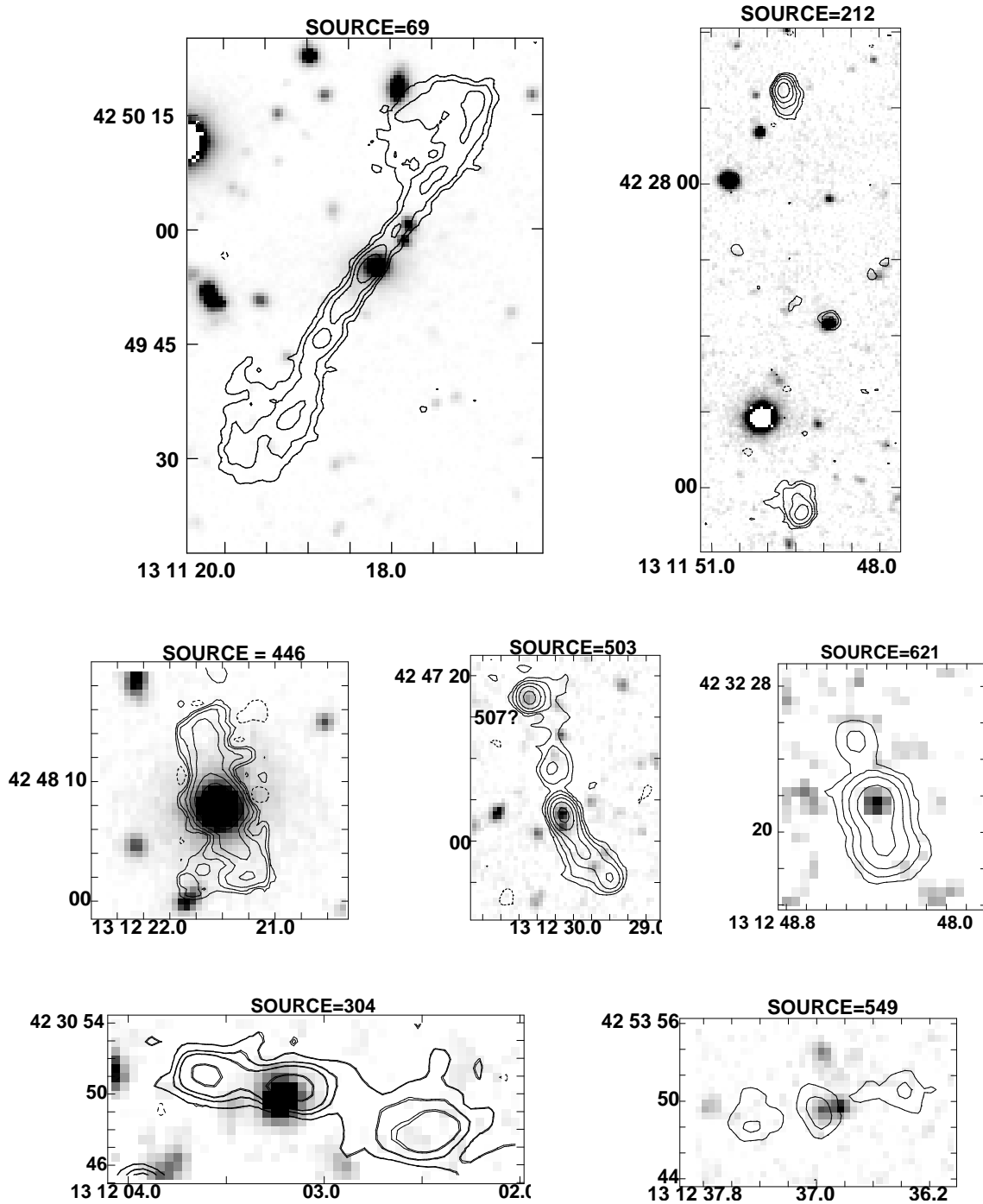


Fig. 8.— **Extended Active Galaxies:** The uncorrected radio contours, from Fig. 1, superimposed on the z-band optical gray-scale, of the seven AGNs in the SSA13 field are displayed. The source number from the catalog is given above each plot. The minimum contour level of these images is $27.5 \mu\text{Jy}/\text{beam}$ with levels at $-1, 1, 2, 4, 8, 16, \dots$ times the minimum level. The gray-scale contrast has been adjusted to best display the radio/optical alignment.

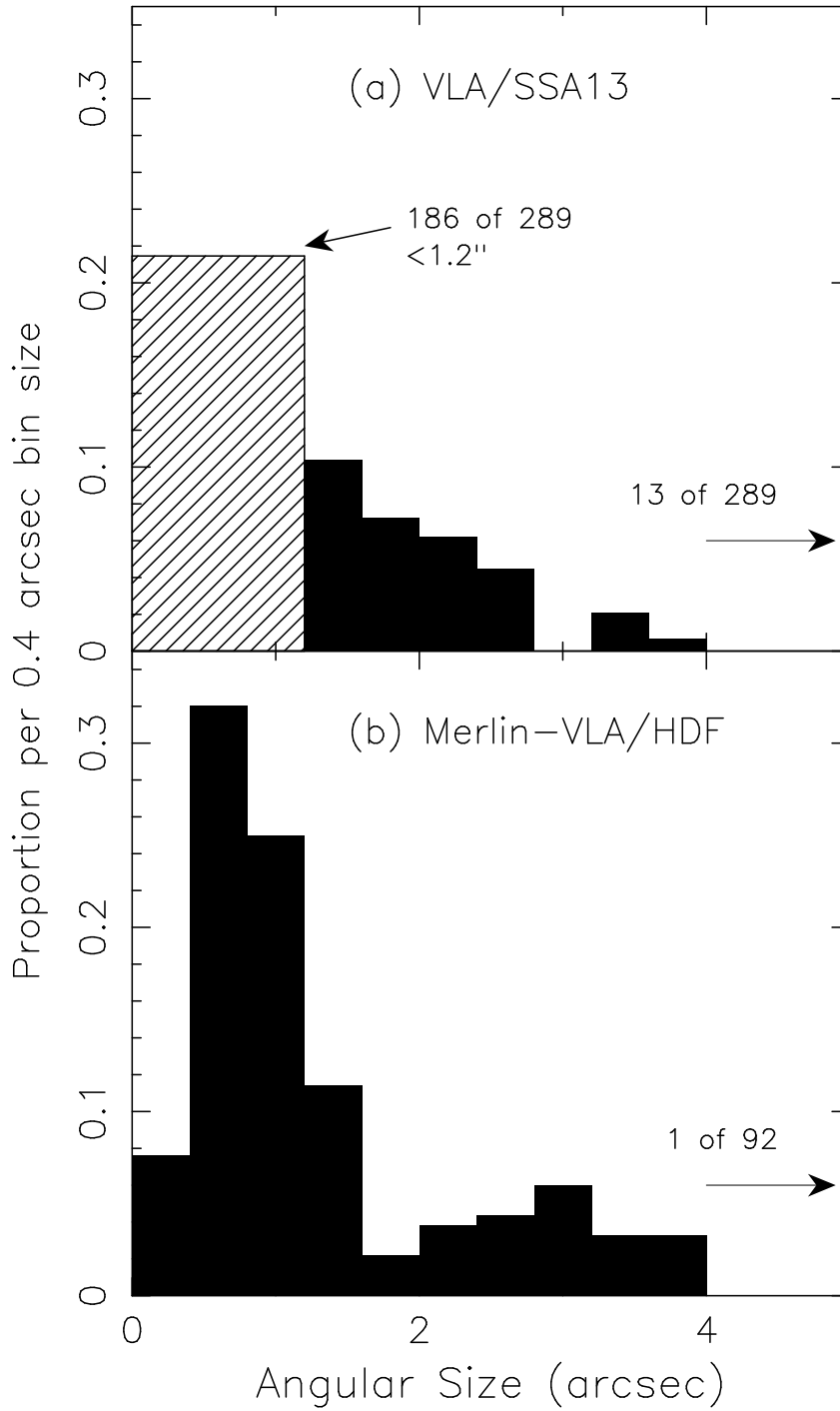


Fig. 9.— **The Angular Size Distribution at 1.4 GHz:** (a) The distribution of 289 sources in the complete SSA13 sample having $\text{SNR} > 8$. The unresolved sources, those largest angular size less than $1.2''$, are shown by the hashed distribution, equally spread over the angular size range. Thirteen of the 289 are larger than $4''$. (b) The distribution of 92 sources from the combined MERLIN/VLA observations of the HDF-North field. All sources are resolved with the $0.2''$ resolution of this survey (Muxlow et al. 2005). See text about the number of source larger than $4''$

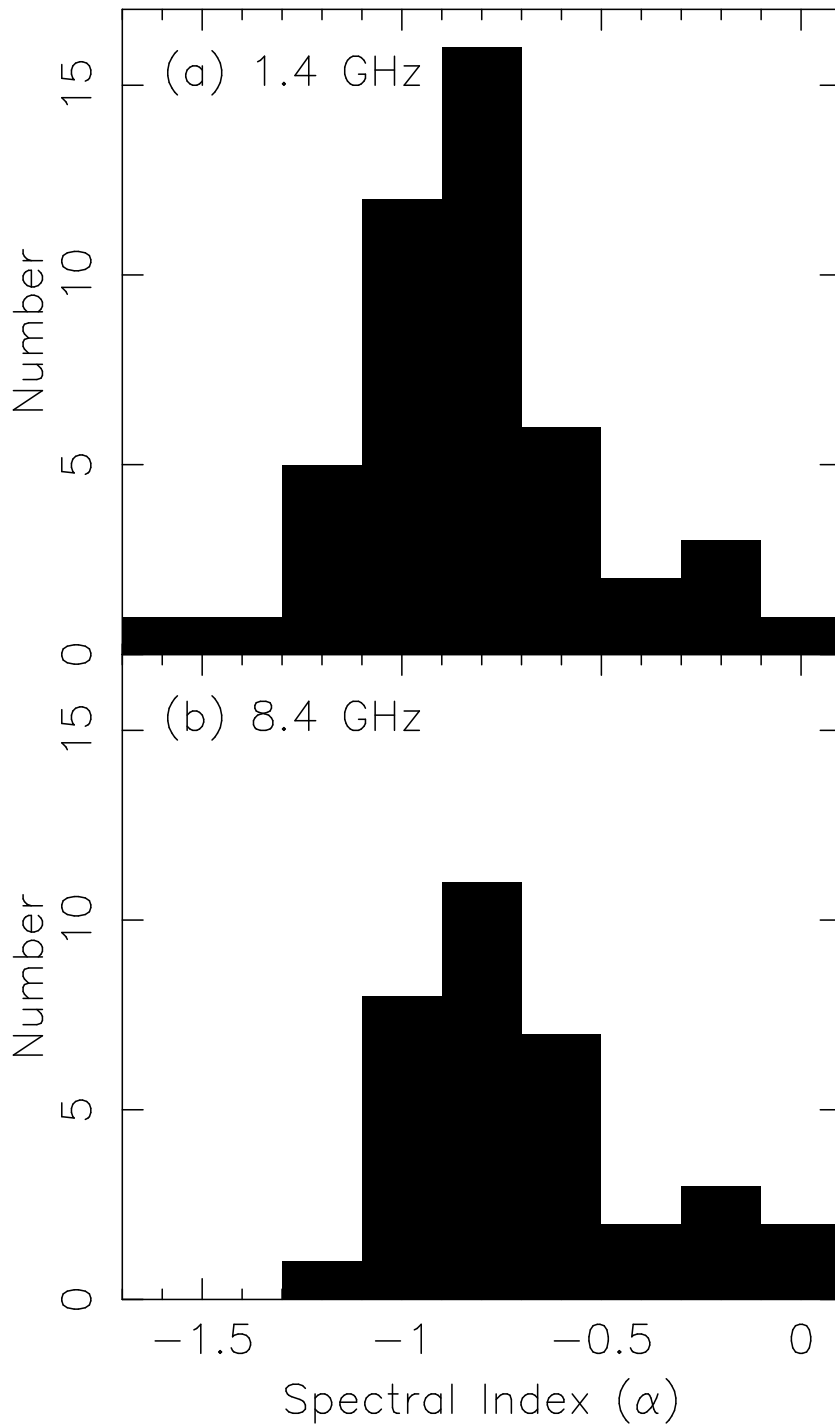


Fig. 10.— **The Spectral Index Distribution versus Frequency:** (a) The spectral index distribution of 47 sources in SSA13 from a complete sample at 1.4 GHz. (b) The spectral index distribution of 34 sources from a complete sample at 8.4 GHz.

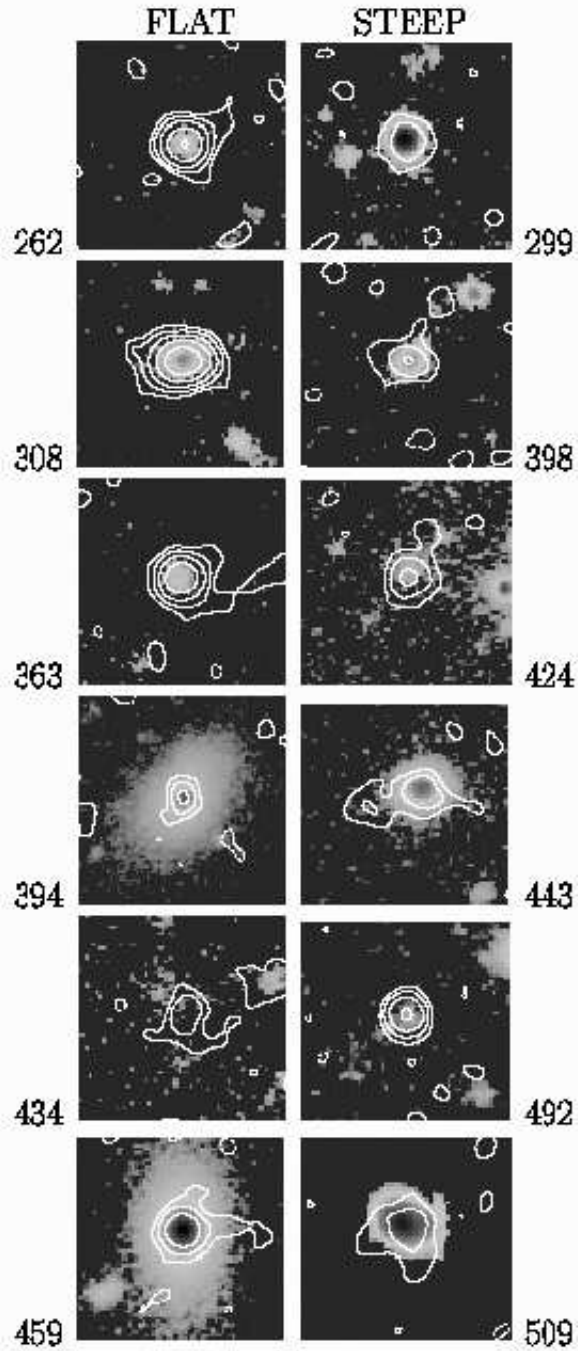


Fig. 11.— **Sources with Extreme Spectral Indices:** The images of these sources have been taken from Fig. 6, with contour levels= $-10,10,20,40,160 \mu\text{Jy}/\text{beam}$. The left column shows the radio/optical structure of the six sources with the flattest spectral index. The right column shows the six sources with the steepest spectral index. The source catalog number is given at the lower edge of each diagram.

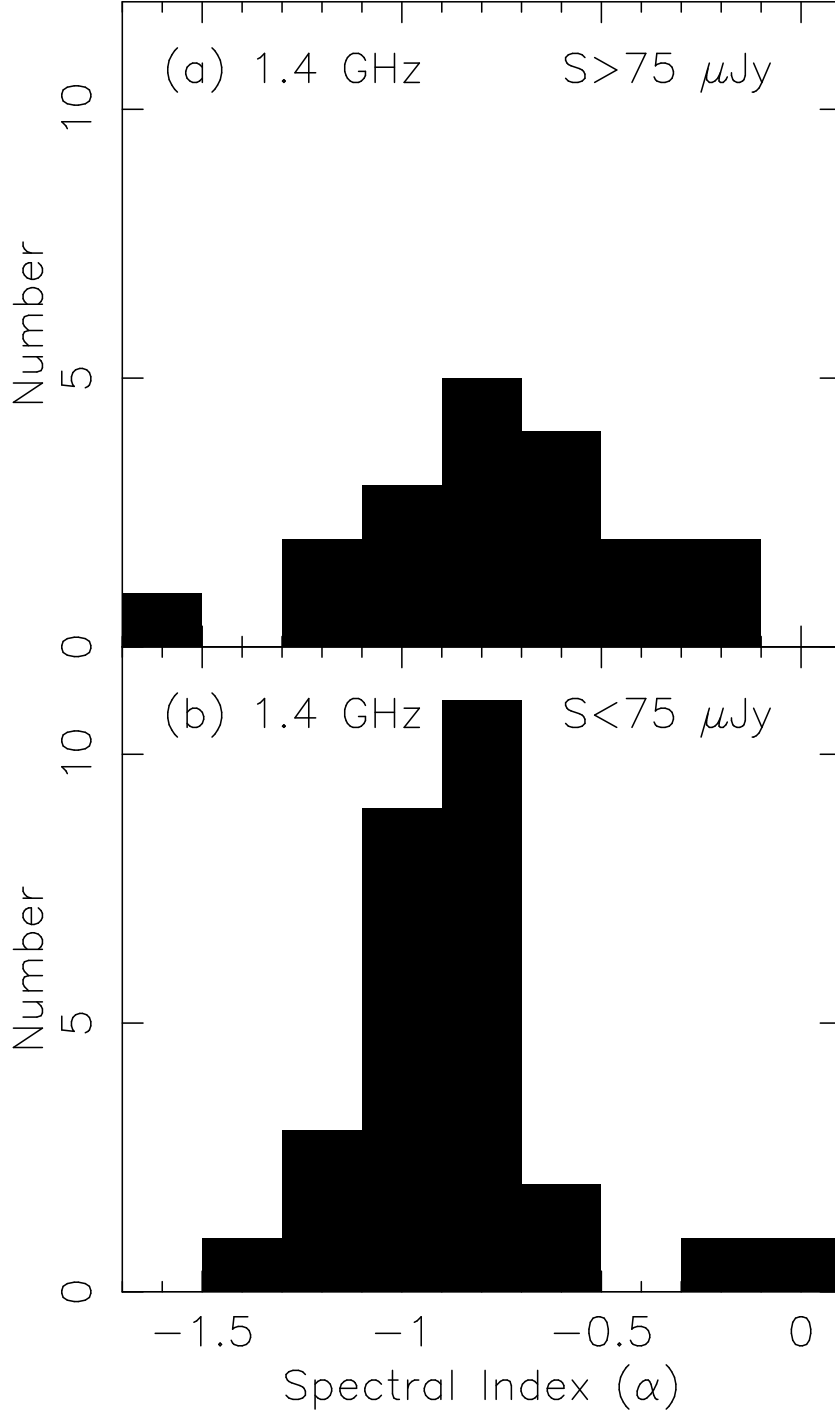


Fig. 12.— **The Spectral Index Distribution versus Flux Density:** (a) The spectral index distribution of 19 sources from a complete sample at 1.4 GHz with flux densities $> 75 \mu\text{Jy}$. (b) The spectral index distribution of 28 sources from a complete sample at 1.4 GHz with flux densities $< 75 \mu\text{Jy}$.

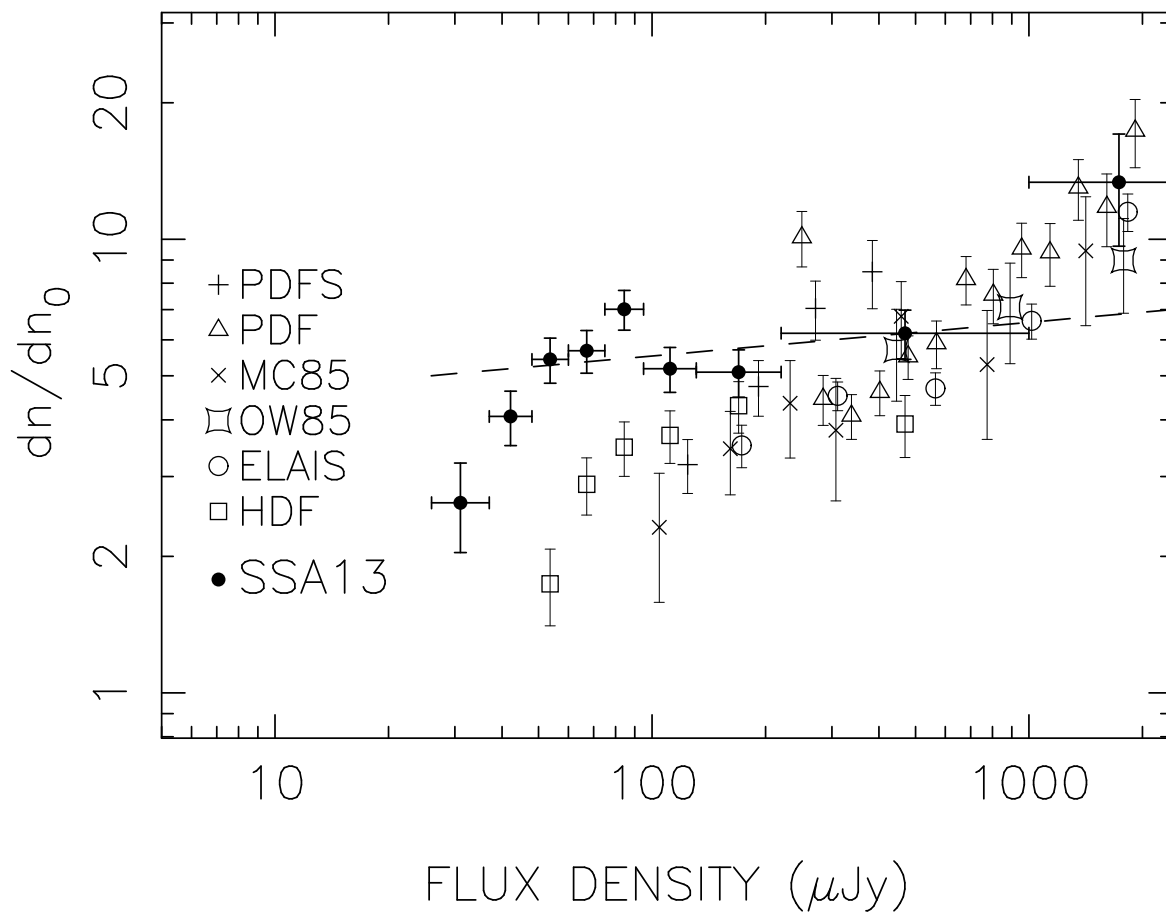


Fig. 13.— **The Micro-Jansky Counts of Radio Sources at 1.4 GHz:** The plotted points show the corrected differential count observed between 25 μJy and 2000 μJy at 1.4 GHz from a variety of deep surveys. The solid circles are the counts from SSA13. The dashed line gives the best fit power law to the SSA13 observation, with the lowest flux density point excluded. References are given in the text.

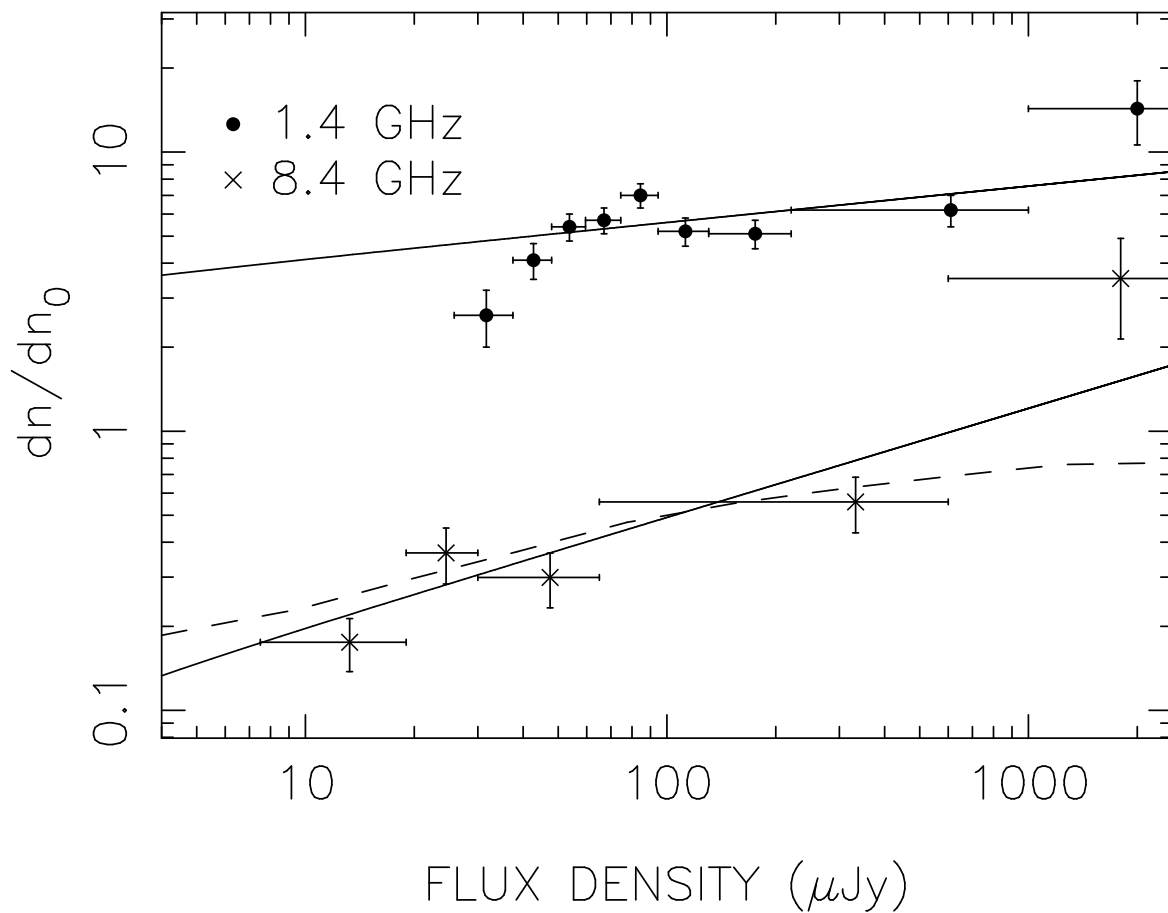


Fig. 14.— **Conversion of Count Between 1.4 and 8.4 GHz** The 1.4 GHz and 8.4 GHz differential counts from the SSA13 field are shown by the plotted points, with the solid lines as the best power-law fits. The dashed curve shows the derived 8.4 GHz source count modeled from the 1.4 GHz count and the spectral index distribution, shown in Fig. 12.

TABLE 1
SSA13 VLA OBSERVATION LOG

Date	No. Hours	Config.
1999 July 02	11	A
1999 July 04	11	A
1999 July 05	12	A
1999 July 16	12	A
1999 July 17	8	A
1999 July 19	11	A
1999 July 23	13	A
1999 August 30	13	A
2000 January 14	13	B

TABLE 2
RADIO/OPTICAL SOURCE CATALOG

(1) No	(2) Source	(3) SNR	(4) S _{1.4}	(5) RA	(6) DEC	(7)	(8)	(9)	(10) ROM	(11) r	(12) z
N001	J131047.4+424218	4.9	132(35)	13 10 47.481 (0.033)	42 42 18.03 (0.17)	2.8	< 1.2	92	Ge	22.7	21.2
N002	J131048.1+424012	6.6	149(36)	13 10 48.182 (0.020)	42 40 12.86 (0.17)	< 2.5			Gc	25.0	22.7
N003	J131049.0+423614	3.8	77(29)	13 10 49.081 (0.028)	42 36 14.56 (0.27)	< 2.8			U	> 26.0	> 23.4
N004	J131049.7+423623	7.4	131(32)	13 10 49.797 (0.016)	42 36 23.44 (0.19)	< 2.4			F	> 26.4	24.9
N005	J131051.7+424308	4.3	71(24)	13 10 51.705 (0.018)	42 43 08.95 (0.26)	< 2.2			Gd	21.6	21.0
N006	J131054.2+423929	6.6	96(24)	13 10 54.211 (0.015)	42 39 29.92 (0.18)	< 1.9			Gc	18.4	17.9
N007	J131055.7+424346	6.1	86(22)	13 10 55.757 (0.017)	42 43 46.53 (0.15)	< 1.3			F	> 26.3	23.9
N008	J131056.1+423022	14.5	295(31)	13 10 56.153 (0.010)	42 30 22.28 (0.10)	< 1.3			Bc		21.6
009	J131056.8+423721	5.7	92(23)	13 10 56.869 (0.016)	42 37 21.80 (0.17)	< 1.9			Gc?	19.1	18.3
010	J131057.3+423804	5.5	192(44)	13 10 57.311 (0.041)	42 38 04.69 (0.22)	4.7	1.8	86	Be	18.4	17.9
N011	J131057.9+423238	29.5	768(32)	13 10 57.909 (0.010)	42 32 38.66 (0.10)	2.4	1.1	19	Gd	25.2	22.5
N012	J131057.9+423535	4.7	65(24)	13 10 57.935 (0.026)	42 35 35.71 (0.27)	< 2.8			Gc	25.0	22.2
013	J131058.8+424151	6.9	119(22)	13 10 58.881 (0.016)	42 41 51.39 (0.11)	1.9	< 0.7	119	Be	24.0	22.3
N014	J131059.2+423229	7.1	122(25)	13 10 59.212 (0.015)	42 32 29.78 (0.13)	< 1.6			U	> 26.5	> 25.2
015	J131102.0+423914	14.2	195(22)	13 11 02.086 (0.010)	42 39 14.11 (0.10)	< 1.3			Gd	23.6	22.7
016	J131102.5+423318	6.3	80(20)	13 11 02.599 (0.019)	42 33 18.10 (0.13)	2.1	< 1.0	110	Be	21.1	19.9
N017	J131102.8+423836	4.9	60(19)	13 11 02.895 (0.020)	42 38 36.55 (0.20)	< 2.0			Gc	20.9	19.8
018	J131103.0+423229	32.0	522(23)	13 11 03.077 (0.010)	42 32 29.60 (0.10)	1.4	< 0.4	62	Ge	24.0	22.0
019	J131103.2+424116	23.6	312(20)	13 11 03.254 (0.010)	42 41 16.84 (0.10)	< 1.1			U	> 26.5	> 25.1
020	J131103.3+423637	5.9	76(17)	13 11 03.343 (0.014)	42 36 37.94 (0.13)	< 1.6			Gc?	23.8	22.1
N021	J131103.4+423212	3.7	73(36)	13 11 03.424 (0.042)	42 32 12.41 (0.37)	3.8	2.8	83	Be?	22.1	20.6
N022	J131103.6+424400	5.2	71(22)	13 11 03.630 (0.021)	42 44 00.90 (0.18)	< 2.1			U	> 26.4	> 25.8
023	J131104.5+423834	10.9	133(19)	13 11 04.582 (0.010)	42 38 34.79 (0.10)	< 1.4			Bc	25.1	23.2
N024	J131105.0+423058	5.2	95(26)	13 11 05.090 (0.018)	42 30 58.64 (0.20)	< 2.2			Gc	24.1	22.3
N025	J131105.6+423941	3.9	75(25)	13 11 05.692 (0.035)	42 39 41.41 (0.31)	3.7	< 1.0	47	U	> 26.4	> 25.4
026	J131105.7+423439	10.2	120(19)	13 11 05.762 (0.010)	42 34 39.57 (0.10)	< 1.5			F	23.8	24.0
N027	J131105.9+424827	5.3	185(47)	13 11 05.986 (0.029)	42 48 27.11 (0.31)	2.2	< 1.1	18	U ?	> 25.9	> 24.9
028	J131106.0+424434	12.5	188(22)	13 11 06.068 (0.010)	42 44 34.28 (0.10)	1.6	-1.4	125	Be	24.3	23.3
N029	J131106.1+424701	14.2	281(28)	13 11 06.117 (0.010)	42 47 01.12 (0.10)	< 1.5			Gc	22.5	20.7
030	J131106.3+424305	7.8	125(25)	13 11 06.379 (0.013)	42 43 05.01 (0.14)	< 1.9			Gc	19.6	18.5
031	J131106.9+424403	15.4	230(21)	13 11 06.937 (0.010)	42 44 03.33 (0.10)	1.8	< 1.0	120	Be	24.2	22.8
N032	J131107.0+424739	6.4	112(26)	13 11 07.095 (0.017)	42 47 39.51 (0.14)	< 2.0			Gd?	21.0	20.2
033	J131107.1+423743	5.6	65(20)	13 11 07.157 (0.021)	42 37 43.62 (0.19)	< 2.0			Bc	24.2	23.3
034	J131107.5+423505	5.7	64(18)	13 11 07.577 (0.017)	42 35 05.91 (0.18)	< 1.3			Gc	23.5	21.8
035	J131107.6+424457	6.5	179(40)	13 11 07.603 (0.050)	42 44 57.00 (0.60)	3.0			B2	20.3	19.3
A		6.5	121(25)	13 11 07.599 (0.014)	42 44 56.10 (0.14)	< 2.0				20.3	19.3
B		5.1	58(32)	13 11 07.607 (0.039)	42 44 59.08 (0.51)	< 3.6				21.0	19.9
036	J131107.9+424545	5.9	96(25)	13 11 07.966 (0.016)	42 45 45.05 (0.18)	< 1.9			Gc	21.9	20.5
037	J131108.0+423816	5.7	100(23)	13 11 08.016 (0.019)	42 38 16.18 (0.23)	3.0	< 0.9	150	Ge	20.9	19.6
038	J131108.6+423016	20.2	331(25)	13 11 08.621 (0.010)	42 30 16.89 (0.10)	< 1.4			Gd	21.4	19.6
N039	J131108.6+423417	4.7	95(24)	13 11 08.640 (0.031)	42 34 17.97 (0.18)	3.5	< 0.9	113	Ge	23.8	22.2
N040	J131109.6+424152	5.1	111(33)	13 11 09.661 (0.029)	42 41 52.21 (0.50)	4.0	2.3	54	F	25.1	24.4
N041	J131109.8+422647	6.6	148(29)	13 11 09.807 (0.018)	42 26 47.07 (0.12)	2.5	< 0.8	116	Ge		19.2
042	J131109.9+423355	8.2	106(20)	13 11 09.910 (0.011)	42 33 55.79 (0.12)	< 1.7			Gc	24.9	22.7
043	J131110.0+423514	40.6	449(16)	13 11 10.084 (0.010)	42 35 14.91 (0.10)	0.6	< 0.3	79	Ge	21.8	19.9
044	J131110.2+423938	99.9	43400(870)	13 11 10.208 (0.010)	42 39 38.03 (0.10)	1.3	0.7	61	Ge	24.1	21.9
N045	J131110.3+422752	9.1	147(27)	13 11 10.398 (0.013)	42 27 52.57 (0.13)	< 1.7			Gc		19.9
046	J131110.4+423256	7.1	107(24)	13 11 10.474 (0.016)	42 32 56.62 (0.14)	< 2.2			Gc	19.4	18.6
047	J131110.8+423136	6.9	154(29)	13 11 10.870 (0.014)	42 31 36.92 (0.23)	3.3	< 0.9	163	Ge	20.3	19.4
048	J131112.1+424631	5.6	60(13)	13 11 12.170 (0.012)	42 46 31.90 (0.10)	< 1.0			Gc	21.2	20.2
049	J131112.2+424044	8.2	118(19)	13 11 12.233 (0.013)	42 40 44.55 (0.12)	2.2	< 0.7	64	Be	21.6	20.4
050	J131112.5+424012	7.1	74(18)	13 11 12.513 (0.015)	42 40 12.90 (0.14)	< 1.7			Be?	23.8	22.0
N051	J131112.9+423951	4.8	95(25)	13 11 12.951 (0.028)	42 39 51.56 (0.34)	3.5	< 0.9	37	Gd	20.8	20.3
N052	J131113.0+424802	13.9	259(28)	13 11 13.058 (0.010)	42 48 02.82 (0.10)	< 1.7			Gc	19.1	18.3
N053	J131113.1+423911	4.7	102(38)	13 11 13.188 (0.048)	42 39 11.57 (0.76)	3.3	2.5	80	Be?	19.6	19.5
N054	J131113.5+424023	5.3	47(12)	13 11 13.503 (0.011)	42 40 23.31 (0.16)	< 1.2			U	> 24.1	> 23.6
N055	J131113.6+422706	7.9	146(28)	13 11 13.625 (0.013)	42 27 06.43 (0.14)	< 1.8			Gc		21.8
056	J131114.4+423120	9.7	132(20)	13 11 14.481 (0.010)	42 31 20.04 (0.10)	< 1.4			Gc	22.5	20.8
N057	J131114.5+424939	4.3	130(52)	13 11 14.589 (0.036)	42 49 39.25 (0.37)	3.7	2.7	113	Be	19.9	19.2
058	J131115.4+424235	8.1	81(14)	13 11 15.458 (0.010)	42 42 35.87 (0.10)	< 0.9			Bc	25.2	24.2
059	J131116.4+423349	7.0	77(19)	13 11 16.440 (0.015)	42 33 49.59 (0.15)	< 1.9			Gd	19.9	19.0
060	J131116.7+424417	11.7	149(19)	13 11 16.776 (0.010)	42 44 17.71 (0.10)	< 1.3			Gc	26.1	23.2
N061	J131117.1+424223	5.1	64(20)	13 11 17.146 (0.021)	42 42 23.33 (0.20)	< 1.8	< 1.2	130	Bc	22.7	20.8

TABLE 2—Continued

(1)	(2)	(3)	(4)	(5)	(6)	(7)	(8)	(9)	(10)	(11)	(12)
No	Source	SNR	S _{1,4}	RA	DEC	Radio Size	ROM	ROM	r	z	
062	J131117.1+423734	7.1	68(15)	13 11 17.171 (0.013)	42 37 34.92 (0.12)	< 1.5			Gc	22.9	21.4
063	J131117.1+423619	7.5	75(18)	13 11 17.194 (0.016)	42 36 19.96 (0.13)	< 1.7			Gc	25.2	24.2
064	J131117.2+424116	7.5	83(19)	13 11 17.292 (0.013)	42 41 16.41 (0.16)	< 2.0			Bc	24.8	23.2
065	J131117.4+424509	5.6	73(26)	13 11 17.412 (0.022)	42 45 09.07 (0.28)	< 2.6			Gc	20.1	19.9
066	J131117.5+423152	6.3	66(14)	13 11 17.556 (0.013)	42 31 52.11 (0.10)	< 1.3			Gc	23.1	21.7
067	J131117.9+423651	5.6	97(23)	13 11 17.954 (0.027)	42 36 51.97 (0.20)	3.3 < 1.4	115		Ge	20.8	19.9
068	J131118.2+424243	31.6	313(15)	13 11 18.249 (0.010)	42 42 43.03 (0.10)	1.5 < 0.3	125		Be	23.6	23.0
N069	J131118.2+424954	40.3	9570(250)	13 11 18.266 (0.010)	42 49 54.89 (0.10)	60.0	8.0	140	EG?	20.2	19.0
070	J131119.2+422846	5.4	70(18)	13 11 19.254 (0.016)	42 28 46.84 (0.15)	< 1.3			U		> 24.1
N071	J131119.4+423345	5.3	51(17)	13 11 19.477 (0.016)	42 33 45.90 (0.23)	< 1.9			Bc	23.7	22.7
072	J131119.7+423628	9.8	235(28)	13 11 19.748 (0.013)	42 36 28.47 (0.16)	4.1	1.4	35	Ge	18.0	17.2
073	J131119.8+423652	33.6	311(13)	13 11 19.800 (0.010)	42 36 52.90 (0.10)	0.5 < 0.3	81		Ge	22.0	20.5
N074	J131120.1+423602	5.2	69(18)	13 11 20.101 (0.023)	42 36 02.20 (0.16)	2.1 < 1.2	81		Ge	22.4	21.8
075	J131121.1+424712	6.0	92(26)	13 11 21.198 (0.018)	42 47 12.26 (0.20)	< 2.2			Gc	23.5	22.6
N076	J131121.2+424742	3.9	84(30)	13 11 21.290 (0.028)	42 47 42.69 (0.45)	2.7 < 1.9	1		Be	24.9	23.1
N077	J131121.3+422440	5.7	129(36)	13 11 21.323 (0.020)	42 24 40.48 (0.22)	< 2.3			sg	20.0	19.0
N078	J131121.7+422431	4.2	100(36)	13 11 21.741 (0.030)	42 24 31.25 (0.26)	< 2.9			sg	22.4	19.4
079	J131122.0+422834	8.1	101(21)	13 11 22.002 (0.013)	42 28 34.77 (0.13)	< 1.3			Gc		19.1
080	J131122.2+423205	51.7	526(15)	13 11 22.236 (0.010)	42 32 05.18 (0.10)	0.8 < 0.3	56		Ge	20.4	19.6
081	J131122.3+422915	7.8	93(18)	13 11 22.361 (0.013)	42 29 15.62 (0.11)	1.5 < 1.0	35		Ge	22.5	20.5
082	J131122.4+423614	5.9	53(14)	13 11 22.453 (0.013)	42 36 14.28 (0.15)	< 1.4			F	26.1	24.3
083	J131122.6+424310	86.2	819(14)	13 11 22.682 (0.010)	42 43 10.09 (0.10)	0.8 < 0.2	119		Ge	24.4	22.6
084	J131122.9+424415	14.2	146(15)	13 11 22.903 (0.010)	42 44 15.51 (0.10)	< 1.2			Bc	19.5	18.5
085	J131123.2+423828	56.5	486(13)	13 11 23.241 (0.010)	42 38 28.70 (0.10)	0.8 < 0.3	89		Ge	20.9	19.5
086	J131123.3+423916	6.2	53(13)	13 11 23.340 (0.011)	42 39 16.70 (0.15)	1.5	0.7	155	Ge	20.7	20.0
N087	J131123.3+424349	4.5	42(12)	13 11 23.373 (0.013)	42 43 49.25 (0.16)	< 1.1			U	> 26.7	> 25.1
088	J131124.4+424606	6.4	76(16)	13 11 24.408 (0.013)	42 46 06.59 (0.11)	< 1.5			Gc	23.3	23.1
N089	J131124.8+422446	7.1	113(23)	13 11 24.801 (0.011)	42 24 46.91 (0.14)	< 1.2			sg	24.0	21.2
090	J131124.8+422719	5.5	104(26)	13 11 24.810 (0.040)	42 27 19.98 (0.30)	3.0	1.5	80	Ge		19.3
091	J131125.1+424220	5.6	50(15)	13 11 25.142 (0.016)	42 42 20.70 (0.20)	< 1.8			Gd?	23.2	22.0
092	J131125.2+423652	12.5	107(13)	13 11 25.213 (0.010)	42 36 52.71 (0.10)	< 1.2			F	25.2	23.8
093	J131125.2+423401	34.0	316(14)	13 11 25.229 (0.010)	42 34 01.43 (0.10)	< 0.9			Gc	23.3	22.4
N094	J131125.8+423508	5.0	40(13)	13 11 25.857 (0.018)	42 35 08.79 (0.17)	< 1.7			Gd	20.7	19.8
095	J131126.1+424223	5.6	51(13)	13 11 26.104 (0.012)	42 42 23.22 (0.15)	< 1.4			U	> 26.5	> 25.0
096	J131126.7+423428	9.3	108(17)	13 11 26.754 (0.012)	42 34 28.98 (0.11)	2.1 < 1.0	51		Be?	26.3	23.9
097	J131126.8+422906	9.5	114(18)	13 11 26.839 (0.010)	42 29 06.46 (0.10)	< 1.2			Gc	22.8	21.0
098	J131126.8+423348	99.9	894(13)	13 11 26.890 (0.010)	42 33 48.79 (0.10)	0.4 < 0.2	66		F	> 26.0	25.0
099	J131127.6+422956	87.0	958(16)	13 11 27.616 (0.010)	42 29 56.56 (0.10)	0.8 < 0.2	45		Be	23.3	22.1
100	J131127.7+423511	9.8	85(13)	13 11 27.742 (0.010)	42 35 11.03 (0.10)	< 1.1			F	25.3	24.6
101	J131127.9+423154	5.8	87(17)	13 11 27.920 (0.020)	42 31 54.95 (0.40)	4.3	2.0	0	C ?	20.4	19.4
A		5.8	49(13)	13 11 27.926 (0.014)	42 31 54.17 (0.14)	< 1.1			Gc		
B		4.5	38(14)	13 11 27.915 (0.023)	42 31 56.43 (0.15)	< 1.9			Gd		
102	J131128.0+424033	6.3	48(11)	13 11 28.022 (0.013)	42 40 33.16 (0.10)	< 1.3			Gc	24.9	22.5
N103	J131128.1+425124	4.9	83(30)	13 11 28.165 (0.017)	42 51 24.74 (0.37)	< 3.1			Gc	21.1	20.4
104	J131128.5+424938	10.3	253(30)	13 11 28.525 (0.012)	42 49 38.35 (0.10)	2.5 < 1.4	76		Ge?	19.0	18.3
105	J131128.5+424945	11.2	239(27)	13 11 28.599 (0.011)	42 49 45.22 (0.10)	2.5 < 0.7	65		Ge?	19.4	18.7
106	J131129.3+423517	7.3	60(15)	13 11 29.311 (0.013)	42 35 17.40 (0.14)	< 1.6			F	26.2	24.4
N107	J131129.5+423234	4.7	73(20)	13 11 29.504 (0.020)	42 32 34.68 (0.29)	2.9 < 1.2	133		Ge	21.7	20.4
N108	J131129.6+424359	3.9	117(34)	13 11 29.610 (0.060)	42 43 59.50 (0.50)	4.5			Ge	19.7	18.9
109	J131129.7+424150	12.1	90(12)	13 11 29.785 (0.010)	42 41 50.82 (0.10)	< 0.8			Ge?	21.7	20.7
110	J131130.0+423913	6.2	49(12)	13 11 30.001 (0.012)	42 39 13.48 (0.14)	< 1.5			U	> 26.5	> 25.4
N111	J131130.2+425117	99.9	2400(85)	13 11 30.244 (0.010)	42 51 17.90 (0.10)	1.2 < 0.4	154		Ge	25.4	22.9
112	J131130.4+423516	10.7	81(11)	13 11 30.410 (0.010)	42 35 16.51 (0.10)	< 0.9			F ?	24.8	24.0
N113	J131130.7+422506	4.8	114(38)	13 11 30.745 (0.026)	42 25 06.96 (0.26)	< 2.9			U		> 23.8
N114	J131131.1+422537	6.2	92(23)	13 11 31.147 (0.014)	42 25 37.52 (0.19)	< 2.0			Bc		22.2
115	J131131.8+424705	7.0	83(19)	13 11 31.855 (0.014)	42 47 05.32 (0.15)	< 1.7			Gc	22.2	20.8
116	J131131.9+423129	7.6	64(13)	13 11 31.968 (0.010)	42 31 29.01 (0.13)	< 1.4			Gc	24.9	23.3
117	J131132.1+423133	6.9	68(15)	13 11 32.101 (0.014)	42 31 33.55 (0.11)	< 1.8			Gc	24.6	22.2
118	J131132.2+422546	7.6	121(24)	13 11 32.208 (0.013)	42 25 46.11 (0.14)	< 1.4			Gc		22.0
119	J131132.3+424453	6.1	55(13)	13 11 32.326 (0.013)	42 44 53.50 (0.13)	1.7 < 1.2	106		Be	20.1	19.3
120	J131132.4+424243	6.1	59(15)	13 11 32.464 (0.017)	42 42 43.99 (0.16)	< 2.0			U	> 25.8	> 25.3
121	J131132.5+423731	7.9	61(13)	13 11 32.550 (0.011)	42 37 31.62 (0.12)	< 1.5			Bc	23.8	22.6
N122	J131132.8+424357	4.8	37(10)	13 11 32.806 (0.015)	42 43 57.11 (0.12)	< 1.1			U ?	24.3	23.2

TABLE 2—Continued

(1)	(2)	(3)	(4)	(5)	(6)	(7)	(8)	(9)	(10)	(11)	(12)
No	Source	SNR	S _{1.4}	RA	DEC	Radio Size	ROM	r	z		
123	J131132.9+423526	10.0	71(11)	13 11 32.992 (0.010)	42 35 26.25 (0.10)	< 1.0			U	> 26.4	> 24.8
N124	J131133.0+423422	10.4	104(13)	13 11 33.021 (0.010)	42 34 22.74 (0.10)	2.5	1.5	35	Ge	19.9	18.9
125	J131133.0+422700	5.4	67(19)	13 11 33.044 (0.018)	42 27 00.24 (0.17)	< 1.8			Gc		21.9
126	J131133.1+424300	6.4	54(14)	13 11 33.119 (0.014)	42 43 00.87 (0.13)	< 1.5			Bc	25.5	24.7
127	J131133.3+423506	6.4	49(12)	13 11 33.364 (0.012)	42 35 06.65 (0.13)	< 1.5			Bc	21.1	20.4
128	J131133.8+424230	51.9	415(13)	13 11 33.862 (0.010)	42 42 30.17 (0.10)	< 0.8			Bc	25.6	23.4
129	J131134.1+423031	5.6	86(23)	13 11 34.178 (0.021)	42 30 31.74 (0.32)	3.2	< 1.4	21	U	> 26.5	> 24.7
130	J131134.2+422948	28.2	412(20)	13 11 34.297 (0.010)	42 29 48.87 (0.10)	2.0	0.9	138	Ge		17.4
131	J131134.4+424510	6.0	88(19)	13 11 34.431 (0.015)	42 45 10.46 (0.21)	2.5	< 1.1	25	Be	19.0	18.1
N132	J131134.5+424309	4.7	35(11)	13 11 34.518 (0.016)	42 43 09.26 (0.15)	< 1.1			Bc	24.4	22.6
133	J131134.6+423400	7.1	53(13)	13 11 34.673 (0.012)	42 34 00.08 (0.14)	< 1.4			F	> 26.1	24.5
134	J131134.8+424843	6.4	67(14)	13 11 34.823 (0.010)	42 48 43.97 (0.14)	< 1.1			Bc	24.0	22.3
135	J131134.9+425020	7.5	196(29)	13 11 34.908 (0.013)	42 50 20.45 (0.14)	2.8	< 0.8	53	Ge	21.7	20.0
136	J131135.1+424321	8.6	74(14)	13 11 35.186 (0.010)	42 43 21.30 (0.11)	< 1.5			Gc	23.6	21.5
137	J131135.4+422708	7.1	87(20)	13 11 35.405 (0.012)	42 27 08.71 (0.15)	< 1.4			U		> 25.0
138	J131135.4+423038	11.9	99(16)	13 11 35.410 (0.014)	42 30 38.87 (0.10)	2.4	< 0.7	102	Ge	25.4	23.7
N139	J131135.6+424315	5.0	104(27)	13 11 35.616 (0.031)	42 43 15.55 (0.30)	2.9			U	> 25.8	> 25.5
140	J131135.6+424852	5.5	81(21)	13 11 35.628 (0.017)	42 48 52.58 (0.16)	< 2.0			Bc	21.5	20.2
141	J131135.8+423037	17.1	213(17)	13 11 35.836 (0.010)	42 30 37.05 (0.10)	1.7	< 1.1	147	F ?	25.6	24.6
142	J131135.8+423920	7.7	75(15)	13 11 35.838 (0.017)	42 39 20.14 (0.13)	2.1	< 1.3	80	Ge	19.4	18.6
N143	J131136.1+423139	5.1	84(23)	13 11 36.115 (0.022)	42 31 39.85 (0.36)	3.4	< 1.7	17	Be?	23.2	21.7
144	J131136.2+424031	5.9	90(22)	13 11 36.251 (0.022)	42 40 31.23 (0.29)	2.5			F	25.1	24.5
145	J131136.3+424040	7.8	59(12)	13 11 36.399 (0.011)	42 40 40.76 (0.10)	< 1.3			Gc	21.2	20.2
146	J131136.5+423630	5.7	37(12)	13 11 36.509 (0.018)	42 36 30.35 (0.15)	< 1.7			Gc	22.4	20.7
147	J131136.6+422511	8.8	138(24)	13 11 36.652 (0.010)	42 25 11.43 (0.13)	< 1.4			su	> 23	> 22
148	J131136.7+423541	10.5	73(10)	13 11 36.754 (0.010)	42 35 41.37 (0.10)	< 0.8			Bc	25.4	22.9
149	J131136.7+423828	5.6	33(09)	13 11 36.782 (0.014)	42 38 28.19 (0.10)	< 1.0			Gc	26.8	24.3
150	J131136.9+423440	8.9	78(13)	13 11 36.918 (0.012)	42 34 40.04 (0.10)	2.1	< 0.6	110	F	25.5	24.4
N151	J131137.5+424237	4.4	40(17)	13 11 37.553 (0.026)	42 42 37.01 (0.29)	2.4			Ge	18.2	17.5
152	J131137.6+423059	8.7	90(15)	13 11 37.634 (0.011)	42 30 59.30 (0.10)	1.5	< 0.6	74	Ge	22.7	21.6
N153	J131137.6+423131	5.0	42(13)	13 11 37.693 (0.018)	42 31 31.86 (0.15)	< 1.6			Gc	23.3	20.6
154	J131138.2+423727	7.2	87(17)	13 11 38.261 (0.014)	42 37 27.81 (0.19)	2.4	1.3	178	Be	22.0	20.8
155	J131138.7+424420	7.1	50(12)	13 11 38.747 (0.014)	42 44 20.68 (0.12)	< 1.4			U	> 26.7	> 25.5
156	J131138.7+424457	8.2	102(18)	13 11 38.774 (0.014)	42 44 57.37 (0.15)	2.5	< 1.1	45	Ge?	20.1	20.1
157	J131139.0+423100	6.5	57(14)	13 11 39.048 (0.012)	42 31 00.20 (0.14)	< 1.6			Gc	25.1	22.8
158	J131139.8+424454	11.7	171(18)	13 11 39.850 (0.010)	42 44 54.16 (0.10)	2.5	< 0.9	70	Ge?	20.1	19.4
159	J131140.1+423747	6.4	62(13)	13 11 40.172 (0.018)	42 37 47.77 (0.12)	2.8	< 0.7	116	F ?	> 26.7	> 25.2
160	J131140.2+423434	7.8	52(11)	13 11 40.264 (0.010)	42 34 34.93 (0.11)	< 1.1			U	> 26.3	> 25.2
161	J131141.4+424053	10.7	91(13)	13 11 41.407 (0.010)	42 40 53.10 (0.10)	1.5	< 0.8	160	Be	21.2	20.4
162	J131141.4+424312	12.1	99(14)	13 11 41.495 (0.010)	42 43 12.75 (0.10)	< 1.4			Gc	24.5	23.2
N163	J131141.5+423022	4.7	37(12)	13 11 41.526 (0.017)	42 30 22.50 (0.16)	< 1.3			Gc	23.5	21.8
164	J131141.7+423316	7.5	68(14)	13 11 41.757 (0.015)	42 33 16.84 (0.12)	1.8	< 1.0	78	U	> 26.6	> 25.5
N165	J131141.8+423944	5.0	31(10)	13 11 41.842 (0.014)	42 39 44.59 (0.15)	< 1.0			U	> 26.6	> 25.3
166	J131142.0+424420	7.6	210(31)	13 11 42.060 (0.019)	42 44 20.78 (0.23)	4.6	2.2	40	B2	20.4	19.5
A		6.3	94(15)	13 11 42.165 (0.020)	42 44 21.81 (0.32)	< 2.0				20.4	19.5
B		7.2	116(17)	13 11 42.001 (0.019)	42 44 20.16 (0.28)	< 2.0				20.9	19.7
167	J131142.2+423957	8.7	56(12)	13 11 42.269 (0.010)	42 39 57.11 (0.12)	< 1.5			Bc	23.5	21.6
N168	J131142.4+425218	6.9	234(36)	13 11 42.430 (0.015)	42 52 18.29 (0.20)	2.5	2.5	0	Ge	18.7	18.1
169	J131142.7+424618	7.9	76(14)	13 11 42.796 (0.010)	42 46 18.78 (0.11)	< 1.1			S ?	22.2	22.6
170	J131143.2+422947	7.0	77(18)	13 11 43.223 (0.016)	42 29 47.93 (0.20)	2.5	< 0.9	137	F	24.8	23.7
171	J131143.2+424123	15.7	99(10)	13 11 43.253 (0.010)	42 41 23.81 (0.10)	< 0.9			F ?	25.9	24.8
172	J131143.3+425050	28.0	415(22)	13 11 43.342 (0.010)	42 50 50.31 (0.10)	< 1.3			Gc	23.7	22.6
N173	J131143.4+423357	5.0	56(14)	13 11 43.412 (0.018)	42 33 57.30 (0.15)	2.0	< 1.0	117	Gd	23.1	21.2
174	J131143.4+423808	11.7	72(10)	13 11 43.456 (0.010)	42 38 08.90 (0.10)	< 0.9			F	25.4	24.2
175	J131143.5+424740	8.8	140(21)	13 11 43.527 (0.015)	42 47 40.55 (0.12)	2.8	< 1.1	105	Be?	23.6	22.0
176	J131143.5+422841	7.0	64(14)	13 11 43.534 (0.012)	42 28 41.24 (0.12)	< 1.0			Gc		22.5
177	J131143.5+423148	9.1	69(11)	13 11 43.583 (0.010)	42 31 48.03 (0.10)	< 1.0			F	> 26.2	25.0
178	J131143.6+423030	12.7	111(13)	13 11 43.616 (0.010)	42 30 30.85 (0.10)	< 0.9			Gc	25.7	23.4
179	J131144.0+424158	13.7	87(10)	13 11 44.070 (0.010)	42 41 58.65 (0.10)	< 0.8			Gc	20.9	19.7
180	J131144.2+424302	7.9	167(25)	13 11 44.204 (0.017)	42 43 02.54 (0.19)	3.5	2.4	44	Ge	18.3	17.5
181	J131144.3+422930	7.4	80(15)	13 11 44.390 (0.010)	42 29 30.46 (0.13)	1.7	< 0.7	139	Ge	20.7	20.0
182	J131144.5+424501	10.2	133(18)	13 11 44.511 (0.013)	42 45 01.36 (0.10)	2.8	< 0.8	68	Ge	19.1	18.2
183	J131144.5+423437	35.6	228(10)	13 11 44.577 (0.010)	42 34 37.41 (0.10)	< 0.4			Gc?	24.2	22.9

TABLE 2—Continued

(1) No	(2) Source	(3) SNR	(4) S _{1,4}	(5) RA	(6) DEC	(7) Radio Size	(8)	(9)	(10) ROM	(11) r	(12) z
184	J131144.5+424613	5.8	51(13)	13 11 44.598 (0.014)	42 46 13.43 (0.13)	< 1.4			F	> 26.6	24.9
185	J131144.6+423825	6.2	149(28)	13 11 44.638 (0.070)	42 38 25.82 (0.55)	6.5			C ?	23.6	22.1
A		6.2	63(20)	13 11 44.633 (0.017)	42 38 26.20 (0.22)	< 1.0			Gc	23.6	22.1
B		6.1	39(07)	13 11 44.792 (0.017)	42 38 22.77 (0.22)	3.5	< 1.5	120	Ge	22.6	21.4
C		6.0	47(16)	13 11 44.514 (0.022)	42 38 27.56 (0.28)	< 2.0	0		S	22.9	22.2
186	J131145.0+422930	5.5	46(14)	13 11 45.097 (0.018)	42 29 30.20 (0.13)	< 1.8			Gd	24.8	23.6
187	J131145.1+424518	9.1	101(16)	13 11 45.103 (0.012)	42 45 18.63 (0.10)	2.3	< 0.7	71	Ge	24.1	22.1
188	J131145.2+423952	9.3	179(24)	13 11 45.202 (0.023)	42 39 52.95 (0.31)	5.0			C ?	20.5	19.7
189	J131145.2+423842	6.6	47(11)	13 11 45.284 (0.013)	42 38 42.78 (0.12)	< 1.4			F	> 26.5	24.9
190	J131145.3+423912	21.3	301(18)	13 11 45.367 (0.010)	42 39 12.91 (0.10)	2.6	2.0	89	Ge	18.1	17.3
191	J131145.4+423509	5.5	52(16)	13 11 45.475 (0.018)	42 45 09.89 (0.19)	< 2.0			Gc	24.0	23.1
192	J131145.6+423242	45.4	351(12)	13 11 45.666 (0.010)	42 32 42.51 (0.10)	1.1	< 0.3	142	Ge	24.9	23.3
193	J131145.9+423215	5.7	36(10)	13 11 45.909 (0.015)	42 32 15.97 (0.12)	< 1.3			Bc	24.2	22.2
194	J131145.9+423145	5.9	99(22)	13 11 45.946 (0.021)	42 31 45.15 (0.26)	2.5			Ge	19.1	18.5
195	J131146.0+423828	5.8	38(12)	13 11 46.076 (0.018)	42 38 28.37 (0.14)	1.7	< 1.0	55	Be?	25.6	24.7
196	J131146.1+424751	6.3	155(28)	13 11 46.150 (0.019)	42 47 51.80 (0.22)	3.2	1.8	45	Ge	18.5	17.7
N197	J131146.1+422325	7.8	165(27)	13 11 46.169 (0.015)	42 23 25.26 (0.11)	2.4	< 0.7	93	sg	19.6	18.9
198	J131146.3+422707	16.7	295(22)	13 11 46.327 (0.010)	42 27 07.97 (0.10)	2.3	< 1.0	88	Ge		18.3
199	J131146.5+424718	5.9	82(19)	13 11 46.510 (0.015)	42 47 18.28 (0.22)	2.2	< 1.4	29	Be	23.6	21.6
N200	J131146.6+423639	3.9	26(11)	13 11 46.651 (0.020)	42 36 39.41 (0.22)	< 1.9			Bc	23.1	22.2
201	J131146.9+425126	6.3	159(29)	13 11 46.940 (0.030)	42 51 26.23 (0.33)	3.8			B2?	25.4	23.9
A		6.3	83(19)	13 11 46.831 (0.011)	42 51 26.07 (0.16)	< 1.1				25.6	24.3
B		4.2	76(25)	13 11 47.084 (0.030)	42 51 26.79 (0.26)	2.9	< 1.1	62		25.4	23.9
202	J131147.1+424509	6.3	67(14)	13 11 47.131 (0.019)	42 45 09.42 (0.10)	2.7	< 0.7	82	Ge	23.8	22.9
N203	J131147.2+423759	4.3	30(12)	13 11 47.233 (0.025)	42 37 59.22 (0.20)	< 2.0			Gc	25.2	23.0
204	J131147.2+422939	5.6	49(14)	13 11 47.298 (0.018)	42 29 39.13 (0.17)	2.3	< 0.8	126	Ge	23.7	21.6
205	J131147.3+424244	7.1	68(14)	13 11 47.388 (0.014)	42 42 44.02 (0.12)	1.7	< 1.2	70	U	> 25.9	> 25.3
206	J131147.4+423444	20.5	128(11)	13 11 47.475 (0.010)	42 34 44.81 (0.10)	< 0.9			Gc	22.9	21.3
207	J131147.5+424801	12.3	118(14)	13 11 47.557 (0.010)	42 48 01.55 (0.10)	< 0.7			Gc	23.9	21.6
208	J131148.2+424814	14.5	150(15)	13 11 48.262 (0.010)	42 48 14.53 (0.10)	< 1.1			Gc	23.8	21.9
209	J131148.4+424647	13.2	138(15)	13 11 48.453 (0.010)	42 46 47.96 (0.10)	1.6	< 0.7	111	Be	22.6	21.5
N210	J131148.6+424523	4.9	43(17)	13 11 48.625 (0.022)	42 45 23.09 (0.24)	< 2.1			U	> 26.5	> 25.2
211	J131148.6+423216	6.1	50(13)	13 11 48.662 (0.015)	42 32 16.63 (0.13)	< 1.7			Gc	25.6	23.5
212	J131148.8+422733	13.1	149(18)	13 11 48.865 (0.010)	42 27 33.09 (0.10)	90.0			EG?		19.7
213	J131149.3+423910	13.3	82(10)	13 11 49.382 (0.010)	42 39 10.17 (0.10)	1.2	< 0.5	85	Ge	25.6	23.2
N214	J131149.5+423906	4.5	32(10)	13 11 49.583 (0.023)	42 39 06.63 (0.31)	< 1.1			Gc	24.8	22.8
215	J131149.6+423212	6.4	56(14)	13 11 49.646 (0.019)	42 32 12.96 (0.14)	2.1	< 0.8	101	Ge	25.2	23.4
N216	J131150.1+424331	4.4	26(12)	13 11 50.132 (0.026)	42 43 31.12 (0.21)	< 2.1			U	> 26.4	> 25.6
217	J131150.2+424355	6.3	42(10)	13 11 50.228 (0.011)	42 43 55.05 (0.11)	< 1.2			F	25.7	24.5
N218	J131150.3+423923	4.6	103(27)	13 11 50.333 (0.044)	42 39 23.33 (0.33)	4.4			B2	23.9	21.7
A		4.6	35(10)	13 11 50.250 (0.013)	42 39 23.80 (0.12)	< 1.2				23.9	21.7
B		3.2	68(23)	13 11 50.432 (0.045)	42 39 22.80 (0.50)	3.5	3.0	90		23.6	23.1
N219	J131150.5+422746	4.8	50(15)	13 11 50.544 (0.017)	42 27 46.85 (0.16)	< 1.6			F		23.6
220	J131150.5+424157	7.0	47(12)	13 11 50.579 (0.012)	42 41 57.18 (0.15)	< 1.5			Gc	23.9	21.9
221	J131150.9+424407	16.9	122(12)	13 11 50.975 (0.010)	42 44 07.50 (0.10)	< 0.9			U	> 25.5	> 25.1
N222	J131151.0+423940	4.8	27(10)	13 11 51.002 (0.018)	42 39 40.84 (0.18)	< 1.6			Gc	24.4	22.9
223	J131151.0+424820	7.0	88(15)	13 11 51.086 (0.020)	42 48 20.93 (0.30)	2.8			Be	23.7	22.4
224	J131151.1+424121	12.1	74(10)	13 11 51.140 (0.010)	42 41 21.47 (0.10)	< 1.0			Bc	25.1	23.1
225	J131151.3+423530	6.4	38(11)	13 11 51.330 (0.014)	42 35 30.33 (0.14)	< 1.4			Gc	25.1	23.1
226	J131151.3+424137	16.7	150(13)	13 11 51.379 (0.010)	42 41 37.66 (0.10)	1.5			Be	23.2	21.5
227	J131151.4+423159	6.9	47(12)	13 11 51.449 (0.012)	42 31 59.22 (0.14)	< 1.4			Gc	24.8	22.4
228	J131151.5+423653	5.8	39(11)	13 11 51.539 (0.015)	42 36 53.23 (0.14)	< 1.5			Bc	25.4	25.0
229	J131151.9+424431	5.7	40(11)	13 11 51.974 (0.013)	42 44 31.05 (0.14)	< 1.2			U ?		24.4
N230	J131152.0+424228	4.9	34(13)	13 11 52.046 (0.023)	42 42 28.70 (0.20)	< 2.0			Bc	25.7	23.7
231	J131152.3+424808	9.1	83(12)	13 11 52.311 (0.010)	42 48 08.14 (0.10)	< 0.8			Bc	19.2	18.1
N232	J131152.3+423952	5.1	54(17)	13 11 52.321 (0.033)	42 39 52.07 (0.25)	3.0	< 1.8	84	Be	23.8	21.8
233	J131152.3+423201	34.0	241(11)	13 11 52.323 (0.010)	42 32 01.11 (0.10)	1.0	< 0.3	109	Ge	24.2	22.3
234	J131152.4+423014	6.1	88(18)	13 11 52.492 (0.019)	42 30 14.69 (0.16)	2.6	< 1.3	53	F ?	> 25.2	24.5
235	J131152.7+423007	99.9	1452(32)	13 11 52.702 (0.010)	42 30 07.73 (0.10)	< 0.8			U	> 26.4	> 25.2
236	J131153.1+423026	6.4	49(12)	13 11 53.135 (0.011)	42 30 26.83 (0.13)	< 0.9			Gc?	20.4	19.6
237	J131153.1+423129	10.3	90(13)	13 11 53.162 (0.010)	42 31 29.40 (0.10)	1.6	< 0.6	107	Be	21.1	20.2
238	J131153.1+424126	12.7	80(10)	13 11 53.180 (0.010)	42 41 26.34 (0.10)	1.2	< 0.5	121	Ge	20.1	19.6
239	J131153.4+423415	8.4	45(08)	13 11 53.420 (0.010)	42 34 15.65 (0.10)	1.2	< 0.5	30	Ge?	20.1	19.2

TABLE 2—Continued

(1) No	(2) Source	(3) SNR	(4) S _{1,4}	(5) RA	(6) DEC	(7)	(8) Radio Size	(9)	(10) ROM	(11) r	(12) z
240	J131153.5+424535	6.6	46(14)	13 11 53.529 (0.013)	42 45 35.63 (0.19)	< 1.7			F	26.9	25.4
241	J131153.6+423455	6.0	37(12)	13 11 53.614 (0.013)	42 34 55.18 (0.22)	< 2.1			U	> 26.9	> 25.3
N242	J131153.9+424440	4.9	31(09)	13 11 53.951 (0.014)	42 44 40.91 (0.12)	< 1.0			Gc	23.8	22.2
243	J131153.9+423821	8.9	53(10)	13 11 53.971 (0.010)	42 38 21.59 (0.10)	< 0.8			Gc	24.4	22.3
244	J131154.0+425006	7.6	140(23)	13 11 54.040 (0.055)	42 50 06.11 (0.44)	2.8			C ?	20.2	20.2
A		7.6	93(20)	13 11 54.141 (0.013)	42 50 06.72 (0.15)	< 1.9			S	20.7	20.4
B		4.4	47(11)	13 11 53.971 (0.024)	42 50 04.66 (0.31)	< 1.0			U		
245	J131154.1+423542	5.6	55(15)	13 11 54.104 (0.020)	42 35 42.13 (0.27)	2.6	< 1.5	154	Ge	20.7	19.9
N246	J131154.2+424729	4.6	80(21)	13 11 54.239 (0.028)	42 47 29.99 (0.23)	3.5	< 1.0	61	Ge	23.1	22.3
247	J131154.3+423652	39.8	268(11)	13 11 54.310 (0.010)	42 36 52.38 (0.10)	1.2	0.5	37	F	24.8	24.1
248	J131154.3+424636	7.0	233(44)	13 11 54.366 (0.011)	42 46 36.31 (0.12)	2.7	< 1.0	110	Ge	23.6	22.5
N249	J131154.7+424731	4.9	61(17)	13 11 54.753 (0.023)	42 47 31.42 (0.17)	2.3	< 0.9	105	Be	23.9	23.1
250	J131154.8+424641	8.9	82(14)	13 11 54.871 (0.010)	42 46 41.02 (0.10)	1.6	< 0.7	71	Be	25.7	24.7
N251	J131155.0+424607	4.8	76(19)	13 11 55.021 (0.027)	42 46 07.61 (0.16)	3.3	< 0.9	98	Gd	25.3	25.3
N252	J131155.2+425103	3.6	58(24)	13 11 55.281 (0.026)	42 51 03.63 (0.29)	< 2.3			Gc	23.2	22.3
253	J131155.8+424058	60.1	394(11)	13 11 55.871 (0.010)	42 40 58.77 (0.10)	1.3	< 0.5	30	Be	22.8	21.3
254	J131156.4+424158	6.5	40(09)	13 11 56.483 (0.011)	42 41 58.13 (0.10)	< 1.1			U ?	> 26.6	> 25.2
N255	J131156.6+424203	4.6	25(10)	13 11 56.657 (0.025)	42 42 03.34 (0.16)	< 1.7			F ?	> 26.2	25.2
256	J131156.6+424359	7.9	52(11)	13 11 56.697 (0.010)	42 43 59.20 (0.11)	< 1.1			Gc	23.2	22.5
N257	J131156.7+424416	4.3	55(17)	13 11 56.783 (0.018)	42 44 16.24 (0.14)	2.2	< 0.8	106	Ge?	24.1	22.8
258	J131156.8+423655	6.0	36(10)	13 11 56.837 (0.014)	42 36 55.93 (0.13)	< 1.4			Gc	20.0	19.0
259	J131156.9+424202	6.6	80(17)	13 11 56.927 (0.020)	42 42 02.18 (0.18)	2.6	1.7	100	F	25.8	24.7
260	J131157.1+424138	5.4	41(14)	13 11 57.106 (0.017)	42 41 38.05 (0.20)	< 1.9			Gd	21.9	20.6
261	J131157.2+424129	6.4	36(09)	13 11 57.259 (0.012)	42 41 29.97 (0.10)	< 1.1			Gc	25.5	23.4
262	J131157.5+423910	34.6	183(09)	13 11 57.503 (0.010)	42 39 10.09 (0.10)	< 0.4			Gc	24.8	22.6
263	J131157.6+424412	6.6	71(15)	13 11 57.603 (0.016)	42 44 12.70 (0.15)	2.0	< 1.4	99	Ge?	19.6	18.9
N264	J131157.8+424718	5.1	43(15)	13 11 57.822 (0.017)	42 47 18.56 (0.21)	< 1.9			Bc?	22.6	22.1
265	J131157.8+424643	7.9	64(13)	13 11 57.862 (0.010)	42 46 43.26 (0.11)	< 1.2			Gc	23.6	21.4
266	J131157.8+423022	21.6	263(17)	13 11 57.882 (0.010)	42 50 22.76 (0.10)	0.7	< 0.4	161	Ge?	18.8	17.9
267	J131157.9+423630	99.9	599(09)	13 11 57.911 (0.010)	42 36 30.31 (0.10)	< 0.3			F ?	26.3	24.1
N268	J131158.0+424518	4.8	82(20)	13 11 58.010 (0.030)	42 45 18.50 (0.30)	5.2			Ge?	21.5	20.7
A		4.8	27(10)	13 11 58.059 (0.020)	42 45 17.91 (0.18)	< 1.3			Ge	21.5	20.7
B		3.2	29(12)	13 11 57.803 (0.042)	42 45 19.48 (0.36)	2.8	1.5	114			
C		3.0	26(12)	13 11 58.228 (0.049)	42 45 18.95 (0.36)	3.0	1.0	70			
269	J131158.1+423722	6.8	58(13)	13 11 58.154 (0.016)	42 37 22.10 (0.17)	2.4	< 1.1	49	Be	23.6	23.0
270	J131158.3+424141	16.0	89(09)	13 11 58.394 (0.010)	42 41 41.18 (0.10)	< 0.6			Gc	25.0	24.3
271	J131158.5+423244	7.1	44(09)	13 11 58.546 (0.011)	42 32 44.78 (0.10)	< 1.2			Gd	24.3	22.2
272	J131158.7+423754	8.1	74(13)	13 11 58.769 (0.012)	42 37 54.39 (0.13)	2.0	1.2	37	Ge	19.6	18.7
N273	J131159.2+424517	4.9	44(16)	13 11 59.281 (0.022)	42 45 17.41 (0.20)	< 2.2			U	> 26.6	> 25.3
274	J131159.2+422444	21.8	304(20)	13 11 59.295 (0.010)	42 24 44.90 (0.10)	< 0.9			su	> 23	> 22
N275	J131159.3+422827	4.8	37(12)	13 11 59.335 (0.015)	42 28 27.30 (0.16)	< 1.1			F ?		24.2
276	J131159.3+423928	17.6	86(08)	13 11 59.351 (0.010)	42 39 28.46 (0.10)	< 0.5			Gc	24.2	22.4
277	J131159.3+423915	9.7	67(11)	13 11 59.375 (0.010)	42 39 15.75 (0.10)	1.4	< 1.0	139	Ge	19.7	19.0
278	J131159.5+424736	10.6	93(14)	13 11 59.576 (0.010)	42 47 36.91 (0.10)	< 1.2			Gc	24.4	22.9
279	J131159.5+424616	6.3	103(22)	13 11 59.590 (0.022)	42 46 16.66 (0.21)	3.1	1.5	60	Be	21.6	20.4
N280	J131159.6+424154	4.6	27(12)	13 11 59.635 (0.018)	42 41 54.61 (0.30)	< 2.1			Bc?	24.4	22.8
281	J131159.6+423541	5.6	35(11)	13 11 59.653 (0.017)	42 35 41.96 (0.16)	1.8	1.0	124	Ge	21.1	19.8
N282	J131200.0+424012	5.3	59(15)	13 12 00.011 (0.024)	42 40 12.23 (0.19)	2.8	< 1.4	111	Ge	20.2	19.5
283	J131200.0+424806	31.6	313(14)	13 12 00.029 (0.010)	42 48 06.58 (0.10)	1.1	< 0.4	158	Ge	21.7	20.2
284	J131200.2+424037	7.1	42(10)	13 12 00.216 (0.011)	42 40 37.46 (0.10)	< 1.2			U	> 26.6	> 25.6
285	J131200.2+425209	12.2	274(33)	13 12 00.230 (0.030)	42 52 09.55 (0.22)	3.7			B2	24.6	23.2
A		12.2	205(24)	13 12 00.261 (0.010)	42 52 09.10 (0.10)	< 1.5				25.1	23.5
B		4.8	69(24)	13 12 00.007 (0.023)	42 52 11.50 (0.23)	< 2.2				24.6	23.2
286	J131200.2+422846	16.8	204(19)	13 12 00.250 (0.030)	42 28 46.71 (0.23)	3.5			B2		21.5
A		16.8	52(13)	13 12 00.221 (0.010)	42 28 46.59 (0.19)	< 1.7					22.6
B		5.0	152(13)	13 12 00.284 (0.011)	42 28 46.88 (0.10)	3.0	1.5	93			21.5
287	J131200.5+424553	10.3	80(12)	13 12 00.570 (0.010)	42 45 53.80 (0.10)	< 1.0			Gc	22.0	20.3
288	J131200.6+422746	5.9	48(13)	13 12 00.687 (0.016)	42 27 46.08 (0.13)	< 1.6			Gc		19.5
289	J131201.1+424350	8.8	99(16)	13 12 01.157 (0.013)	42 43 50.47 (0.12)	2.6	< 1.1	95	Ge	19.6	18.9
290	J131201.1+424208	6.0	59(16)	13 12 01.172 (0.024)	42 42 08.39 (0.28)	3.2	< 1.4	42	Ge	24.2	23.0
291	J131201.3+423935	12.5	82(11)	13 12 01.349 (0.010)	42 39 35.72 (0.10)	1.2	< 0.9	13	Be	20.8	20.0
292	J131201.4+423050	7.4	120(21)	13 12 01.437 (0.025)	42 30 50.54 (0.13)	4.4	< 0.8	100	Ge	21.2	20.5
293	J131201.5+423331	99.9	2870(59)	13 12 01.545 (0.010)	42 33 31.79 (0.10)	1.2	< 0.4	118	Be	23.4	21.5

TABLE 2—Continued

(1) No	(2) Source	(3) SNR	(4) S _{1.4}	(5) RA	(6) DEC	(7) Radio Size	(8)	(9)	(10) ROM	(11) r	(12) z
294	J131201.8+424950	13.2	146(17)	13 12 01.852 (0.010)	42 49 50.87 (0.10)	< 1.4			Bc?	24.6	24.0
295	J131202.1+424807	16.6	155(14)	13 12 02.179 (0.010)	42 48 07.19 (0.10)	< 1.0			Gd?	21.9	21.0
296	J131202.4+423804	6.3	34(09)	13 12 02.415 (0.011)	42 38 04.87 (0.13)	< 1.1			Bc	23.6	22.0
N297	J131202.4+424002	4.9	49(13)	13 12 02.470 (0.018)	42 40 02.33 (0.25)	2.8	< 1.0	15	Be	23.6	22.2
298	J131202.5+424750	16.6	142(12)	13 12 02.521 (0.010)	42 47 50.37 (0.10)	< 0.7			Bc	20.5	19.4
299	J131202.6+423833	6.0	44(12)	13 12 02.671 (0.014)	42 38 33.93 (0.15)	< 1.4			S ?	21.6	20.8
N300	J131202.8+423303	4.5	24(09)	13 12 02.802 (0.013)	42 33 03.98 (0.22)	< 1.6			F	26.1	24.2
301	J131203.0+424030	67.4	379(09)	13 12 03.087 (0.010)	42 40 30.62 (0.10)	0.6	< 0.4	73	Ge	24.9	23.4
N302	J131203.0+425042	4.7	45(14)	13 12 03.092 (0.015)	42 50 42.01 (0.20)	< 1.3			Bc	23.0	21.1
303	J131203.1+423715	8.0	63(12)	13 12 03.128 (0.012)	42 37 15.83 (0.12)	2.0	< 0.9	53	Ge	23.5	21.5
304	J131203.1+423050	16.8	458(29)	13 12 03.165 (0.010)	42 30 50.31 (0.10)	20.0	5.0	75	EG	22.8	21.0
305	J131203.2+425119	6.9	102(22)	13 12 03.205 (0.014)	42 51 19.62 (0.16)	< 2.1			Gc	25.6	23.6
306	J131203.2+423747	6.6	34(08)	13 12 03.233 (0.010)	42 37 47.33 (0.11)	< 1.1			U	> 26.3	> 25.4
307	J131203.3+424525	7.2	74(15)	13 12 03.226 (0.015)	42 45 25.22 (0.15)	1.7	< 1.7	95	Ge	19.6	18.5
308	J131203.5+423331	99.9	1580(31)	13 12 03.515 (0.010)	42 33 31.55 (0.10)	1.6	0.3	96	Ge	23.2	21.8
N309	J131203.5+423748	3.8	27(10)	13 12 03.555 (0.027)	42 37 48.37 (0.36)	< 1.5			Gc	24.5	22.8
310	J131203.6+424746	19.1	266(18)	13 12 03.601 (0.033)	42 47 46.07 (0.17)	3.5			B2	19.6	18.8
A		19.1	168(13)	13 12 03.695 (0.010)	42 47 46.31 (0.10)	< 0.9				19.6	18.8
B		11.7	98(12)	13 12 03.421 (0.010)	42 47 45.83 (0.10)	< 0.7				22.6	21.3
311	J131203.6+425058	6.8	74(15)	13 12 03.699 (0.010)	42 50 58.68 (0.12)	< 1.0			Gc	22.8	20.9
312	J131203.7+422805	6.4	55(12)	13 12 03.738 (0.010)	42 28 05.91 (0.11)	< 1.0			F		23.9
313	J131203.7+422434	6.1	84(20)	13 12 03.768 (0.015)	42 24 34.96 (0.15)	< 1.7			su	> 23	> 22
N314	J131203.7+424900	5.2	138(35)	13 12 03.781 (0.039)	42 49 00.87 (0.28)	4.4	< 2.2	79	Be?	19.4	18.8
315	J131203.7+424644	29.7	302(27)	13 12 03.794 (0.016)	42 46 44.46 (0.33)	3.4			B2?	21.9	20.5
A		29.7	239(13)	13 12 03.808 (0.010)	42 46 44.02 (0.10)	< 0.9				21.9	20.5
B		5.6	63(15)	13 12 03.715 (0.015)	42 46 46.64 (0.18)	2.0	< 1.0	48		23.4	21.8
316	J131203.8+424637	6.2	59(14)	13 12 03.854 (0.016)	42 46 37.20 (0.16)	2.3	< 0.8	54	Ge	23.6	21.7
317	J131203.9+423506	5.4	78(19)	13 12 03.925 (0.023)	42 35 06.04 (0.28)	3.1	2.1	34	Ge	22.6	21.4
318	J131203.9+423044	8.0	53(10)	13 12 03.925 (0.011)	42 30 44.74 (0.10)	< 1.2			Bc	24.8	22.6
N319	J131203.9+423211	4.9	58(20)	13 12 03.947 (0.036)	42 32 11.85 (0.36)	3.5	< 1.9	53	Be?	21.9	20.8
320	J131203.9+424338	6.5	51(12)	13 12 03.972 (0.016)	42 43 38.66 (0.10)	2.1	< 0.7	100	Ge	22.1	21.0
N321	J131204.5+422253	5.6	83(22)	13 12 04.526 (0.015)	42 22 53.42 (0.18)	< 1.3			sg	22.1	20.8
322	J131204.9+424317	9.1	95(16)	13 12 04.914 (0.012)	42 43 17.50 (0.17)	2.6	1.5	155	Be	20.4	19.4
323	J131204.9+423055	7.5	48(11)	13 12 04.935 (0.011)	42 30 55.58 (0.13)	< 1.1			U	> 27.0	> 25.6
N324	J131204.9+422158	99.9	13800(280)	13 12 04.969 (0.010)	42 21 58.43 (0.10)	1.2			su	> 23	> 22
325	J131205.3+423209	5.4	73(21)	13 12 05.317 (0.037)	42 32 09.39 (0.29)	3.9	< 1.8	114	Ge	21.7	20.5
N326	J131205.4+422729	5.3	50(15)	13 12 05.490 (0.015)	42 27 29.72 (0.19)	< 1.3			Gc		22.5
327	J131205.4+422434	5.9	92(24)	13 12 05.492 (0.018)	42 24 34.47 (0.17)	< 2.2			su	> 23	> 22
N328	J131205.5+424221	4.9	29(09)	13 12 05.510 (0.014)	42 42 21.83 (0.11)	< 1.2			Bc	25.3	23.9
329	J131205.5+423305	11.4	68(09)	13 12 05.551 (0.010)	42 33 05.19 (0.10)	< 0.8			Bc	24.7	23.5
330	J131205.6+424718	23.9	207(15)	13 12 05.660 (0.030)	42 47 18.38 (0.20)	4.1			B2?	22.4	21.0
A		23.9	135(06)	13 12 05.759 (0.010)	42 47 18.44 (0.10)	1.1				22.9	21.1
B		5.7	72(13)	13 12 05.467 (0.018)	42 47 18.30 (0.24)	2.0	0.9	87		22.4	21.0
331	J131205.7+423852	8.9	50(10)	13 12 05.711 (0.010)	42 38 52.84 (0.10)	< 1.2			Bc	26.2	24.1
332	J131205.7+423007	56.1	408(11)	13 12 05.725 (0.010)	42 30 07.59 (0.10)	< 0.8			Gc		21.0
N333	J131205.8+422252	12.7	223(24)	13 12 05.869 (0.010)	42 22 52.43 (0.10)	< 1.3			su	> 23	> 22
334	J131205.9+422456	6.4	78(18)	13 12 05.995 (0.013)	42 24 56.88 (0.15)	< 1.6			su	> 23	> 22
335	J131206.2+424709	57.2	512(20)	13 12 06.244 (0.010)	42 47 09.12 (0.32)	3.4			B2?	21.9	20.6
A		57.2	435(12)	13 12 06.270 (0.010)	42 47 08.88 (0.10)	0.7	< 0.3	161		21.9	20.6
B		7.3	77(15)	13 12 06.080 (0.013)	42 47 11.51 (0.12)	2.3	< 0.7	61		23.0	21.0
336	J131206.3+422838	6.2	53(15)	13 12 06.320 (0.015)	42 28 38.81 (0.16)	< 1.8			Gc		21.3
337	J131206.4+424126	8.0	52(12)	13 12 06.439 (0.015)	42 41 26.72 (0.13)	2.0	< 0.8	114	Be	17.2	16.2
338	J131206.4+422932	7.7	65(14)	13 12 06.451 (0.011)	42 29 32.18 (0.13)	< 1.5			Gc	22.1	20.6
N339	J131206.5+424141	4.7	24(10)	13 12 06.544 (0.021)	42 41 41.91 (0.19)	< 1.7			Gc	21.2	20.0
N340	J131206.5+424532	3.9	41(15)	13 12 06.572 (0.028)	42 45 32.58 (0.32)	< 3.2			Gc?	22.4	21.0
341	J131206.6+423703	8.5	45(09)	13 12 06.619 (0.010)	42 37 03.85 (0.10)	< 1.0			Bc	23.0	21.4
N342	J131206.7+424013	4.9	63(19)	13 12 06.788 (0.033)	42 40 13.19 (0.33)	3.2	2.1	0	Ge	18.4	17.9
343	J131207.0+424308	6.9	40(10)	13 12 07.065 (0.010)	42 43 08.56 (0.13)	< 1.3			Gc	22.9	21.2
344	J131207.0+422910	6.0	60(18)	13 12 07.098 (0.031)	42 29 10.07 (0.22)	2.5	1.5	106	Ge	24.0	22.3
345	J131207.1+422934	5.8	83(20)	13 12 07.110 (0.021)	42 29 34.98 (0.21)	2.9	2.3	50	Gd	21.8	20.1
346	J131207.2+423202	7.4	150(28)	13 12 07.288 (0.020)	42 32 02.44 (0.30)	5.1			B2?	25.7	24.5
A		7.4	101(14)	13 12 07.325 (0.014)	42 32 01.84 (0.19)	3.4	2.2	116		26.2	25.1
B		5.2	49(10)	13 12 07.135 (0.020)	42 32 03.82 (0.27)	1.9	0.8	0		25.7	24.5

TABLE 2—Continued

(1) No	(2) Source	(3) SNR	(4) S _{1,4}	(5) RA	(6) DEC	(7)	(8) Radio Size	(9)	(10) ROM	(11) r	(12) z
347	J131207.3+422454	5.9	80(22)	13 12 07.307 (0.017)	42 24 54.43 (0.17)	< 1.9			su	> 23	> 22
348	J131207.4+424236	7.3	44(10)	13 12 07.424 (0.011)	42 42 36.05 (0.10)	< 1.8	< 1.0	87	Be	22.7	21.3
N349	J131207.6+423147	5.3	45(13)	13 12 07.631 (0.025)	42 31 47.62 (0.13)	2.8	< 0.8	92	Ge	23.3	21.9
350	J131207.6+424522	8.7	54(10)	13 12 07.637 (0.010)	42 45 22.53 (0.10)	< 1.0			F ?	> 24.6	23.5
351	J131207.7+423944	9.1	61(10)	13 12 07.737 (0.010)	42 39 44.92 (0.10)	1.5	< 0.7	125	F	24.0	23.1
352	J131208.0+424009	8.4	41(09)	13 12 08.062 (0.010)	42 40 09.16 (0.11)	< 0.9			U	> 25.8	> 25.7
N353	J131208.0+423609	4.4	77(20)	13 12 08.076 (0.033)	42 36 09.88 (0.33)	3.8			C ?		
A		4.4	23(09)	13 12 08.088 (0.027)	42 36 10.89 (0.14)	< 2.4			Gd	> 25.9	25.0
B		3.9	54(17)	13 12 08.054 (0.027)	42 36 8.20 (0.32)	2.8	1.6	138	Ge	25.3	24.3
N354	J131208.0+422939	5.2	37(11)	13 12 08.081 (0.013)	42 29 39.82 (0.16)	< 1.3			F		24.0
N355	J131208.1+424007	4.1	22(08)	13 12 08.172 (0.018)	42 40 07.56 (0.20)	< 1.5			Gc	24.8	24.2
N356	J131208.3+422644	4.9	52(16)	13 12 08.358 (0.014)	42 26 44.28 (0.20)	< 1.7			Gd		19.9
N357	J131208.3+424144	5.1	37(15)	13 12 08.367 (0.027)	42 41 44.77 (0.23)	2.5	< 1.3	120	Gd	23.4	22.4
358	J131208.4+423527	8.1	42(09)	13 12 08.439 (0.010)	42 35 27.92 (0.11)	< 1.1			U	> 26.6	> 25.6
359	J131208.5+424832	13.1	127(16)	13 12 08.529 (0.010)	42 48 32.40 (0.10)	< 1.3			F ?	25.6	24.4
360	J131208.6+424536	5.5	47(13)	13 12 08.602 (0.014)	42 45 36.71 (0.19)	1.8	< 0.8	142	U ?		
361	J131208.6+424305	7.1	87(16)	13 12 08.610 (0.030)	42 43 05.98 (0.33)	2.6			B2	21.9	20.5
A		7.1	47(12)	13 12 08.683 (0.015)	42 43 05.77 (0.20)	< 1.0				22.9	21.9
B		6.8	40(12)	13 12 08.512 (0.016)	42 43 06.30 (0.21)	< 1.0				21.9	20.5
362	J131208.8+424129	12.9	73(10)	13 12 08.819 (0.010)	42 41 29.23 (0.10)	< 1.0			Gc	24.7	23.3
363	J131209.0+424217	30.1	172(09)	13 12 09.075 (0.010)	42 42 17.26 (0.10)	< 0.6			Gc	24.3	22.7
N364	J131209.1+425413	8.9	249(38)	13 12 09.154 (0.013)	42 54 13.97 (0.19)	2.0	< 1.2	121	Ge	21.3	20.0
365	J131209.1+425110	10.9	140(20)	13 12 09.159 (0.010)	42 51 10.37 (0.10)	< 1.3			Gc	25.0	23.6
N366	J131209.4+423113	5.2	34(11)	13 12 09.426 (0.018)	42 31 13.24 (0.15)	< 1.5			F	25.5	24.0
367	J131209.6+424249	13.9	76(09)	13 12 09.608 (0.010)	42 42 49.92 (0.10)	< 0.7			Gc	23.6	21.2
368	J131209.6+422946	5.7	83(21)	13 12 09.663 (0.025)	42 29 46.64 (0.25)	2.5	2.1	90	U	> 25.9	> 25.6
N369	J131209.6+422250	7.1	193(34)	13 12 09.691 (0.014)	42 22 50.53 (0.23)	2.5	1.4	21	su	> 23	> 22
370	J131209.7+422930	6.3	46(11)	13 12 09.761 (0.011)	42 29 30.16 (0.13)	< 1.2			F		23.6
371	J131210.0+423010	37.4	269(12)	13 12 10.067 (0.010)	42 30 10.01 (0.10)	< 0.8			Gc	23.3	21.5
372	J131210.5+423146	15.2	117(12)	13 12 10.582 (0.010)	42 31 46.78 (0.10)	1.7	< 0.5	85	Be	20.5	19.4
373	J131210.5+424735	5.5	46(14)	13 12 10.590 (0.014)	42 47 35.42 (0.19)	< 1.7			U	> 26.4	> 25.4
N374	J131210.7+425025	5.3	69(20)	13 12 10.780 (0.016)	42 50 25.22 (0.21)	< 2.0			Gc	19.8	18.9
375	J131210.8+422331	99.9	1737(41)	13 12 10.839 (0.010)	42 23 31.25 (0.10)	1.0	0.4	2	su	> 23	> 22
N376	J131210.8+422120	5.4	107(32)	13 12 10.897 (0.017)	42 21 20.00 (0.27)	< 2.4			su	> 23	> 22
377	J131211.0+424053	99.9	2102(58)	13 12 11.023 (0.010)	42 40 53.50 (0.10)	< 0.7			Bc	22.3	20.4
N378	J131211.0+423129	4.9	51(15)	13 12 11.040 (0.029)	42 31 29.72 (0.18)	3.1	< 0.9	102	Be	21.6	20.9
379	J131211.1+423623	7.3	56(11)	13 12 11.192 (0.016)	42 36 23.87 (0.10)	2.4	< 0.7	88	Ge	24.4	23.8
380	J131211.3+424106	7.6	59(10)	13 12 11.371 (0.014)	42 41 06.36 (0.19)	1.6	1.1	155	Ge	23.0	21.4
N381	J131211.4+423005	4.9	36(13)	13 12 11.493 (0.021)	42 30 05.16 (0.17)	< 1.9			Gc	21.8	20.9
382	J131211.6+423050	7.5	83(16)	13 12 11.604 (0.014)	42 30 50.43 (0.15)	2.1	< 1.4	123	Ge	21.2	19.9
N383	J131211.8+422202	5.6	95(32)	13 12 11.856 (0.023)	42 22 02.54 (0.29)	< 3.1			sg	21.4	20.4
384	J131211.9+424656	8.8	64(11)	13 12 11.987 (0.010)	42 46 56.99 (0.10)	< 0.7			Gc	25.6	24.0
385	J131212.1+422543	16.4	253(25)	13 12 12.194 (0.010)	42 25 43.33 (0.22)	5.5			C ?		
A		16.4	199(19)	13 12 12.161 (0.010)	42 25 42.92 (0.10)	< 1.5			Gc		22.6
B		5.1	54(18)	13 12 12.406 (0.015)	42 25 46.22 (0.25)	< 1.9			Gc		22.6
N386	J131212.6+424503	4.4	36(17)	13 12 12.613 (0.027)	42 45 03.68 (0.35)	< 2.7			U ?	> 26.5	> 25.8
387	J131212.6+424422	15.6	97(11)	13 12 12.693 (0.010)	42 44 22.54 (0.10)	< 1.0			U	> 26.5	> 25.6
N388	J131212.7+423223	4.5	27(10)	13 12 12.728 (0.017)	42 32 23.57 (0.16)	< 1.3			Gc	21.1	20.0
389	J131212.8+424401	9.3	55(10)	13 12 12.830 (0.010)	42 44 01.10 (0.10)	< 1.0			Gc	> 26.2	> 25.7
390	J131212.8+424806	7.4	66(14)	13 12 12.899 (0.011)	42 48 06.56 (0.12)	< 1.3			Gc?	23.5	22.0
N391	J131212.9+424459	5.2	36(11)	13 12 12.964 (0.016)	42 44 59.47 (0.12)	< 1.4			U ?	> 26.5	> 25.8
392	J131213.0+423114	18.1	137(12)	13 12 13.025 (0.010)	42 31 14.38 (0.10)	1.2	< 0.8	104	Be	24.7	22.3
393	J131213.1+423555	7.2	49(11)	13 12 13.142 (0.013)	42 35 55.44 (0.16)	1.9	< 1.0	30	Be	20.3	19.5
394	J131213.4+424129	9.6	51(09)	13 12 13.425 (0.010)	42 41 29.27 (0.10)	< 0.9			Gc	19.8	18.9
395	J131213.8+423706	8.8	47(09)	13 12 13.864 (0.010)	42 37 06.66 (0.10)	< 1.3			F	25.2	25.0
396	J131214.2+424225	5.4	33(13)	13 12 14.272 (0.018)	42 42 25.82 (0.27)	< 2.3			Gc	23.5	22.1
397	J131214.5+423324	64.3	390(10)	13 12 14.506 (0.010)	42 33 24.86 (0.10)	1.0	< 0.4	76	Ge	19.0	18.0
398	J131214.5+423821	8.5	59(11)	13 12 14.564 (0.013)	42 38 21.79 (0.11)	1.9	< 1.0	79	Be	23.0	21.8
399	J131214.8+422733	6.9	81(17)	13 12 14.825 (0.013)	42 27 33.39 (0.18)	1.6	< 1.3	140	F		23.1
N400	J131215.1+423702	4.4	34(13)	13 12 15.171 (0.017)	42 37 02.25 (0.22)	< 1.5			Gc?	20.5	19.9
401	J131215.2+424637	92.2	710(12)	13 12 15.243 (0.010)	42 46 37.56 (0.10)	< 0.7			Gc	20.6	19.3
402	J131215.2+422459	14.4	184(19)	13 12 15.265 (0.010)	42 24 59.38 (0.10)	< 1.2			sg	18.7	17.6
403	J131215.2+423900	8.4	84(14)	13 12 15.269 (0.014)	42 39 00.86 (0.12)	2.5	1.4	86	S ?	18.4	18.1

TABLE 2—Continued

(1) No	(2) Source	(3) SNR	(4) $S_{1.4}$	(5) RA	(6) DEC	(7) Radio Size	(8)	(9)	(10) ROM	(11) r	(12) z
404	J131215.2+425111	6.3	143(26)	13 12 15.272 (0.015)	42 51 11.72 (0.20)	2.8	< 1.4	46	Be	25.7	23.8
N405	J131215.2+422234	9.7	190(29)	13 12 15.290 (0.010)	42 22 34.79 (0.12)	< 2.1			sg	20.0	19.0
406	J131215.4+423253	8.3	43(09)	13 12 15.493 (0.010)	42 32 53.25 (0.10)	< 0.6			Gc	23.9	22.3
407	J131216.0+423913	5.9	38(11)	13 12 16.042 (0.015)	42 39 13.24 (0.13)	1.8	0.9	120	F ?	25.5	24.8
408	J131216.0+423921	28.2	156(09)	13 12 16.085 (0.010)	42 39 21.64 (0.10)	0.6			U	> 26.5	> 25.4
409	J131216.0+424926	8.5	94(17)	13 12 16.094 (0.010)	42 49 26.24 (0.13)	< 1.5			Bc?	22.4	21.7
410	J131216.1+423215	7.3	44(09)	13 12 16.188 (0.010)	42 32 15.92 (0.10)	< 1.0			Bc	23.0	21.4
411	J131216.3+423452	7.0	42(10)	13 12 16.338 (0.010)	42 34 52.25 (0.15)	1.7	< 0.7	15	Ge	23.4	21.7
412	J131216.4+424833	7.7	81(16)	13 12 16.407 (0.012)	42 48 33.13 (0.15)	2.3	< 0.7	46	S ?	19.3	18.1
413	J131216.7+423356	8.0	67(13)	13 12 16.787 (0.010)	42 33 56.33 (0.16)	2.2	< 1.0	179	Ge?	22.3	23.4
414	J131217.1+423912	12.7	72(09)	13 12 17.182 (0.010)	42 39 12.27 (0.10)	1.1	< 0.5	165	Be	20.8	19.9
415	J131217.5+423930	13.0	68(09)	13 12 17.560 (0.010)	42 39 30.22 (0.10)	< 0.9			F	26.3	24.9
416	J131217.5+423058	38.0	241(10)	13 12 17.575 (0.010)	42 30 58.87 (0.10)	0.7	< 0.3	88	S ?	20.1	20.1
N417	J131217.6+423645	5.2	46(12)	13 12 17.670 (0.023)	42 36 45.72 (0.22)	2.3			F	25.6	24.4
418	J131217.6+423506	6.0	48(13)	13 12 17.647 (0.027)	42 35 06.08 (0.17)	3.5	< 0.8	68	Ge?		23.2
419	J131217.6+424829	19.4	183(14)	13 12 17.664 (0.010)	42 48 29.49 (0.10)	< 1.1			S ?	17.6	18.1
420	J131218.0+424344	80.8	465(10)	13 12 18.088 (0.010)	42 43 44.92 (0.10)	< 0.5			Bc	19.6	18.6
421	J131218.1+424742	8.0	64(12)	13 12 18.151 (0.010)	42 47 42.29 (0.10)	< 0.9			U	> 26.5	> 25.5
422	J131218.1+422656	8.5	85(15)	13 12 18.151 (0.010)	42 26 56.60 (0.10)	< 1.2			F		23.8
N423	J131218.2+424318	4.9	63(18)	13 12 18.248 (0.028)	42 43 18.21 (0.27)	2.8	1.8	114	Gd	19.8	18.9
424	J131218.2+423908	9.6	50(10)	13 12 18.295 (0.010)	42 39 08.86 (0.10)	< 1.2			Bc	24.9	24.6
425	J131218.4+423843	19.4	122(10)	13 12 18.407 (0.010)	42 38 43.86 (0.10)	1.1	0.8	24	Be	21.9	20.5
N426	J131218.6+423114	4.6	33(11)	13 12 18.684 (0.018)	42 31 14.99 (0.15)	< 1.4			Bc	23.7	22.7
427	J131218.7+424034	6.6	34(08)	13 12 18.746 (0.011)	42 40 34.86 (0.10)	< 0.9			Ge	22.3	21.3
428	J131219.0+423339	15.2	98(10)	13 12 19.020 (0.010)	42 33 39.32 (0.10)	< 0.9			Gc	21.7	19.9
429	J131219.3+424856	10.6	116(15)	13 12 19.384 (0.033)	42 48 56.68 (0.11)	2.1			Ge		
430	J131219.5+423833	6.8	55(12)	13 12 19.596 (0.017)	42 38 33.00 (0.12)	2.4	< 1.0	94	Ge	21.3	20.6
431	J131219.8+423608	17.7	157(10)	13 12 19.898 (0.010)	42 36 08.95 (0.22)	3.5			C ?	22.9	21.8
A		17.7	107(06)	13 12 19.759 (0.010)	42 36 09.32 (0.10)	1.1	0.4	135	Be	22.9	21.8
B		9.1	50(06)	13 12 20.068 (0.011)	42 36 07.58 (0.15)	< 1.0			Bc	22.9	21.8
432	J131219.9+423924	9.9	50(08)	13 12 19.977 (0.010)	42 39 24.34 (0.10)	< 0.7			U	> 26.4	> 25.5
433	J131220.1+423704	14.2	84(10)	13 12 20.178 (0.010)	42 37 04.20 (0.10)	1.2	< 0.5	112	U	> 26.5	> 25.4
434	J131220.2+424029	8.3	53(10)	13 12 20.252 (0.010)	42 40 29.49 (0.14)	1.9	< 0.7	169	F ?	25.1	23.0
435	J131220.6+423109	7.8	87(16)	13 12 20.624 (0.014)	42 31 09.84 (0.14)	2.2	1.1	67	C ?	23.6	22.7
436	J131220.9+424753	6.5	126(24)	13 12 20.905 (0.014)	42 47 53.51 (0.28)	4.0	1.2	15	U	> 26.7	> 25.6
437	J131220.9+423535	11.0	74(11)	13 12 20.924 (0.010)	42 35 35.75 (0.10)	1.4	< 0.9	166	F	25.4	23.5
N438	J131220.9+423923	4.9	100(31)	13 12 20.993 (0.032)	42 39 23.70 (0.34)	4.2	2.5	118	Ge?	19.1	18.3
N439	J131221.0+424205	4.2	27(09)	13 12 21.099 (0.025)	42 42 05.37 (0.33)	< 1.2			Gc	23.1	21.6
N440	J131221.1+423240	5.2	38(15)	13 12 21.148 (0.020)	42 32 40.58 (0.27)	2.3			Ge	22.3	20.9
N441	J131221.2+424723	4.4	74(28)	13 12 21.288 (0.050)	42 47 23.04 (0.50)	4.2			B2	21.8	20.7
A		4.4	46(20)	13 12 21.220 (0.031)	42 47 21.81 (0.27)	< 2.7				21.8	20.7
B		2.4	28(14)	13 12 21.380 (0.034)	42 47 25.35 (0.22)	< 2.2				22.7	21.8
N442	J131221.2+423723	3.8	71(22)	13 12 21.293 (0.036)	42 37 23.22 (0.38)	3.1			Ge?	19.2	18.5
443	J131221.3+423616	7.4	74(15)	13 12 21.301 (0.033)	42 36 16.58 (0.22)	2.4			Ge?	21.0	20.1
A		7.4	41(10)	13 12 21.239 (0.013)	42 36 16.85 (0.10)	< 1.6			Gc	21.0	20.1
B		4.1	33(08)	13 12 21.494 (0.026)	42 36 16.11 (0.34)	< 1.0			Gd		
444	J131221.3+423507	11.0	57(08)	13 12 21.349 (0.010)	42 35 07.22 (0.10)	< 0.8			Gc	24.2	22.2
445	J131221.3+424423	58.4	373(10)	13 12 21.384 (0.010)	42 44 23.37 (0.10)	0.9	< 0.3	92	Ge	21.6	20.4
446	J131221.4+424808	99.9	3020(60)	13 12 21.430 (0.010)	42 48 08.84 (0.10)	12.0	3.0	10	EG?	20.6	18.9
447	J131221.5+424202	13.9	120(13)	13 12 21.516 (0.010)	42 42 02.77 (0.10)	1.9	1.4	108	Ge	21.5	20.5
448	J131221.8+423827	10.3	95(13)	13 12 21.831 (0.010)	42 38 27.36 (0.10)	2.2	1.1	124	Be	22.7	22.0
449	J131221.9+422816	13.4	116(14)	13 12 21.960 (0.010)	42 28 16.76 (0.10)	< 1.1			F ?		23.9
N450	J131222.3+423814	5.2	29(10)	13 12 22.344 (0.014)	42 38 14.14 (0.17)	< 1.3			S ?	21.0	20.0
451	J131222.4+422832	5.8	92(22)	13 12 22.450 (0.023)	42 28 32.54 (0.25)	3.2	< 1.7	128	Ge		21.8
N452	J131222.6+422610	5.2	54(17)	13 12 22.615 (0.017)	42 26 10.24 (0.20)	< 1.4			F		23.2
453	J131223.2+423907	9.8	110(14)	13 12 23.282 (0.012)	42 39 07.94 (0.10)	2.6	1.4	92	Ge?	21.0	19.6
454	J131223.6+423303	9.3	74(13)	13 12 23.626 (0.012)	42 33 03.29 (0.11)	1.9	< 1.1	90	Ge	25.0	22.9
455	J131223.6+424517	99.9	3670(73)	13 12 23.646 (0.010)	42 45 17.16 (0.10)	1.4	0.5	93	Ge	24.7	22.5
456	J131223.6+424750	28.5	244(13)	13 12 23.646 (0.010)	42 47 50.44 (0.10)	< 0.7			Gc	22.4	20.6
457	J131223.6+423712	19.5	152(12)	13 12 23.690 (0.010)	42 37 12.01 (0.10)	1.9	1.1	98	Be?	19.9	18.9
N458	J131223.9+423434	5.0	25(11)	13 12 23.987 (0.017)	42 34 34.51 (0.25)	< 1.8			Gc	24.6	22.8
459	J131223.9+423525	15.9	97(10)	13 12 23.994 (0.010)	42 35 25.72 (0.10)	1.0	< 0.7	91	Ge	20.0	18.9
460	J131224.3+424323	13.4	76(09)	13 12 24.372 (0.010)	42 43 23.61 (0.10)	< 0.8			F	25.8	24.8

TABLE 2—Continued

(1) No	(2) Source	(3) SNR	(4) S _{1,4}	(5) RA	(6) DEC	(7)	(8) Radio Size	(9)	(10) ROM	(11) r	(12) z
461	J131224.4+424416	7.5	77(15)	13 12 24.421 (0.018)	42 44 16.02 (0.13)	3.1	< 0.8	110	Be?	22.6	21.4
462	J131224.6+422738	5.4	35(14)	13 12 24.730 (0.027)	42 27 37.60 (0.30)	3.1	1.3	40	B2?		21.2
A		5.4	41(08)	13 12 24.680 (0.014)	42 27 36.91 (0.19)	< 1.8					22.5
B		3.8	32(08)	13 12 24.816 (0.018)	42 27 38.66 (0.25)	< 2.5					21.2
463	J131225.1+423512	6.0	31(08)	13 12 25.137 (0.011)	42 35 12.92 (0.10)	< 1.0			U	> 26.5	> 25.5
464	J131225.1+424601	5.5	57(20)	13 12 25.156 (0.020)	42 46 01.81 (0.22)	2.5			F	26.1	25.0
N465	J131225.2+424557	4.2	36(14)	13 12 25.220 (0.024)	42 45 57.74 (0.20)	< 1.9			F	26.2	24.7
N466	J131225.2+423256	3.2	18(08)	13 12 25.249 (0.027)	42 32 56.98 (0.20)	< 1.8			F?	> 26.1	24.4
467	J131225.2+424221	11.7	60(09)	13 12 25.261 (0.010)	42 42 21.98 (0.10)	< 0.6			F	> 26.7	24.7
468	J131225.2+424103	20.9	126(10)	13 12 25.263 (0.010)	42 41 03.97 (0.10)	1.1	< 0.6	94	Ge	24.8	23.7
469	J131225.2+424345	10.0	95(19)	13 12 25.286 (0.044)	42 43 45.05 (0.33)	3.5			B2?	23.1	21.3
A		10.0	64(11)	13 12 25.213 (0.010)	42 43 44.65 (0.10)	< 1.1				23.1	21.3
B		4.4	31(13)	13 12 25.528 (0.018)	42 43 46.05 (0.27)	< 1.6				25.0	23.3
N470	J131225.3+422340	5.1	84(24)	13 12 25.326 (0.015)	42 23 40.83 (0.23)	< 2.0			sg	20.8	19.9
N471	J131225.4+423258	2.6	32(16)	13 12 25.400 (0.040)	42 32 58.78 (0.56)	< 1.4			F?	> 26.5	25.0
N472	J131225.5+423826	4.5	22(08)	13 12 25.581 (0.018)	42 38 26.46 (0.13)	< 1.5			Gc	24.3	22.3
473	J131225.7+423941	99.9	781(10)	13 12 25.734 (0.010)	42 39 41.47 (0.10)	1.4	< 0.3	179	Be	25.6	23.8
N474	J131225.7+424941	5.2	51(17)	13 12 25.746 (0.017)	42 49 41.69 (0.23)	< 1.8			U	> 26.3	> 25.6
475	J131226.1+423243	12.8	101(12)	13 12 26.129 (0.010)	42 32 43.67 (0.10)	< 1.1			Gc	19.5	18.9
476	J131226.2+424227	16.1	84(09)	13 12 26.283 (0.010)	42 42 27.00 (0.10)	< 0.6			Gc	18.9	18.0
N477	J131226.6+425151	4.8	122(32)	13 12 26.688 (0.032)	42 51 51.81 (0.27)	3.8	< 1.3	113	Ge?	21.0	19.9
N478	J131226.7+425451	4.1	79(26)	13 12 26.795 (0.016)	42 54 51.97 (0.31)	< 2.1			F	25.9	24.4
479	J131226.8+423621	8.7	51(10)	13 12 26.873 (0.010)	42 36 21.49 (0.10)	1.6	< 0.6	117	U	> 26.8	> 25.7
480	J131226.9+423315	6.4	39(10)	13 12 26.945 (0.013)	42 33 15.07 (0.12)	1.5	0.6	74	Ge	20.2	19.7
N481	J131226.9+424052	4.9	35(14)	13 12 26.993 (0.023)	42 40 52.56 (0.21)	< 1.6			Gd	20.2	19.7
482	J131227.1+423516	6.4	38(10)	13 12 27.141 (0.011)	42 35 16.66 (0.12)	< 1.2			Gc	23.4	22.1
483	J131227.4+423800	15.7	139(13)	13 12 27.487 (0.010)	42 38 00.53 (0.10)	2.2	1.2	175	Ge?	20.5	19.5
484	J131227.6+424536	6.6	54(12)	13 12 27.645 (0.014)	42 45 36.75 (0.10)	1.7	< 0.7	79	Be	23.2	22.0
485	J131227.6+423014	9.2	93(16)	13 12 27.648 (0.011)	42 30 14.40 (0.14)	1.6			Ge		19.3
N486	J131227.7+424709	5.3	36(11)	13 12 27.741 (0.017)	42 47 09.69 (0.16)	< 1.4			U	> 25.1	> 24.3
487	J131227.9+424638	7.7	61(12)	13 12 27.944 (0.010)	42 46 38.60 (0.11)	< 0.9			Gc	23.9	21.8
N488	J131228.2+424508	4.6	30(12)	13 12 28.228 (0.023)	42 45 08.88 (0.19)	< 1.7			Gc	22.9	22.3
489	J131228.3+424454	7.1	42(10)	13 12 28.306 (0.014)	42 44 54.79 (0.10)	< 1.5			Gc	25.0	24.0
490	J131228.3+424951	14.4	159(16)	13 12 28.399 (0.010)	42 49 51.74 (0.10)	< 0.9			Gc?	17.6	16.4
491	J131228.4+424603	37.8	272(11)	13 12 28.492 (0.010)	42 46 03.33 (0.10)	1.0	< 0.3	94	Be	24.6	22.4
492	J131228.6+423620	18.5	93(08)	13 12 28.671 (0.010)	42 36 20.17 (0.10)	< 0.4			Bc	25.4	24.5
493	J131228.6+423147	5.6	59(14)	13 12 28.693 (0.021)	42 31 47.71 (0.16)	2.8	< 0.8	67	Ge	22.8	21.9
N494	J131229.1+423451	5.0	30(10)	13 12 29.123 (0.019)	42 34 51.90 (0.14)	< 1.6			Gc	21.1	20.2
N495	J131229.1+424757	5.3	53(14)	13 12 29.180 (0.014)	42 47 57.94 (0.19)	2.0	< 0.8	133	Be	25.9	23.7
N496	J131229.2+423731	4.7	79(20)	13 12 29.234 (0.026)	42 37 31.65 (0.28)	2.8			Ge	19.0	18.2
497	J131229.3+425152	8.6	131(24)	13 12 29.379 (0.011)	42 51 52.61 (0.14)	< 1.8			Gd	23.8	23.3
N498	J131229.4+425316	5.4	101(28)	13 12 29.430 (0.017)	42 53 16.69 (0.21)	< 1.9			U	> 26.5	> 25.8
499	J131229.4+425208	6.2	103(24)	13 12 29.467 (0.016)	42 52 08.75 (0.16)	2.0	1.0	81	Ge	19.9	19.1
500	J131229.5+423152	7.1	86(17)	13 12 29.501 (0.330)	42 31 52.94 (0.35)	3.8			B2	22.3	21.7
A		7.1	45(07)	13 12 29.547 (0.015)	42 31 52.45 (0.20)	< 1.0				22.3	21.7
B		3.4	41(12)	13 12 29.352 (0.031)	42 31 53.98 (0.40)	2.5	1.5	118		24.6	23.2
N501	J131229.5+424854	3.8	82(33)	13 12 29.528 (0.036)	42 48 54.30 (0.72)	4.5	< 2.4	9	Ge	19.8	19.3
502	J131229.8+424618	5.4	42(12)	13 12 29.868 (0.014)	42 46 18.11 (0.17)	1.8	< 1.4	130	Be	24.3	22.3
503	J131229.9+424703	99.9	1805(85)	13 12 29.909 (0.010)	42 47 03.14 (0.10)	20.0	5.0	25	EG?	24.8	22.5
504	J131229.9+423519	7.2	41(10)	13 12 29.920 (0.011)	42 35 19.97 (0.13)	< 1.3			Gc?		20.4
505	J131229.9+423628	5.5	28(09)	13 12 29.997 (0.017)	42 36 28.04 (0.13)	< 1.7			Gc	24.1	23.3
506	J131230.0+423106	11.1	109(14)	13 12 30.042 (0.010)	42 31 06.40 (0.10)	2.2	< 0.7	85	U	> 26.3	> 25.0
507	J131230.2+424717	65.6	542(13)	13 12 30.283 (0.010)	42 47 17.43 (0.10)	< 1.0			Gc?	24.6	22.9
508	J131230.3+424220	8.8	52(09)	13 12 30.305 (0.010)	42 42 20.86 (0.10)	< 1.0			Bc	21.3	20.6
509	J131230.7+423737	6.5	81(17)	13 12 30.786 (0.019)	42 37 37.67 (0.21)	2.4			Ge	20.5	19.8
510	J131230.8+423903	8.7	64(12)	13 12 30.852 (0.012)	42 39 03.51 (0.10)	1.8	< 1.0	76	Be	20.8	19.6
N511	J131230.9+424051	5.1	30(11)	13 12 30.950 (0.020)	42 40 51.14 (0.18)	< 1.6			F	25.0	23.6
512	J131231.4+422503	6.1	82(21)	13 12 31.440 (0.015)	42 25 03.72 (0.17)	< 1.5			Gc		19.7
N513	J131231.4+422747	4.5	48(16)	13 12 31.442 (0.032)	42 27 47.01 (0.18)	3.3	< 0.8	105	F		22.1
514	J131231.4+424552	14.9	153(15)	13 12 31.482 (0.010)	42 45 52.59 (0.10)	1.7	1.0	71	Ge	18.9	18.0
515	J131231.5+424041	8.3	72(14)	13 12 31.502 (0.012)	42 40 41.90 (0.17)	2.2	1.2	0	S ?	17.6	16.4
516	J131231.9+424429	19.4	130(11)	13 12 31.921 (0.010)	42 44 29.82 (0.10)	< 0.8			F	26.0	25.1
517	J131232.1+422628	27.8	311(23)	13 12 32.101 (0.010)	42 26 28.41 (0.10)	4.9			Ge		20.7

TABLE 2—Continued

(1) No	(2) Source	(3) SNR	(4) S _{1.4}	(5) RA	(6) DEC	(7) Radio Size	(8)	(9)	(10) ROM	(11) r	(12) z
518	J131232.3+423949	18.4	97(09)	13 12 32.308 (0.010)	42 39 49.58 (0.10)	0.9	< 0.5	128	F	24.7	24.1
519	J131232.3+424109	8.0	41(08)	13 12 32.359 (0.010)	42 41 09.94 (0.10)	< 0.7			Gd	23.0	22.5
N520	J131232.4+424808	4.9	50(19)	13 12 32.424 (0.027)	42 48 08.13 (0.23)	2.4	< 1.5	75	Ge	20.2	20.2
521	J131232.6+422655	6.4	61(13)	13 12 32.629 (0.010)	42 26 55.68 (0.13)	< 1.1			U		> 24.0
522	J131232.8+424038	99.9	706(09)	13 12 32.804 (0.010)	42 40 38.54 (0.10)	< 0.4			Gc	25.1	23.4
523	J131232.8+422850	9.6	79(12)	13 12 32.813 (0.010)	42 28 50.22 (0.10)	< 1.2			Gc		20.7
524	J131233.2+423508	10.7	57(09)	13 12 33.215 (0.010)	42 35 08.13 (0.10)	< 1.0			F	25.6	23.8
N525	J131233.4+422522	4.2	70(24)	13 12 33.456 (0.034)	42 25 22.14 (0.43)	4.3	< 1.9	135	C		20.3
N526	J131234.0+422215	19.4	426(33)	13 12 34.072 (0.010)	42 22 15.75 (0.10)	< 1.7			sg	17.2	16.5
527	J131234.4+424309	7.6	63(12)	13 12 34.498 (0.013)	42 43 09.18 (0.11)	1.8	< 0.8	77	Ge	20.2	19.2
528	J131234.6+423607	12.9	69(09)	13 12 34.637 (0.010)	42 36 00.54 (0.10)	< 0.8			Bc	24.8	23.1
529	J131234.6+424342	5.5	39(11)	13 12 34.691 (0.013)	42 43 42.64 (0.16)	< 1.4			Gc	20.2	19.5
N530	J131234.7+423624	5.1	28(09)	13 12 34.738 (0.012)	42 36 24.63 (0.18)	< 1.5			Gc	21.3	20.3
531	J131234.8+422429	6.6	96(19)	13 12 34.870 (0.011)	42 24 29.97 (0.13)	< 1.3			sg	20.6	19.9
532	J131234.9+423252	6.3	39(11)	13 12 34.997 (0.014)	42 32 52.35 (0.15)	< 1.6			Gd	25.0	
533	J131235.2+424423	6.0	36(09)	13 12 35.252 (0.012)	42 44 23.81 (0.11)	< 1.0			U	> 26.6	> 24.9
534	J131235.2+423016	5.8	42(11)	13 12 35.257 (0.011)	42 30 16.42 (0.13)	< 1.2			Gc	20.7	19.6
535	J131235.4+423619	6.4	38(09)	13 12 35.455 (0.010)	42 36 19.69 (0.11)	< 1.1			Gc?	18.0	16.8
N536	J131235.7+425334	5.9	94(22)	13 12 35.756 (0.011)	42 53 34.12 (0.19)	< 1.3			Gc	21.2	20.0
537	J131235.7+423245	10.5	77(12)	13 12 35.757 (0.010)	42 32 45.06 (0.10)	1.7	< 0.7	63	Be	23.7	22.9
538	J131235.9+424222	14.4	84(09)	13 12 35.931 (0.010)	42 42 22.45 (0.10)	< 0.7			F	> 26.5	24.6
539	J131236.0+423811	5.5	30(12)	13 12 36.026 (0.014)	42 38 11.29 (0.29)	< 2.6			Gc	24.0	23.0
540	J131236.0+424044	8.8	54(10)	13 12 36.066 (0.010)	42 40 44.17 (0.10)	< 1.0			F	24.7	24.3
541	J131236.0+423219	5.8	35(10)	13 12 36.069 (0.017)	42 32 19.02 (0.10)	1.5	1.0	98	Be	21.7	20.9
N542	J131236.1+425402	7.4	134(30)	13 12 36.173 (0.013)	42 54 02.80 (0.19)	< 1.9			Gc	20.4	20.2
543	J131236.2+424027	15.9	106(10)	13 12 36.227 (0.010)	42 40 27.57 (0.10)	1.1	< 0.8	18	Ge	19.3	18.6
544	J131236.2+423516	9.8	57(10)	13 12 36.284 (0.010)	42 35 16.08 (0.10)	< 1.1			F	26.1	24.7
545	J131236.7+425223	12.9	222(25)	13 12 36.704 (0.010)	42 52 23.43 (0.10)	< 1.5			Bc	22.8	20.9
N546	J131236.8+425319	6.2	135(30)	13 12 36.806 (0.014)	42 53 19.58 (0.24)	2.3	< 1.4	11	Be	21.9	20.9
547	J131236.8+422609	5.4	61(18)	13 12 36.847 (0.017)	42 26 09.95 (0.20)	< 2.0			Gc		21.9
N548	J131236.9+423205	5.1	77(23)	13 12 36.971 (0.030)	42 32 05.22 (0.34)	2.6			Ge	25.6	23.5
N549	J131236.9+425349	8.0	170(30)	13 12 36.982 (0.011)	42 53 49.33 (0.16)	10.0	3.0	100	EG?	24.5	23.0
550	J131237.0+423536	6.3	38(11)	13 12 37.008 (0.016)	42 35 36.75 (0.12)	< 1.8			F	26.1	25.0
551	J131237.2+424340	23.0	146(10)	13 12 37.232 (0.010)	42 43 40.17 (0.10)	< 0.8			Bc	25.5	24.6
552	J131237.3+424845	15.0	160(16)	13 12 37.321 (0.010)	42 48 45.99 (0.10)	< 1.2			Bc	22.7	21.0
553	J131237.3+423101	9.9	107(15)	13 12 37.397 (0.010)	42 31 01.28 (0.10)	1.6			Ge	23.0	21.6
554	J131237.4+423026	8.7	70(12)	13 12 37.499 (0.010)	42 30 26.82 (0.10)	1.5	< 0.7	80	U	> 25.7	> 25.5
555	J131237.5+424247	49.3	289(10)	13 12 37.543 (0.010)	42 42 47.89 (0.10)	0.7	< 0.3	115	Be	23.9	22.5
556	J131237.7+422908	11.8	94(12)	13 12 37.775 (0.010)	42 29 08.43 (0.10)	< 0.8			F	25.8	22.8
557	J131237.9+424127	5.6	30(09)	13 12 37.927 (0.011)	42 41 27.60 (0.15)	< 1.1			Gc	24.1	22.4
558	J131237.9+424005	7.7	46(11)	13 12 37.953 (0.010)	42 40 05.97 (0.13)	< 1.5			Gc	24.2	23.6
N559	J131238.2+425244	6.5	103(22)	13 12 38.218 (0.011)	42 52 44.00 (0.16)	< 1.2			Gc	19.5	18.7
560	J131238.2+422818	8.2	75(16)	13 12 38.296 (0.012)	42 28 18.42 (0.12)	< 1.6			Gc		22.7
561	J131238.3+423201	8.4	64(12)	13 12 38.348 (0.010)	42 32 01.72 (0.10)	1.2	< 0.7	101	F	25.8	25.0
N562	J131238.3+424916	4.7	89(25)	13 12 38.352 (0.037)	42 49 16.59 (0.25)	4.0	< 1.1	71	Ge	24.0	22.6
563	J131238.5+423441	6.2	35(09)	13 12 38.524 (0.013)	42 34 41.25 (0.10)	< 1.3			Bc?	23.4	22.3
N564	J131238.7+423017	4.1	32(14)	13 12 38.715 (0.027)	42 30 17.52 (0.21)	< 2.2			Gc	22.0	20.8
N565	J131238.8+422803	4.8	44(14)	13 12 38.836 (0.016)	42 28 03.16 (0.23)	< 2.0			U		> 24.4
566	J131239.0+423945	15.4	88(10)	13 12 39.073 (0.010)	42 39 45.94 (0.10)	0.9	< 0.5	92	F ?	> 26.5	24.9
N567	J131239.3+423732	4.9	44(14)	13 12 39.323 (0.040)	42 37 32.30 (0.15)	5.0	1.5	85	B2?	23.0	21.6
A		4.9	25(09)	13 12 39.101 (0.017)	42 37 32.13 (0.12)	< 1.4				23.6	22.0
B		4.3	19(09)	13 12 39.564 (0.020)	42 37 32.56 (0.16)	< 2.0				23.0	21.6
568	J131239.1+424155	9.8	57(10)	13 12 39.143 (0.010)	42 41 55.61 (0.10)	< 0.8			F	25.7	24.6
569	J131239.3+424249	8.3	83(15)	13 12 39.382 (0.016)	42 42 49.19 (0.15)	2.7	< 1.2	58	Ge?	16.6	15.4
N570	J131239.4+423158	4.1	63(20)	13 12 39.445 (0.039)	42 31 58.28 (0.30)	4.0	< 1.5	126	Ge	23.4	22.4
N571	J131239.4+422539	3.9	41(17)	13 12 39.447 (0.028)	42 25 39.61 (0.20)	< 2.3			U		> 24.4
572	J131239.6+423910	33.6	195(10)	13 12 39.698 (0.010)	42 39 10.81 (0.10)	0.9	< 0.5	120	Ge	23.3	21.2
573	J131239.7+424524	5.7	56(15)	13 12 39.749 (0.026)	42 45 24.90 (0.14)	3.2	< 0.8	102	Ge	24.4	22.6
574	J131239.7+424551	9.2	92(15)	13 12 39.785 (0.010)	42 45 51.14 (0.12)	2.0	< 0.7	131	Be	23.4	21.5
575	J131239.8+422642	48.6	547(16)	13 12 39.840 (0.010)	42 26 42.18 (0.10)	1.2	< 0.3	161	Ge?		21.6
576	J131240.0+423721	6.8	57(13)	13 12 40.086 (0.014)	42 37 21.82 (0.16)	2.1	< 1.0	38	U	> 26.4	> 25.7
577	J131240.3+422846	5.8	52(15)	13 12 40.382 (0.017)	42 28 46.69 (0.14)	< 2.0			Gc	17.9	19.7
N578	J131240.4+424257	5.2	35(12)	13 12 40.435 (0.018)	42 42 57.49 (0.20)	< 1.7			Gc	23.8	21.9

TABLE 2—Continued

(1) No	(2) Source	(3) SNR	(4) S _{1.4}	(5) RA	(6) DEC	(7)	(8) Radio Size	(9)	(10) ROM	(11) r	(12) z
579	J131240.4+423753	11.0	62(09)	13 12 40.471 (0.010)	42 37 53.48 (0.10)	1.4	< 0.5	79	Be	22.2	20.4
580	J131240.5+423922	19.7	111(00)	13 12 40.590 (0.010)	42 39 22.78 (0.10)	< 0.8			Gc	25.7	23.6
581	J131240.7+423434	31.0	192(10)	13 12 40.736 (0.010)	42 34 34.53 (0.10)	< 0.7			Gc	19.8	19.0
582	J131240.7+424859	8.3	127(23)	13 12 40.784 (0.016)	42 48 59.10 (0.18)	2.3	< 1.8	105	Be?	24.6	23.2
583	J131241.0+423420	15.4	100(11)	13 12 41.019 (0.010)	42 34 20.33 (0.10)	1.0	< 0.6	99	Be	22.9	21.1
584	J131241.1+423443	39.0	229(10)	13 12 41.158 (0.010)	42 34 43.80 (0.10)	< 0.7			Gc	23.5	22.7
585	J131241.3+424751	6.8	61(16)	13 12 41.366 (0.016)	42 47 51.14 (0.15)	< 1.9			Gc	23.2	20.9
N586	J131241.7+423817	4.7	36(15)	13 12 41.744 (0.024)	42 38 17.48 (0.22)	< 1.7			Bc	21.7	20.4
587	J131241.9+422744	14.3	241(21)	13 12 41.971 (0.010)	42 27 44.90 (0.10)	2.1	1.3	83	Be		18.3
588	J131242.2+423824	5.4	49(13)	13 12 42.285 (0.023)	42 38 24.73 (0.17)	2.7	< 0.9	115	Ge	24.7	23.9
589	J131242.3+422852	5.5	39(11)	13 12 42.346 (0.012)	42 28 52.35 (0.14)	< 1.0			F ?	> 25.3	23.6
590	J131242.5+425036	6.9	119(25)	13 12 42.577 (0.022)	42 50 36.35 (0.15)	3.0	< 0.9	88	Ge	20.9	19.9
591	J131242.7+422800	5.9	58(16)	13 12 42.745 (0.015)	42 28 00.06 (0.18)	< 1.7			F		23.3
592	J131242.9+424138	7.7	67(12)	13 12 42.940 (0.010)	42 41 38.74 (0.12)	1.5	< 1.0	21	F	26.1	24.6
593	J131243.0+423422	5.5	49(12)	13 12 43.098 (0.017)	42 34 22.91 (0.16)	2.1	< 0.8	52	Ge	21.8	20.5
594	J131243.3+423217	5.5	41(13)	13 12 43.377 (0.016)	42 32 17.01 (0.18)	< 1.7			Gd?	24.1	22.9
595	J131243.5+424936	6.0	98(21)	13 12 43.556 (0.016)	42 49 36.00 (0.19)	2.0	< 1.4	47	Be	25.3	23.0
N596	J131243.6+424708	4.9	51(14)	13 12 43.641 (0.016)	42 47 08.84 (0.14)	2.2			F	25.0	24.5
597	J131244.1+423607	8.1	44(09)	13 12 44.123 (0.010)	42 36 07.57 (0.12)	< 1.3			U	> 26.2	> 25.7
598	J131244.3+422648	11.3	131(17)	13 12 44.330 (0.010)	42 26 48.78 (0.10)	< 1.1			U		23.7
599	J131244.4+423837	11.2	79(11)	13 12 44.453 (0.010)	42 38 37.19 (0.10)	1.1	< 0.9	161	F	24.3	24.3
600	J131244.6+423615	13.8	77(09)	13 12 44.632 (0.010)	42 36 15.83 (0.10)	1.0	< 0.5	43	Be	23.8	23.1
601	J131245.2+424436	6.4	53(11)	13 12 45.265 (0.014)	42 44 36.31 (0.10)	1.3	< 0.7	80	Be?	25.1	23.4
602	J131245.4+423940	7.4	46(10)	13 12 45.447 (0.011)	42 39 40.99 (0.10)	< 0.9			Gc	20.2	19.0
603	J131245.4+424114	6.0	55(13)	13 12 45.493 (0.018)	42 41 14.90 (0.15)	2.0	< 1.1	70	Ge	19.9	19.1
N604	J131245.9+422246	4.3	82(37)	13 12 45.930 (0.034)	42 22 46.13 (0.35)	3.0	3.0		sg	20.7	19.8
N605	J131246.3+423055	5.3	46(13)	13 12 46.380 (0.021)	42 30 55.49 (0.15)	2.3	< 0.8	111	Ge	21.0	20.2
N606	J131246.4+424800	4.2	41(14)	13 12 46.445 (0.020)	42 48 00.66 (0.27)	< 2.5			U		
607	J131246.4+423518	26.3	208(12)	13 12 46.467 (0.010)	42 45 18.14 (0.10)	< 0.9			Bc	25.7	24.3
N608	J131246.6+424838	4.1	43(17)	13 12 46.677 (0.028)	42 48 38.11 (0.18)	< 2.5			U	> 25.9	> 25.2
609	J131246.6+422728	6.6	67(16)	13 12 46.687 (0.013)	42 27 28.99 (0.14)	< 1.5			Gc		18.5
610	J131246.7+424757	8.3	194(33)	13 12 46.745 (0.023)	42 47 57.15 (0.21)	3.8	2.3	107	Be	22.2	20.8
611	J131246.7+423251	14.9	142(14)	13 12 46.754 (0.010)	42 32 51.24 (0.10)	1.7	1.0	154	F ?	25.6	24.9
N612	J131246.7+423828	4.8	34(11)	13 12 46.764 (0.021)	42 38 28.82 (0.14)	< 1.9			Gc	25.6	23.6
613	J131246.9+424147	11.2	81(12)	13 12 46.939 (0.010)	42 41 47.29 (0.10)	1.6	< 0.7	126	F	26.1	24.4
614	J131246.9+423400	7.5	65(14)	13 12 46.958 (0.015)	42 34 00.57 (0.15)	2.5	< 0.8	49	F	26.4	24.3
N615	J131247.5+423846	4.4	32(15)	13 12 47.509 (0.030)	42 38 46.47 (0.25)	< 2.4			Gc	24.1	23.3
616	J131247.8+423602	6.2	40(11)	13 12 47.883 (0.012)	42 36 02.16 (0.14)	< 1.3			F	> 26.2	24.4
617	J131247.8+424537	7.7	65(14)	13 12 47.887 (0.012)	42 45 37.68 (0.13)	< 1.6			Bc	25.5	24.2
618	J131248.1+424044	6.4	41(11)	13 12 48.116 (0.012)	42 40 44.12 (0.14)	1.6	< 1.0	20	Ge	21.0	20.2
619	J131248.1+423020	7.2	56(11)	13 12 48.167 (0.012)	42 30 20.17 (0.10)	1.7	1.0	83	Be	25.0	23.9
620	J131248.2+423956	12.4	72(08)	13 12 48.260 (0.010)	42 39 56.54 (0.10)	< 0.5			Gc	21.9	20.4
621	J131248.3+423221	41.9	643(16)	13 12 48.358 (0.010)	42 32 21.66 (0.10)	8.0	2.0	10	EG?	24.9	24.3
N622	J131248.4+422204	4.5	207(54)	13 12 48.411 (0.026)	42 22 04.28 (0.41)	3.2	< 2.4	18	sg	22.2	20.8
N623	J131248.7+425236	12.8	223(27)	13 12 48.733 (0.010)	42 52 36.68 (0.10)	< 1.5			Gc	17.4	16.3
N624	J131248.7+423611	5.0	45(12)	13 12 48.769 (0.020)	42 36 11.24 (0.19)	2.2	< 1.0	130	Ge	21.1	20.2
625	J131249.5+423532	5.6	37(11)	13 12 49.584 (0.016)	42 35 32.02 (0.13)	< 1.6			Gc		17.3
N626	J131249.7+425132	4.1	52(17)	13 12 49.788 (0.015)	42 51 32.64 (0.24)	< 1.4			Gd?	24.5	23.7
N627	J131250.0+425354	4.4	165(44)	13 12 50.004 (0.035)	42 53 54.80 (0.25)	3.7	2.0	85	Be	23.4	22.4
628	J131250.0+423110	11.3	110(14)	13 12 50.023 (0.010)	42 31 10.04 (0.10)	1.7	< 0.6	46	Ge		21.4
629	J131250.0+424217	10.2	126(21)	13 12 50.033 (0.016)	42 42 17.22 (0.22)	4.6			B2	21.6	20.3
A		10.2	82(13)	13 12 50.165 (0.010)	42 42 16.58 (0.11)	2.0	< 0.6	155		21.6	20.3
B		4.9	44(13)	13 12 49.835 (0.025)	42 42 18.58 (0.14)	2.5	< 0.8	94		21.9	20.7
N630	J131250.4+422955	4.5	35(11)	13 12 50.432 (0.016)	42 29 55.78 (0.15)	< 1.2			Gc		21.3
631	J131250.5+424333	5.4	64(17)	13 12 50.533 (0.018)	42 43 33.21 (0.23)	1.9	< 1.4	19	F	26.1	24.5
632	J131250.5+423130	48.8	371(12)	13 12 50.538 (0.010)	42 31 30.26 (0.10)	< 0.6			Gc	23.1	22.7
633	J131251.0+423406	6.5	41(10)	13 12 51.045 (0.013)	42 34 06.43 (0.11)	< 1.4			Bc	24.1	22.5
634	J131251.1+423809	11.2	91(12)	13 12 51.159 (0.010)	42 38 09.46 (0.10)	1.7	< 0.8	103	Ge?	23.6	22.3
N635	J131251.2+423016	5.3	47(16)	13 12 51.233 (0.020)	42 30 16.68 (0.21)	< 2.2			Bc	24.7	23.2
N636	J131251.2+423901	5.2	44(16)	13 12 51.254 (0.021)	42 39 01.94 (0.22)	< 1.6			U		
N637	J131251.4+425208	4.7	149(38)	13 12 51.446 (0.035)	42 52 08.76 (0.31)	4.4	< 1.3	61	Ge	23.3	21.8
638	J131251.8+424619	6.8	59(14)	13 12 51.839 (0.011)	42 46 19.98 (0.15)	< 1.5			Gc	23.8	21.5
639	J131251.8+423330	20.5	202(14)	13 12 51.855 (0.010)	42 33 30.65 (0.10)	1.5	0.9	35	Be	19.7	18.6

TABLE 2—Continued

(1) No	(2) Source	(3) SNR	(4) S _{1,4}	(5) RA	(6) DEC	(7) Radio Size	(8)	(9)	(10) ROM	(11) r	(12) z
640	J131251.8+423100	6.1	61(18)	13 12 51.886 (0.016)	42 31 00.95 (0.19)	< 1.6			Gc	21.8	20.4
641	J131252.1+423359	14.9	130(13)	13 12 52.194 (0.010)	42 33 59.18 (0.10)	1.4	< 1.0	41	Ge	25.1	23.3
642	J131252.2+422819	6.9	69(16)	13 12 52.205 (0.012)	42 28 19.44 (0.15)	< 1.4			Gc		18.4
643	J131252.3+423626	11.1	68(09)	13 12 52.396 (0.010)	42 36 26.55 (0.10)	< 0.6			Bc	23.0	20.9
N644	J131252.4+423642	4.3	33(16)	13 12 52.441 (0.021)	42 36 42.02 (0.39)	3.2	2.0	160	Be	24.6	23.5
N645	J131252.5+424508	5.1	69(18)	13 12 52.573 (0.024)	42 45 08.11 (0.18)	2.6	< 1.3	82	Ge	19.9	19.4
N646	J131252.6+423843	4.9	81(22)	13 12 52.671 (0.050)	42 38 43.86 (0.18)	5.5	< 1.2	88	Be	23.3	23.1
N647	J131252.8+423838	5.2	44(18)	13 12 52.876 (0.027)	42 38 38.97 (0.27)	2.0			Ge	22.6	21.0
648	J131253.0+422735	5.7	99(25)	13 12 53.077 (0.029)	42 27 35.46 (0.24)	3.4	< 1.4	114	U		> 24.2
649	J131253.1+422943	6.6	64(17)	13 12 53.104 (0.013)	42 29 43.86 (0.17)	< 1.9			Bc	23.5	21.9
N650	J131253.3+422516	5.3	35(12)	13 12 53.377 (0.015)	42 35 16.88 (0.21)	< 1.6			Gc	24.9	22.5
651	J131253.4+422748	5.4	68(19)	13 12 53.423 (0.020)	42 27 48.95 (0.16)	< 2.3			Gc		21.7
N652	J131253.5+423755	4.8	54(17)	13 12 53.512 (0.020)	42 37 55.46 (0.36)	3.2	< 1.3	171	Ge	20.3	19.3
N653	J131253.7+424148	4.5	48(16)	13 12 53.729 (0.034)	42 41 48.54 (0.20)	3.0	< 1.1	102	U	> 26.1	> 25.3
654	J131253.7+423917	14.5	187(20)	13 12 53.783 (0.022)	42 39 17.03 (0.22)	2.5			F ?		
A		14.4	107(12)	13 12 53.709 (0.010)	42 39 16.65 (0.10)	1.0	< 0.8	99	Gc	24.0	23.2
B		14.5	80(09)	13 12 53.899 (0.010)	42 39 17.75 (0.10)	< 0.6			U	> 25.8	> 23.9
655	J131253.8+423824	6.9	56(12)	13 12 53.854 (0.014)	42 38 24.28 (0.12)	1.5	< 0.9	71	Ge	22.1	20.5
N656	J131254.1+425318	4.6	102(39)	13 12 54.106 (0.030)	42 53 18.43 (0.31)	2.0			U	> 26.5	> 25.4
657	J131254.2+422629	5.8	113(25)	13 12 54.208 (0.020)	42 26 29.41 (0.18)	2.4	< 1.4	103	U		> 24.4
658	J131254.2+423412	7.1	49(10)	13 12 54.212 (0.011)	42 34 12.65 (0.10)	< 1.6	< 1.0		Gc	21.8	20.4
659	J131254.2+423730	6.4	38(09)	13 12 54.245 (0.010)	42 37 30.09 (0.12)	< 1.1			U	> 25.8	> 24.2
660	J131254.6+424008	7.2	64(13)	13 12 54.645 (0.013)	42 40 08.33 (0.13)	1.9	< 0.8	132	Be?	26.5	24.8
N661	J131254.9+425214	5.6	106(32)	13 12 54.998 (0.025)	42 52 14.03 (0.20)	< 2.8			Gc	21.7	20.1
662	J131255.0+424749	6.2	75(17)	13 12 55.020 (0.014)	42 47 49.30 (0.13)	< 1.7			Gc	23.1	21.0
663	J131255.4+424300	9.3	72(13)	13 12 55.493 (0.010)	42 43 00.46 (0.10)	< 1.3			F	25.8	25.2
N664	J131255.5+423505	5.2	36(10)	13 12 55.536 (0.016)	42 35 05.10 (0.12)	< 1.4			Gc	21.4	20.4
665	J131255.7+423724	9.7	61(11)	13 12 55.788 (0.010)	42 37 24.21 (0.10)	< 1.1			Bc	20.6	20.3
666	J131256.0+424433	17.7	144(13)	13 12 56.099 (0.010)	42 44 33.55 (0.10)	< 0.7			Bc	25.3	23.9
667	J131256.1+424910	5.5	62(14)	13 12 56.127 (0.012)	42 49 10.77 (0.14)	< 1.1			Gc	21.3	19.9
N668	J131256.4+423342	4.2	209(55)	13 12 56.432 (0.050)	42 33 42.00 (0.88)	7.5			C ?		
A		4.2	56(20)	13 12 56.592 (0.045)	42 33 45.58 (0.36)	3.4	2.2	122	Ge	22.3	21.1
B		3.9	153(45)	13 12 56.365 (0.087)	42 33 41.09 (0.71)	6.2	3.7	84	Ge	20.3	20.3
N669	J131256.4+422431	4.8	202(49)	13 12 56.441 (0.030)	42 24 31.12 (0.35)	2.9			sg	19.9	19.3
670	J131256.5+423101	7.9	88(16)	13 12 56.561 (0.014)	42 31 01.74 (0.11)	2.0	< 0.7	74	Ge	20.7	19.8
N671	J131256.5+423130	4.3	35(15)	13 12 56.577 (0.029)	42 31 30.73 (0.23)	< 2.3			Bc	24.7	23.5
672	J131256.8+424535	6.5	70(17)	13 12 56.804 (0.014)	42 45 35.23 (0.14)	1.8	1.0	175	Be	23.9	22.1
N673	J131256.8+423916	5.0	54(15)	13 12 56.879 (0.016)	42 39 16.54 (0.24)	2.4	< 1.0	160	U	> 26.3	> 25.6
674	J131257.0+422807	7.4	146(23)	13 12 57.043 (0.017)	42 28 07.55 (0.11)	3.1	1.5	83	Be		20.4
675	J131257.2+423359	7.6	50(11)	13 12 57.211 (0.013)	42 33 59.54 (0.10)	1.1	< 0.7	103	Ge	23.2	21.5
676	J131257.2+424026	8.6	72(12)	13 12 57.265 (0.010)	42 40 26.06 (0.10)	1.0	< 0.8	52	Gd?	20.4	19.4
677	J131257.8+423949	7.5	57(12)	13 12 57.857 (0.012)	42 39 49.18 (0.11)	1.4	< 0.7	46	U		> 25.4
N678	J131257.8+425115	99.9	1887(23)	13 12 57.886 (0.010)	42 51 15.30 (0.10)	1.3	0.5	19	Ge	23.6	23.0
679	J131257.8+424733	53.2	594(16)	13 12 57.896 (0.010)	42 47 33.33 (0.10)	1.0	< 0.3	41	Gd	23.6	23.0
680	J131257.9+424027	6.5	48(12)	13 12 57.924 (0.012)	42 40 27.22 (0.14)	< 1.6			Bc?	21.6	20.3
681	J131258.0+424823	6.6	73(20)	13 12 58.002 (0.018)	42 48 23.27 (0.16)	< 2.1			Gc	20.0	19.5
682	J131258.0+424439	8.8	127(19)	13 12 58.008 (0.013)	42 44 39.04 (0.11)	2.2	< 1.4	93	Be	26.1	24.7
683	J131258.1+423938	10.5	91(13)	13 12 58.190 (0.010)	42 39 38.02 (0.10)	1.4	< 0.8	114	Be	20.9	19.6
684	J131258.2+422721	16.8	219(20)	13 12 58.295 (0.010)	42 27 21.33 (0.10)	< 1.4			Gc		20.6
685	J131258.6+424353	5.4	45(15)	13 12 58.616 (0.015)	42 43 53.07 (0.26)	< 2.2			F ?	24.1	23.6
686	J131258.6+423602	8.2	63(13)	13 12 58.663 (0.011)	42 36 02.66 (0.10)	< 1.5			Gc	23.2	21.9
N687	J131259.2+424925	3.4	48(21)	13 12 59.260 (0.031)	42 49 25.68 (0.24)	< 2.5			Bc	21.3	20.1
688	J131259.2+424038	6.3	113(21)	13 12 59.288 (0.026)	42 40 38.64 (0.18)	4.5	< 1.1	64	Be	20.3	19.0
689	J131259.5+424737	6.4	75(16)	13 12 59.507 (0.011)	42 47 37.89 (0.14)	< 1.2			F	25.7	24.6
690	J131259.7+423819	5.5	57(15)	13 12 59.762 (0.024)	42 38 19.61 (0.18)	2.8	< 0.9	120	Gd	20.2	20.2
N691	J131259.9+423510	4.5	36(13)	13 12 59.939 (0.022)	42 35 10.42 (0.17)	< 1.6			Gc	24.2	22.2
N692	J131259.9+423515	4.3	29(11)	13 12 59.997 (0.018)	42 35 15.63 (0.17)	< 1.3			Gc	24.3	22.7
693	J131300.3+423658	9.6	71(12)	13 13 00.363 (0.010)	42 36 58.72 (0.10)	< 1.2			F	26.1	24.0
694	J131300.6+422724	9.8	161(22)	13 13 00.655 (0.022)	42 27 24.33 (0.33)	2.4			B2		19.5
A		9.8	115(17)	13 13 00.614 (0.010)	42 27 23.92 (0.10)	< 0.9					19.5
B		5.4	46(11)	13 13 00.709 (0.020)	42 27 25.98 (0.25)	< 2.0					20.3
695	J131301.1+424014	8.1	85(16)	13 13 01.152 (0.016)	42 40 14.49 (0.14)	2.0	< 1.5	79	Ge	24.7	22.9
N696	J131301.3+422942	5.0	64(21)	13 13 01.349 (0.022)	42 29 42.82 (0.22)	< 2.3			Gc	22.7	21.8

TABLE 2—Continued

(1)	(2)	(3)	(4)	(5)	(6)	(7)	(8)	(9)	(10)	(11)	(12)
No	Source	SNR	S _{1,4}	RA	DEC	Radio Size	ROM	r	z		
N697	J131301.3+423212	4.9	46(21)	13 13 01.383 (0.025)	42 32 12.89 (0.36)	< 2.7			Gc	21.0	20.0
N698	J131301.4+423823	5.1	94(26)	13 13 01.470 (0.029)	42 38 23.68 (0.38)	3.8	1.9	28	Ge	21.2	19.9
N699	J131301.9+422403	4.3	76(31)	13 13 01.963 (0.027)	42 24 03.08 (0.37)	< 3.0			su	> 23	> 22
700	J131302.0+424747	5.7	76(20)	13 13 02.006 (0.016)	42 47 47.81 (0.18)	< 1.7			Gc	23.9	22.5
701	J131302.2+424258	7.5	91(16)	13 13 02.203 (0.012)	42 42 58.53 (0.13)	2.2	< 0.7	138	Be	24.8	22.8
702	J131302.3+423331	8.7	65(11)	13 13 02.329 (0.010)	42 33 31.93 (0.10)	< 0.9			F	25.6	24.4
N703	J131302.5+422616	4.6	97(27)	13 13 02.594 (0.032)	42 26 16.50 (0.19)	3.6	< 0.9	70	F		22.6
704	J131302.8+423910	5.6	46(14)	13 13 02.872 (0.018)	42 39 10.41 (0.17)	< 1.6			Gc	22.0	20.8
705	J131302.9+423507	5.8	45(12)	13 13 02.991 (0.014)	42 35 07.62 (0.14)	< 1.6			F	25.8	24.1
706	J131303.1+423929	6.0	52(15)	13 13 03.135 (0.015)	42 39 29.79 (0.17)	< 1.9			Bc	25.1	24.7
707	J131303.2+424053	5.5	65(18)	13 13 03.212 (0.022)	42 40 53.22 (0.33)	2.3			Be	22.1	21.5
N708	J131303.5+424655	4.9	51(17)	13 13 03.517 (0.022)	42 46 55.77 (0.19)	< 2.0			Gc	22.8	21.6
709	J131303.5+424033	11.8	138(16)	13 13 03.589 (0.010)	42 40 33.18 (0.10)	2.3	< 1.0	120	Ge	23.0	21.0
710	J131303.6+424608	8.1	85(16)	13 13 03.686 (0.010)	42 46 08.64 (0.12)	< 1.6			Gc	20.2	19.5
711	J131303.8+424125	8.0	201(33)	13 13 03.872 (0.053)	42 41 25.22 (0.89)	6.5			B2?	20.1	19.4
A		8.0	105(17)	13 13 03.756 (0.014)	42 41 23.91 (0.11)	2.1	< 1.3	95		20.1	19.4
B		6.3	96(20)	13 13 04.000 (0.017)	42 41 28.37 (0.22)	2.7	< 1.8	20		21.3	20.3
712	J131304.1+424944	25.7	407(23)	13 13 04.130 (0.010)	42 49 44.17 (0.10)	< 1.4			Gc	19.6	18.5
N713	J131304.5+424840	5.2	71(22)	13 13 04.568 (0.020)	42 48 40.25 (0.22)	< 2.1			Gd	20.9	20.0
N714	J131304.6+422437	4.7	134(34)	13 13 04.604 (0.017)	42 24 37.60 (0.39)	4.3	< 0.9	25	su	> 23	> 22
N715	J131304.7+424131	5.0	42(13)	13 13 04.772 (0.016)	42 41 31.45 (0.17)	< 1.6			F ?	26.1	25.0
716	J131304.8+423526	6.0	55(15)	13 13 04.893 (0.017)	42 35 26.54 (0.22)	2.4	< 0.9	30	Be	23.9	22.0
717	J131305.1+423108	9.0	138(20)	13 13 05.147 (0.010)	42 31 08.47 (0.14)	2.2	< 1.3	170	Ge	22.2	20.7
718	J131305.5+423121	85.5	766(14)	13 13 05.564 (0.010)	42 31 21.93 (0.10)	0.7	0.4	131	Ge	23.2	22.3
719	J131305.7+424454	91.6	834(14)	13 13 05.759 (0.010)	42 44 54.94 (0.10)	0.7	0.4	57	Ge	25.9	22.9
720	J131305.7+424333	7.0	81(18)	13 13 05.772 (0.014)	42 43 33.87 (0.19)	2.0	< 1.3	176	Ge	23.4	21.5
N721	J131306.1+423311	4.3	59(19)	13 13 06.170 (0.032)	42 33 11.64 (0.23)	3.1	< 1.0	62	F ?	26.9	25.1
N722	J131306.3+423443	4.6	82(21)	13 13 06.330 (0.033)	42 34 43.89 (0.66)	5.2			B2	21.5	20.5
A		4.4	44(16)	13 13 06.426 (0.019)	42 34 42.41 (0.24)	< 1.9				23.6	22.1
B		4.6	38(11)	13 13 06.202 (0.023)	42 34 45.03 (0.30)	2.0	1.3	70		21.5	20.5
723	J131306.6+422608	7.1	117(25)	13 13 06.608 (0.015)	42 26 08.40 (0.13)	< 2.0			Bc		17.4
724	J131307.4+424740	8.7	112(19)	13 13 07.428 (0.010)	42 47 40.39 (0.11)	< 1.3			Gc	21.8	20.5
725	J131307.4+423738	7.2	55(11)	13 13 07.431 (0.011)	42 37 38.01 (0.10)	< 0.9			Gc	23.1	20.9
726	J131307.9+422734	7.4	99(21)	13 13 07.987 (0.013)	42 27 34.11 (0.13)	< 1.3			Gc		19.2
N727	J131308.2+423412	5.3	65(17)	13 13 08.240 (0.014)	42 34 12.18 (0.26)	2.7	< 0.9	20	Ge	21.2	20.2
728	J131308.5+422829	7.2	92(20)	13 13 08.508 (0.013)	42 28 29.59 (0.15)	< 1.7			U		> 24.2
729	J131308.7+423643	99.9	8480(170)	13 13 08.720 (0.010)	42 36 43.98 (0.10)	< 0.6			Gc	24.1	22.0
730	J131309.1+424130	8.7	100(16)	13 13 09.124 (0.013)	42 41 30.68 (0.10)	1.9	< 1.0	109	U	> 26.3	> 25.7
731	J131309.1+424600	5.5	64(18)	13 13 09.132 (0.022)	42 46 00.86 (0.16)	2.7	< 0.8	121	Ge	21.5	20.5
N732	J131309.5+425036	9.7	196(32)	13 13 09.537 (0.012)	42 50 36.57 (0.11)	1.8	1.1	73	Ge	20.2	19.2
N733	J131309.6+422722	5.1	71(19)	13 13 09.692 (0.016)	42 27 22.88 (0.16)	< 1.3			Bc		21.8
734	J131310.2+423734	8.0	69(14)	13 13 10.235 (0.010)	42 37 34.79 (0.11)	< 1.5			F	25.7	
735	J131310.3+423429	5.4	47(13)	13 13 10.384 (0.017)	42 34 29.22 (0.11)	1.5	< 0.7	63	U	> 26.8	> 26.0
N736	J131310.5+422634	10.6	164(24)	13 13 10.509 (0.010)	42 26 34.62 (0.10)	< 1.4			U		> 23.6
737	J131311.3+424336	6.6	67(18)	13 13 11.392 (0.015)	42 43 36.01 (0.17)	1.9	1.4	70	Be	23.8	22.8
N738	J131313.0+423430	5.3	74(21)	13 13 13.038 (0.034)	42 34 30.73 (0.17)	3.7	1.5	76	C ?	24.7	23.6
N739	J131313.1+424049	5.2	52(18)	13 13 13.132 (0.021)	42 40 49.37 (0.21)	< 2.1			Gc	24.1	22.7
740	J131313.7+423043	13.6	157(18)	13 13 13.765 (0.010)	42 30 43.81 (0.10)	< 1.3			U ?		> 24.6
741	J131314.1+423047	11.0	126(16)	13 13 14.175 (0.010)	42 30 47.87 (0.10)	< 1.2			Bc	23.6	21.7
742	J131314.1+423542	10.4	125(17)	13 13 14.194 (0.010)	42 35 42.64 (0.10)	1.4	< 1.1	55	Ge	19.8	19.0
743	J131314.3+424611	7.1	80(17)	13 13 14.371 (0.014)	42 46 11.61 (0.12)	1.6	< 0.8	129	Be	22.3	21.4
744	J131314.5+424506	8.7	90(16)	13 13 14.593 (0.010)	42 45 06.67 (0.11)	< 1.3			Gc	24.0	22.9
745	J131315.2+423715	20.7	199(14)	13 13 15.266 (0.010)	42 37 15.44 (0.10)	< 0.8			F	26.4	24.6
N746	J131315.7+424854	5.6	80(20)	13 13 15.798 (0.014)	42 48 54.18 (0.15)	< 1.2			U	> 26.4	> 26.0
747	J131316.6+422815	5.4	87(23)	13 13 16.648 (0.015)	42 28 15.98 (0.20)	< 2.0			U		> 24.5
N748	J131316.8+422514	99.9	2430(89)	13 13 16.861 (0.010)	42 25 14.38 (0.10)	1.3	0.5	146	F ?		23.3
749	J131317.0+424402	6.5	75(19)	13 13 17.024 (0.016)	42 44 02.06 (0.17)	< 1.8			Bc	23.0	22.3
750	J131317.1+423902	6.0	99(23)	13 13 17.197 (0.019)	42 39 02.76 (0.27)	3.1	< 1.5	15	Be	20.8	20.1
751	J131317.2+423608	5.8	85(20)	13 13 17.205 (0.020)	42 36 08.47 (0.17)	< 1.7			Gc	24.6	22.4
752	J131317.2+424139	6.4	95(21)	13 13 17.299 (0.040)	42 41 39.20 (0.22)	4.6			B2	23.5	21.5
A		6.4	55(12)	13 13 17.156 (0.011)	42 41 39.01 (0.12)	< 1.3				24.0	23.2
B		3.7	40(18)	13 13 17.432 (0.037)	42 41 39.49 (0.19)	< 2.6				23.5	21.5
753	J131318.2+423610	5.7	109(29)	13 13 18.213 (0.034)	42 36 10.93 (0.30)	4.3	< 1.6	50	C ?	24.1	22.3

TABLE 2—Continued

(1) No	(2) Source	(3) SNR	(4) S _{1.4}	(5) RA	(6) DEC	(7)	(8)	(9)	(10) ROM	(11) r	(12) z
754	J131318.5+424447	9.5	115(18)	13 13 18.504 (0.010)	42 44 47.53 (0.11)	< 1.5			F ?	26.1	24.9
N755	J131318.7+424856	5.0	101(34)	13 13 18.748 (0.023)	42 48 56.69 (0.28)	2.4	1.6	20	Ge	20.3	19.5
756	J131318.9+424108	10.7	126(18)	13 13 18.962 (0.010)	42 41 08.93 (0.10)	< 1.6			F	26.1	25.4
N757	J131319.0+424757	4.9	70(20)	13 13 19.045 (0.018)	42 47 57.41 (0.20)	2.0	1.5	50	Ge	20.9	19.9
758	J131319.3+424624	24.4	1036(65)	13 13 19.301 (0.040)	42 46 24.50 (0.30)	8.1	2.0	105	Ge	17.5	16.6
A		24.4	405(29)	13 13 19.451 (0.010)	42 46 24.16 (0.10)	2.6	< 1.1	105	Ge?	17.5	16.6
B		11.4	631(48)	13 13 19.162 (0.016)	42 46 24.81 (0.10)	5.9	1.4	102	Ge	17.5	16.6
N759	J131319.3+424806	6.3	100(25)	13 13 19.318 (0.015)	42 48 06.35 (0.19)	< 2.0			Gc	19.6	18.7
760	J131319.9+424122	99.9	6470(130)	13 13 19.924 (0.010)	42 41 22.10 (0.10)	1.4	0.4	108	Ge	22.4	20.2
N761	J131319.9+422630	61.4	1178(26)	13 13 19.976 (0.010)	42 26 30.33 (0.10)	1.1	< 0.4	134	Ge		20.6
762	J131320.5+423212	5.5	62(15)	13 13 20.573 (0.012)	42 32 12.81 (0.14)	< 1.0			U	> 26.4	> 25.4
763	J131321.2+424541	6.4	95(22)	13 13 21.244 (0.015)	42 45 41.54 (0.15)	< 1.5			F	25.4	24.4
N764	J131321.4+423837	4.9	43(11)	13 13 21.499 (0.013)	42 38 37.75 (0.13)	< 1.1			Gc	24.7	23.2
765	J131322.1+423700	84.7	948(16)	13 13 22.152 (0.010)	42 37 00.61 (0.10)	0.9	0.4	99	Ge	18.9	17.9
N766	J131322.4+423710	5.3	54(18)	13 13 22.428 (0.016)	42 37 10.10 (0.25)	2.5	2.0	141	Be	24.2	22.2
767	J131322.4+423557	16.3	199(23)	13 13 22.446 (0.010)	42 35 57.61 (0.10)	1.4	0.6	78	Ge	23.3	21.4
768	J131322.5+423347	7.0	77(17)	13 13 22.532 (0.015)	42 33 47.98 (0.10)	< 1.7			Gc	25.9	24.6
769	J131322.6+423620	7.0	80(17)	13 13 22.666 (0.014)	42 36 20.20 (0.12)	< 1.2			Gc	20.8	19.8
770	J131322.9+423308	9.2	114(18)	13 13 22.950 (0.010)	42 33 08.30 (0.10)	< 1.5			Gc	24.7	22.6
N771	J131323.1+424731	11.4	207(30)	13 13 23.187 (0.011)	42 47 31.56 (0.10)	2.3	1.5	80	Ge?	19.9	18.9
772	J131324.1+423725	7.9	89(15)	13 13 24.134 (0.012)	42 37 25.54 (0.10)	< 1.3			Gc	24.8	23.0
773	J131324.2+424430	11.2	157(19)	13 13 24.279 (0.010)	42 44 30.30 (0.10)	< 1.2			Gc	19.3	18.4
N774	J131324.3+424737	5.3	85(22)	13 13 24.394 (0.019)	42 47 37.45 (0.14)	< 1.8			Bc	24.4	23.1
N775	J131324.9+422904	6.1	104(26)	13 13 24.925 (0.020)	42 29 04.82 (0.15)	< 2.2			F		23.4
776	J131326.9+423416	29.5	399(19)	13 13 26.973 (0.010)	42 34 16.35 (0.10)	0.6	< 0.4	118	Ge	24.4	23.0
N777	J131327.0+422754	3.8	59(24)	13 13 27.004 (0.032)	42 27 54.19 (0.20)	< 2.5			Bc		21.5
N778	J131327.3+422754	5.4	101(28)	13 13 27.324 (0.018)	42 27 54.61 (0.19)	< 1.7			Bc		22.0
779	J131328.9+424102	27.6	365(19)	13 13 28.998 (0.010)	42 41 02.64 (0.10)	1.0	< 0.4	69	F ?	26.2	24.8
N780	J131329.8+424624	4.5	196(55)	13 13 29.817 (0.036)	42 46 24.63 (0.45)	2.6	1.1	90	Be	24.1	23.1
N781	J131330.2+423109	6.8	102(28)	13 13 30.226 (0.018)	42 31 09.12 (0.20)	< 1.9			Gc	23.7	22.0
782	J131330.6+424251	7.0	103(21)	13 13 30.642 (0.017)	42 42 51.23 (0.10)	1.9	< 0.7	106	Be	25.1	22.3
N783	J131330.7+424101	4.9	63(18)	13 13 30.787 (0.023)	42 41 01.86 (0.12)	2.1	1.4	82	Ge	21.9	20.3
N784	J131331.1+423347	4.6	78(28)	13 13 31.177 (0.030)	42 33 47.40 (0.23)	< 2.8			Gc	23.0	21.5
N785	J131331.4+424647	5.6	113(35)	13 13 31.421 (0.020)	42 46 47.27 (0.27)	< 2.8			Bc	21.1	19.9
N786	J131331.8+422952	7.0	114(22)	13 13 31.848 (0.011)	42 29 52.07 (0.12)	< 1.2			Gc	20.4	19.4
N787	J131332.0+422909	8.8	183(30)	13 13 32.092 (0.012)	42 29 09.32 (0.14)	2.5	< 0.8	35	U	> 26.3	< 24.5
N788	J131332.1+423649	4.2	52(18)	13 13 32.104 (0.017)	42 36 49.64 (0.26)	< 1.8			Gc	23.2	21.6
789	J131332.5+423406	10.5	148(22)	13 13 32.576 (0.011)	42 34 06.68 (0.10)	< 1.9			Gc	20.6	19.4
790	J131333.6+423746	6.2	72(18)	13 13 33.692 (0.017)	42 37 46.15 (0.12)	< 1.2			U ?	> 25.2	> 24.5
N791	J131334.5+423049	5.5	82(22)	13 13 34.580 (0.019)	42 30 49.23 (0.15)	< 1.4			Gc	21.9	21.1
N792	J131334.9+422904	5.4	205(55)	13 13 34.959 (0.030)	42 29 04.35 (0.44)	3.9	< 2.4	164	Ge?	22.8	21.2
793	J131335.3+424133	8.7	206(28)	13 13 35.385 (0.013)	42 41 33.94 (0.11)	1.6			Ge	21.1	19.8
N794	J131335.7+424043	4.9	76(25)	13 13 35.752 (0.028)	42 40 43.75 (0.18)	< 2.5			Gc	20.8	19.8
N795	J131336.1+424500	4.7	78(24)	13 13 36.116 (0.024)	42 45 00.12 (0.16)	< 2.0			F	25.8	24.4
N796	J131336.3+423307	4.8	182(45)	13 13 36.332 (0.021)	42 33 07.36 (0.44)	4.7	2.5	4	Ge	18.3	17.6
797	J131336.3+423547	9.9	136(19)	13 13 36.354 (0.010)	42 35 47.99 (0.10)	< 1.4			F	26.2	24.0
N798	J131337.4+424314	32.4	588(24)	13 13 37.444 (0.010)	42 43 14.45 (0.10)	0.7			Ge	23.3	20.9
N799	J131338.3+423406	5.4	165(40)	13 13 38.314 (0.027)	42 34 06.78 (0.32)	3.4	< 2.1	155	Gd	22.9	21.7
N800	J131339.5+423418	5.4	109(31)	13 13 39.516 (0.022)	42 34 18.57 (0.19)	< 2.3			Bc?	25.3	24.4
N801	J131340.2+424343	5.1	111(30)	13 13 40.238 (0.021)	42 43 43.97 (0.19)	< 2.5			Bc	25.1	24.0
N802	J131341.2+424051	99.9	27300(550)	13 13 41.272 (0.010)	42 40 51.46 (0.10)	1.7	0.3	91	Ge	20.5	19.3
N803	J131343.3+424424	71.8	3349(77)	13 13 43.333 (0.033)	42 44 24.50 (0.50)	4.7	2.5	120	Ge	22.0	20.0
N804	J131343.4+423522	5.4	169(40)	13 13 43.419 (0.032)	42 35 22.56 (0.22)	3.1	< 2.0	112	Be	22.1	20.6
N805	J131343.9+424302	13.8	267(29)	13 13 43.953 (0.010)	42 43 02.56 (0.10)	< 1.3			Bc	21.7	19.8
N806	J131344.8+423940	4.6	334(88)	13 13 44.851 (0.070)	42 39 40.88 (0.44)	7.4	2.8	130	C ?	24.8	23.0
N807	J131344.9+423457	7.8	138(26)	13 13 44.914 (0.013)	42 34 57.14 (0.11)	< 1.4			F	26.0	23.7
N808	J131346.6+423844	7.8	179(35)	13 13 46.635 (0.016)	42 38 44.99 (0.14)	3.0	2.0	135	Ge	20.8	19.8
N809	J131349.1+424018	7.9	168(33)	13 13 49.144 (0.016)	42 40 18.80 (0.12)	< 1.9			Gc	22.4	21.1
N810	J131349.1+423809	5.2	97(30)	13 13 49.190 (0.026)	42 38 09.77 (0.19)	< 2.5			Gc	23.3	22.3

TABLE 3
RADIO/OPTICAL MORPHOLOGICAL CLASSIFICATIONS

ROM	Number		Description
	Entire Catalog	Complete Sample	
ALL	810	560	
EG	7	5	ACTIVE GALAXIES WITH EXTENDED EMISSION
S	8	7	STELLAR OBJECTS
G	390	268	ISOLATED GALAXIES, of which
Gc	194	134	Unresolved radio source located near nucleus
Ge	166	118	Resolved radio source located near nucleus
Gd	30	16	Radio source displaced from nucleus.
B	185	138	MULTIPLE SYSTEMS, of which
Bc	72	48	Unresolved radio source located near nucleus of one galaxy
Be	91	72	Resolved radio source located near nucleus of one galaxy
B2	22	18	Radio emission from both galaxies of a binary system.
C	12	12	COMPLEX SYSTEMS
F	98	73	FAINT OBJECTS (≈ 24.5 to 26.0 mag)
U	83	52	UNIDENTIFIED
N	27	9	NO SUBARU DATA
sg	14	2	SDSS identifications
su	13	7	SDSS unidentified

TABLE 4
SSA13 RADIO SOURCE COUNT

S_{min} μJy	S_{max} μJy	S_{avg} μJy	Num	Wt	$n(S > S_{min})$ $\times 10^5 \text{sr}^{-1}$	dn/dS $\times 10^{10} \text{sr}^{-1} \text{Jy}^{-1}$	dn/dn_0
25.8	37.5	34.1	20	15.0	54.3	49.3	2.6 ± 1.6
37.5	48.0	42.4	53	4.20	39.0	35.4	4.1 ± 2.0
48.0	59.5	53.5	77	2.30	31.0	25.8	5.4 ± 2.3
59.5	74.5	67.1	86	1.54	23.2	15.5	5.7 ± 2.4
74.5	94.5	83.8	99	1.24	21.5	10.7	7.0 ± 2.6
94.5	130.5	109.6	77	1.06	14.3	4.0	5.2 ± 2.3
130.5	220.5	164.3	70	1.00	12.3	1.4	5.1 ± 2.3
220.5	999.5	419.0	65	1.00	11.4	0.15	6.2 ± 2.5
> 999.5		6400.0	13	1.00	0.23	0.011	14.3 ± 3.5

This figure "f1.gif" is available in "gif" format from:

<http://arxiv.org/ps/astro-ph/0607058v1>